ABSTRACT

Title of Document:	Toward Optimization of Photomodulation of Azobenzene-Modified PPV Derivatives
	Amy Frances Grimes, Doctor of Philosophy, 2007
Directed By:	Professor Douglas S. English, Department of Chemistry and Biochemistry

Photophysical characterization of a family of photoswitchable conjugated polymers is presented in this work. Additionally the instrumentation constructed for these studies, a time-correlated single photon counting spectrometer, is discussed along with the methods used to characterize the instrument. Sample data and fitting procedures are presented. Overall instrument capabilities are also presented, specifically the use of the spectrometer to measure time-resolved fluorescence anisotropy. An example study probing the interactions between charged fluorophores and surfactant vesicles is included as a demonstration of a time-resolved fluorescence anisotropy application.

Understanding the effect of side chain modifications on the emission of light from conjugated polymers is useful in the design of new polymers for applications in sensing and photovoltaics. This thesis focuses on determining the photophysical interactions between a photochromic side chain, azobenzene, covalently bound to a

poly(p-phenylenevinylene) (PPV) derivative. Time-resolved and steady-state fluorescence measurements were employed in these studies.

The photochromic azobenzene quenches emission from the PPV backbone differentially in its' two isomeric states. Both static quenching and non-radiative energy transfer were found to play important roles in the differential quenching of PPV emission by azobenzene. These studies led to the definition of a parameter to judge degree of difference in quenching between the two isomeric forms. This parameter, modulation efficiency (E_{mod}), serves throughout the studies as an important figure of merit for the depth of modulation observed for structurally modified derivatives of the original azobenzene-modified PPV derivative. Maximizing the modulation efficiency was the aim of the PPV studies.

The results presented here elucidated the complex photophysical processes that influence the emission properties of this family of azobenzene-modified PPV derivatives. Important guidelines to maximize modulation efficiency were determined based on these results which will aid researchers in the design of photomodulated conjugated polymers.

TOWARD OPTIMIZATION OF PHOTOMODULATION OF AZOBENZENE-MODIFIED PPV DERIVATIVES

By

Amy Frances Grimes

Dissertation submitted to the Faculty of the Graduate School of the
University of Maryland, College Park, in partial fulfillment
of the requirements for the degree of
Doctor of Philosophy
2007

Advisory Committee:
Professor Douglas S. English, Chair
Professor Millard H. Alexander
Professor Neil Blough
Professor Sheryl Ehrmann
Professor Robert A. Walker

Dedication

I would like to dedicate this work in honor of my family; my parents, Mom and Max, my sister, Bethany and my husband, William for their love and support.

Also, I would like to dedicate this work in loving memory of my Father.

Acknowledgements

I am grateful to my adviser, Dr. Douglas English, for his help and encouragement through the last four years. He has helped me to gain not only technical skills but also confidence in my ability to solve new problems. His guidance was instrumental in my success.

My group members, Xiang Wang, Sara Lioi, Kathy Goodsen, Chip Luckett, Nikolai Sinkov, Emily Danoff and Sophia Vinnikova have been very helpful in completing this work. They have provided hours of lively discussion on topics scientific and otherwise. I am especially appreciative of the help that Sophia has provided in the vesicle experiments.

I am also indebted to my collaborators, Dr. Elizabeth J. Harbron, Diego Vicente and Scott Call at the College of William and Mary for synthesizing the conjugated polymers in these studies and for the helpful exchange of ideas.

Lastly, I would like to thank my family for their patience, love and support though out this process. I would especially like to thank my Mother for the selflessness she has shown in caring for my sister and me. She continues to be a wonderful role model for her daughters.

Table of Contents

List of Tables

List of Figures

Chapter 1: Introduction

1.1 Conjugated Polymers

The first report of conjugated polymers appeared in 1963 by Weiss and coworkers who synthesized oxidized iodine-doped polypyrrole, which was found to conduct electricity with resistivity of only 1 ohm/cm. Their discovery was documented in a series of papers which discussed the synthesis and conductive properties of polypyrrole.[1-3] The same group also filed for an Austrailian patent for the discovery. In 1965 Weiss and coworkers reported synthesis of polymers from imidazole and pyridine.[4,5] In 1974 McGinness and coworkers reported the construction of a voltage-controlled organic polymer switch made from a mixed copolymer of polyacetylene, polypyrrole and polyaniline.[6]

Despite these reports the discovery of conductivity in conjugated polymers is often attributed to Alan Heeger, Alan MacDiarmid and Hideki Shirakawa who were awarded the Nobel Prize in Chemistry in 2000 "for the discovery and development of conductive polymers."[7] Originally published in 1977, they reported high conducitivity in an oxidized, iodine-doped polyacetylene.[8]

Electroluminescence from conjugated polymers was reported in 1990[9] leading to a renewed interest in these materials.[10-13] Easy to process and inexpensive to synthesize, conjugated polymers can be used in a variety of organic-based optoelectronic devices. In many cases conjugated polymers are being designed for use in devices traditionally based on inorganic semiconductors. Conjugated polymers

offer many advantages over inorganic materials. As "soft" materials they can be used to form a variety of structures with ease by spin casting into films and even being deposited via ink-jet printing methods.[14] Devices such as field effect transistors, light emitting diodes, fluorescence sensors and solar energy cells have been demonstrated.

At the heart of this functionality is the unique structure of conjugated polymers. Conjugated polymers are a sequence of repeating monomer units that are electronically coupled through backbone conjugation. The result of conjugation, alternating double and single bonds, is delocalization of the π-bond electrons across all of the conjugated atoms. Delocalized π electrons means that conjugated polymer excitations are delocalized over the conjugated monomer units. The extended π-system results in properties that are similar to semiconductors with the π-molecular orbital which is the HOMO in conjugated polymers acting as the valence band and the π* molecular orbital (LUMO) as the conductance band. For this reason a singlet excited state on a conjugated polymer chain is often referred to as an exciton. However, unlike an inorganic semiconductor, the exciton formed by photoexcitation is generally bound and the excited state is uncharged. Additionally the band gap in a conjugated polymer is generally 1.5 eV to 3.0 eV which is near to most semiconductors, e.g. silicon has a bandgap of 1.1 eV.

Ideally, conjugated polymers are molecules with linear, fully conjugated backbones. However in practice between monomer units there are frequently chemical and physical defects such as saturated carbons, kinks and torsions. Traditionally it was thought that torsions and kinks as well as saturation points define

the borders between chromophoric units and thus the conjugation length. Recent quantum mechanical studies have shown that in the ground state a kink or torsion does result in a diminished delocalization of the transition density to the first two electronic excited states but that only a saturation point on the carbon backbone is sufficient to fully define the separation between two chromophoric units.[15] The number of consecutive conjugated monomer units that exist before a break in the conjugation is known as the conjugation length. For a common conjugated polymer, poly(p-phenylenevinylene) (PPV) shown in Figure 1, the average conjugation length is 5 monomers.[16] The energy of the excited state for a given segment of the polymer chain is inversely proportional to the conjugation length.[17] The random breaks in conjugation result in a heterogeneous distribution of energetic states on the polymer chain. The distribution of chromophoric unit length is also the source of the very large inhomogeneous broadening of the absorption spectrum of conjugated polymers.

Due to the physical and energetic proximity of the conjugated segments on a chain a conjugated polymer can be thought of as a system of weakly coupled chromophores. When a photon is absorbed and an exciton formed that exciton can migrate along the chain via neighboring segments of longer conjugation length and lower energy. Exciton migration occurs very rapidly by non-radiative energy transfer between neighboring segments. Migration can end when an exciton reaches a chromophoric unit that is lower in energy than all those around it or if it migrates into a state where emission cannot occur, i.e. a trap state.

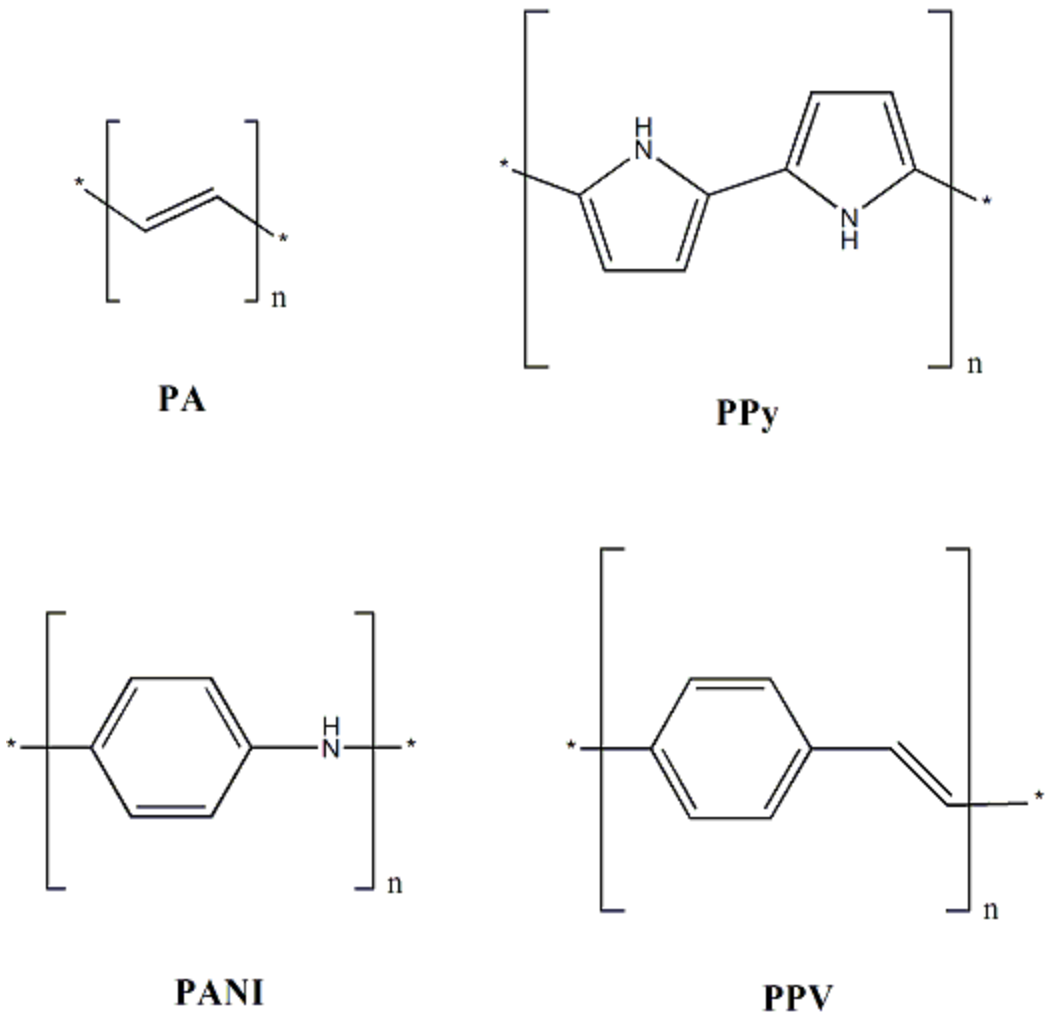

Figure 1.1 The monomer structures of some common conjugated polymers, polyacetylene (PA), polypyrrole (PPy), polyaniline (PANI), poly(p-phenylenevineylen) (PPV)

The chain conformation has a large influence on exciton migration. In a favorable solvent the conjugated polymer is well extended and the exciton makes its way down the chain of chromophoric segments toward lower energy states. However, when in a poor solvent the polymer will take on a compact, coiled conformation, which can result in an exciton moving to a segment on a distant part of the chain that is accessible due to the chain folding back on itself. Coiling and aggregation in a poor solvent can result in decreased photoluminescence efficiency. When two portions of

backbone come into close contact whether two parts of the same chain or from two different chains they can form a trapping site such that an exciton would decay non-radiatively from that segment. Therefore it is important that a solution of conjugated polymers be dilute and to minimize interchain interaction in both the solution and solid state.

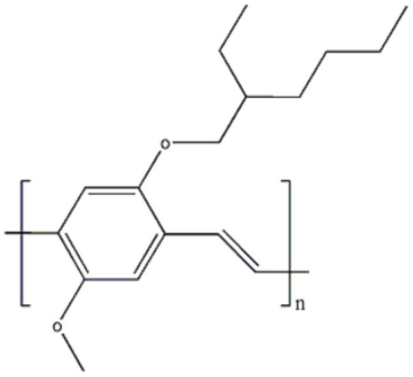

Figure 1.2. The structure of MEH-PPV.

Addition of side chain substituents at various hydrogen positions on the conjugated polymer backbone is one approach to controlling interchain interactions. Braun and Heeger, *et al.* reported the synthesis of a soluble PPV derivatives with bulky side chains, poly(2-methoxy-5-(2'-ethyl)hexoxy-1,4-phenylenevinylene) (MEH-PPV) shown in Figure 1.2, and its application as the emissive layer in a light emitting diode in the early 1990s.[18] Trad, *et al.* reported a small increase in the electroluminescence yield of PPV derivatives with increasing length of alkoxy side chains 4 to 12 carbons long.[19] It is believed that the long side chains cause steric effects which prevent the close approach of other polymer chains when cast into thin films. Additionally alkoxy side chains increase the solubility of PPV derivatives in

common solvents like THF and chloroform that allow for easy spin casting into thin films.

The sensitivity of conjugated polymers to quenching interaction is a direct result of the efficiency of exciton migration along the polymer chain. In a short period of time an exciton is able to sample the energy state of a large number of chromophoric units on the chain. The consequence is that when a quenching site exists on the chain it results in very efficient quenching because it is very likely that an exciton on the chain will experience this site and be quenched. This property of conjugated polymers is a challenge to increasing their quantum efficiency but has been harnessed for the development of very sensitive sensors. Usually each monomer unit contains a site for the binding of the analyte molecule. The binding can result in the quenching of the conjugated polymer's fluorescence for a turn-off sensor or the analyte can inhibit the binding of a quencher for a turn-on sensor.

In addition to using side chains as steric inhibitors of main chain aggregation there have been efforts to add functionality to conjugated polymers by functionalizing their side chains with various types of molecules.

1.2 Functionalized PPV

One approach that scientists have used to develop conjugated polymers with desirable properties is side chain modification. A very common conjugated polymer, PPV, has been modified into hundreds of derivatives. One popular derivative, MEH-PPV, was modified by the addition of two alkoxy side chain units that increase the solubility of the polymer. In addition to solubility, the electron donating alkoxy side

chains result in reducing the polymer's ionization potential making the polymer more easily oxidized than those without alkoxy side chains. The result is to increase the conductivity of the polymer.[20]

The photoconductivity of MEH-PPV can also be increased by blending with C_{60}. The energy conversion efficiency and carrier collection efficiency were found to increase by 2 orders of magnitude when MEH-PPV is blended with C_{60} compared to neat MEH-PPV.[21,22] The mechanism behind this effect is by photoinduced electron transfer from MEH-PPV to C60 at the interface between the two materials. The charge separation takes places efficiently due to the large number of donor-acceptor heterojunctions. This makes the separation of the exciton easier and the result is an increase in the photoconductivity of the material. Cyano-substituted PPV (CN-PPV) has been developed as an alternative to blending with C_{60} and acts in the same manner.

Another approach to increasing the functionality of conjugated polymers is by blending them with dye molecules of different colors in order to increase the emission spectrum. This takes place by energy transfer from the conjugated polymer to the dye molecules. However, these blends tend to suffer from phase separation. An approach to remedy this problem is to covalently attach the dye molecules to the polymer's side chain. The research presented here is in that vein; however the molecule that is covalently bound to the polymer is photochromic. It changes its absorption spectrum and conformation when exposed to certain wavelengths of light. We sought to explore the interactions between the photochromic molecule and the conjugated polymer backbone.

1.3 Current Applications

1.3.1 Sensing

An example of a conjugated polymer sensor developed by Smith, *et. al*. in 2005 detects nitric oxide (NO) which is thought to be an important signaling molecule in the central nervous system. The conjugated polymer, CP1, binds copper (II) which acts to quench fluorescence. When NO is present copper(II) is reduced to copper(I) which does not quench the polymer's fluorescence. This turn-on sensor for NO has a detection sensitivity of 6.3 nM.[23]

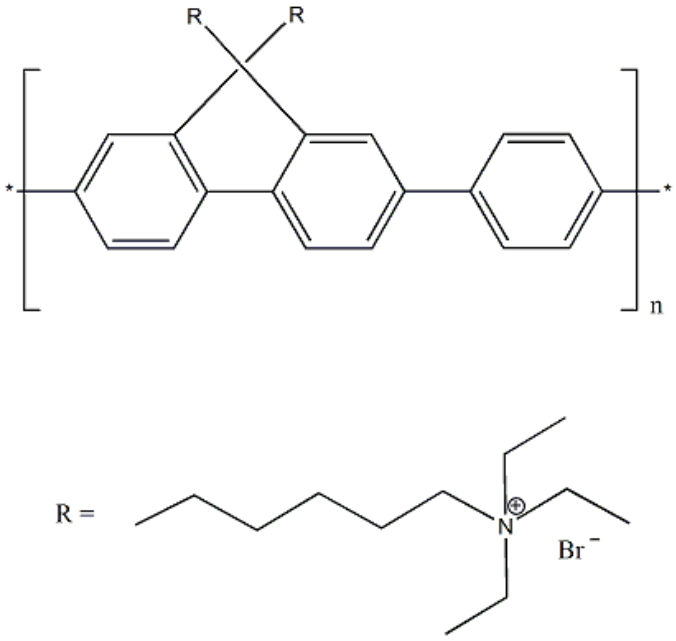

Figure 1.3. The monomer structure of the polyelectrolyte used for single base pair mismatch sensing developed by Tian, *et al.*

There has also been interest in developing conjugated polymer sensors for biological applications, which require that the polymer be water-soluble. The

solution has been to develop charged conjugated polymers known as polyelectrolytes.[24] An application was demonstrated by Tian, *et. al*. using the electrostatic interaction between a cationic polyelectrolyte and anionic ss-DNA to sense single base pair mismatches between two strands of DNA in solution. It was involved in a three part energy transfer process with fluorescein attached to a ss-DNA and ethidium bromide attached to the target ss-DNA. The polyelectrolyte, shown in Figure 1.3, transferred energy to the fluorescein label on the ss-DNA, which emits green light. When a complementary target strand associated with the ss-DNA/polyelectrolyte the energy is transferred from fluorescein to ethidium bromide and yellow emission is observed. By increasing the temperature of the solution it is possible to detect a single mismatched base pair because the ds-DNA will dissociate at a lower temperature when even one base pair is not matched compared to a fully complimentary ds-DNA. The dissociation can be detected by the change in emission color from yellow to green.[25]

1.3.2 Organic Photovoltaics

Polymer-based light emitting diodes (PLEDs) are the focus of a great amount of research over the last 15 years. These devices use conjugated polymers as the emissive layer, which is advantageous because conjugated polymers are easily cast into thin films allowing for thin displays. They are part of a larger class of light emitting diodes that use thin films of organic molecules as the emissive layer known as organic-based light emitting diodes (OLEDs). The general structure of a PLED is shown in Figure 1.4.

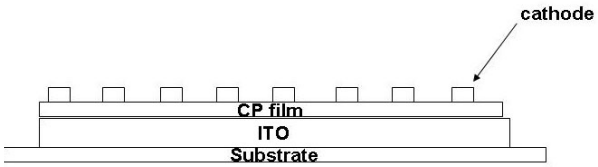

Figure 1.4. Device structure of a PLED. The indium-titanium oxide layer is the anode and applying a voltage across the electode results in the radiatve recombination of electron hole pairs in the conjugated polymer film (CP film). Other semiconductor materials are sometimes place between the ITO anode and CP film to act as a hole transporting layer to increase device efficiency.

Another photovoltaic application of conjugated polymers is in thin film transistors, which is a type of field effect transistor which are capable of controlling the conductivity of a channel in a semiconductor material with an electric field. Thin film transistors are used in the development of active matrix PLEDs which could replace CRT and LCD displays. They are placed in series with the PLED that makes up each pixel of a display to control the voltage across the PLED and therefore the brightness of emission. This is advantageous because it allows the PLED to be continuously operated which eliminates the need for very high voltages to initiate emission each time the pixel is needed.[26,27] The main drawback to PLEDs is the relatively short lifetime of the organic molecules compared to those in liquid crystal displays. Approaches to increasing the lifetime of conjugated polymers are being investigated to allow the technology to advance.

OLEDs have already been used in small displays for digital audio players and color cell phones. Recently some companies have begun to manufacture flexible displays from OLEDs for market testing.

Due to the fast time scales of the processes taking place in conjugated polymers ultrafast spectroscopic techniques and single molecule fluorescence spectroscopy have been applied to study this class of materials. Ultrafast spectroscopy is the experimental technique used in this work, specifically time-resolved fluorescence spectroscopy.

Chapter 2: Fluorescence Theory and Measurements

2.1 Fluorescence

Luminescence is the emission of energy, in the form of a photon, which results from the process of relaxation of an electronically excited molecule to its ground state. Luminescence from an electronically excited molecule in a singlet state in which the excited and ground state electron have opposite spin orientations or are paired is fluorescence. Emission from a triplet state in which the excited and ground state electrons have the same spin orientation or are unpaired is phosphorescence. In order for a molecule to be luminescent it must have delocalized electrons, which are represented as conjugated bonds. At room temperature only the lowest energy electronic states are occupied by electrons as described by the Boltzmann distribution. However, the more closely spaced vibrational levels can be occupied at room temperature.

A Jablonski diagram is often used to depict the processes that an excited state molecule can undergo. An example of a Jablonski diagram is show in Figure 2.1. A vertical arrow represents the absorption of a photon of light by the molecule. The time scale for absorption is $\sim 10^{-15}$ s, the nuclei of the molecule move much more slowly and can be assumed to not be displaced relative to one another during this process. This is known as the Franck-Condon principle. The photon's energy is transferred to the molecule and an electron is promoted from its ground state to the higher energy electronic excited state. The difference in energy between the ground

state of the electron and the excited state that it enters is exactly equal to the energy of the photon that is absorbed. Within each electronic singlet state there are various vibrational states, which are much more closely spaced than electronic energy levels. The electron quickly relaxes to the lowest energy vibrational level of the singlet excited state by emitting energy thermally in a process known as vibrational relaxation. Alternatively, the electron in an excited vibrational state within an excited electronic state (e.g. S_1 or S_2) manifold may undergo internal conversion, crossing into the excited vibrational states of the next lowest electronic state (S_1 or S_0) which occurs on the 10^{-12} s time scale in condensed phases. Internal conversion is a more rapid process than radiative emission; therefore most radiative emission occurs only after internal conversion has occured. In the absence of other molecules to interact with, a few processes can compete to determine the fate of the excited electron including non-radiative relaxation, intersystem crossing to a triplet state, and radiative relaxation or fluorescence. Fluorescence from a singlet excited state generally occurs in 10^{-8} s while phosphorescence happens much more slowly due to the fact that transition between a triplet and singlet state is quantum mechanically forbidden.

Steady-state fluorescence spectra exhibit characteristics that result from the processes described above. In condensed phases, fluorescence emission is lower in energy than the photon of light that was absorbed due to vibrational relaxation and internal conversion, which dissipates some energy thermally. The difference between the excitation energy and emission energy of a fluorophore is known as the Stokes' shift. Emission spectra are also

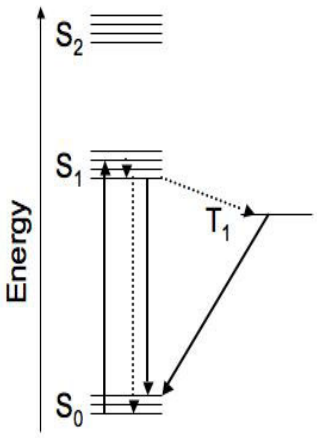

Figure 2.1. A Jablonski diagram depicts the processes possible for a molecule following electronic excitation. The vertical transition represents absorption of a photon, The dotted transitions represent non-radiative processes which can deplete the excited state and the solid transitions show possible radiative processes.

independent of the excitation energy due to the rapid internal conversion to the lowest vibrational level. Additionally the absorption spectrum of a fluorophore and its emission spectrum are related by the fact that the shape of the emission spectrum is typically a mirror image of the absorption spectrum. Normally, only the S_0 to S_1 transition takes place and the corresponding emission is observed. If the probability of absorption is large for S_0 to S_1 then the reverse transition is most probable for emission.

The average amount of time that a molecule spends in the excited state before emitting a photon and returning to its ground state is known as its fluorescence lifetime. The intrinsic fluorescence lifetime of a fluorophore is the lifetime in the absence of non-radiative processes and is inversely related to the rate of radiative decay. The quantum yield of a fluorophore (Q) is the proportion of absorbed photons,

which result in emitted photons. This is related to the radiative rate constant of the fluorophore (Γ) and the rate of non-radiative decay (k) by the following equation:

$$Q = \frac{\Gamma}{(\Gamma + k)} \tag{2.1}$$

2.2 Fluorescence Lifetime Theory

For a group of fluorophores exposed to a pulse of light the number of fluorophores that are initially excited is N_0. The rate with which they relax to the ground state is given be the following expression

$$\frac{dN(t)}{dt} = -(k + j)N(t) \tag{2.2}$$

where k is the rate of nonradiative decay and j is the rate of radiative decay. Integrating this rate,

$$N(t) = N_0 e^{(-t(k+j))} \tag{2.3}$$

The $(k+j)^{-1}$ is the lifetime of the fluorophore or the time that is takes for the initial fluorescence intensity to decay to e^{-1} of its original intensity. Therefore we expect the fluorescence intensity to decay exponentially as a function of time and can be characterized by its fluorescence lifetime.

For systems comprised of multiple species of fluorophores or a single fluorophore in multiple environments the observed fluorescence decay is a sum of exponential functions, each with a lifetime characteristic of one of the subpopulations of fluorophores. Additionally the proportion of total fluorophores with each lifetime is the weighting factor for each exponential in the sum.

The fluorescence lifetime of a molecule can be a powerful indicator of its environment. The intrinsic lifetime of a fluorophore is rarely observed because there are many nonradiative processes, which compete with fluorescence to depopulate the excited electronic state. In general the processes that compete with radiative decay are known as quenching. Forms of quenching include collisional quenching, excited state reactions, energy transfer, electron transfer and ground state complex formation or static quenching. The relationship between the observed fluorescence lifetime, τ, and the native radiative rate is:

$$\tau = (\Gamma + k)^{-1} \tag{2.4}$$

Where gamma is the natural radiative rate and k is the rate for a nonradiative processes. There can be multiple nonradiatve processes taking place in which case each rate would be added to the denominator of the equation above.

For collisional quenching to occur a quencher must diffuse to the fluorophore within its fluorescence lifetime, i.e. while the molecule is in its excited state. When contact is made between the fluorophore and quencher the fluorophore returns to the ground state without emitting a photon. Similarly for static quenching a complex is formed between quencher and fluorophore and no emission occurs. Essentially, collisional quenching and static quenching refer to the same process with two different levels of efficiency. Static quenching is so efficient that the fluorophore never has a chance to emit while in collisional quenching it is possible for emission to occur before quenching. In the steady state all forms of quenching result in a decrease in the emission intensity of the fluorophore. However in time-resolved

fluorescence collisional quenching has the effect of reducing the lifetime of the fluorophore while static quenching does not.

2.3 Fluorescence Anisotropy

Fluorescence anisotropy measurements provide unique information about the inherent properties of a fluorescent molecule as well as the environment it inhabits. Fluorescence anisotropy is a measure of the average angular displacement of a fluorophore in the time between the absorption and emission of a photon. By exposing a group of randomly oriented fluorophores to polarized light, a subset of the fluorophores is excited. Excitation of randomly oriented fluorophores with linearly polarized light results in a population of excited fluorophore symmetrically distributed around the axis of the light's polarization. This is known as photoselection. The probability of a photon of light being absorbed by a fluorophore is

$$P(\theta) \propto \cos^2(\theta) \tag{2.5}$$

where P(θ) is the probability of absorption of a photon when the angle between the polarization of the light and the fluorophore's absorption dipole is θ. The light that is emitted when a fluorophore decays radiatively is polarized in the direction of the fluorophore's emission transition dipole moment. The absorption and emission dipole are usually not collinear. However absorption and emission transition dipole moments into and from the same energy state are often nearly collinear. For this reason the largest anisotropy value can be obtained by exciting in the lowest energy

absorption band of the fluorophore since nearly all emission occurs from the lowest electronically excited state.

To measure fluorescence anisotropy the sample is excited by vertically polarized light and the emission is collected through a polarizer oriented parallel and perpendicular to the excitation polarization. Fluorescence anisotropy is defined by the following equation:

$$r = \frac{I_{para} - I_{perp}}{I_{para} + 2I_{perp}} \tag{2.6}$$

where I_{para} is the intensity when the excitation and emission polarizers are aligned parallel to one another and I_{perp} is the intensity when the two are perpendicular. The numerator is a measure of the amount of depolarization that occurs during the excited state lifetime and the denominator is the total emission intensity. It can be shown that anisotropy is a measure of the average value of $\cos^2 \theta$ where θ is the angle between the emission dipole and the z-axis in the lab frame of reference along which the excitation light is polarized. The relationship is given by the equation

$$r = \frac{3\cos^2(\theta) - 1}{2} \tag{2.7}$$

Photoselection results in a loss of anisotropy due to the distribution of fluorophores with different orientations that are excited. It can be readily shown that the greatest anisotropy that can be measured for fluorophores with collinear absorption and emission dipole moments is 0.4. The experimentally measured anisotropy is actually a product of the loss of anisotropy due to photoselection and that due to angular displacement of the dipoles. Therefore the maximum anisotropy

that can be measured for a fluorophore with angle θ between the absorption and emission dipole moments is given by equation:

$$r_0 = \frac{2}{5}\left(\frac{3\cos^2(\theta)-1}{2}\right). \tag{2.8}$$

Time-resolved fluorescence anisotropy is used to measure the molecular motion that takes place during the fluorophore's excited state lifetime. Following the photoselection of fluorophores with dipoles that are vertically oriented the molecules can undergo rotations and other motions that change the orientation of the emission dipole moment. Anisotropy can be expressed as a function of time by equation 2.9 where τ_{rot} is the rotational correlation time of a spherical molecule that is the amount of time required for the molecule to complete one full rotation.

$$r(t) = r_0 \exp(-t / \tau_{rot}) \tag{2.9}$$

Measurement of time-resolved anisotropy is very similar to measurement of the steady state anisotropy. The fluorescence lifetime decays are collected from fluorophores excited by vertically polarized light with the emission polarizer oriented parallel and then perpendicular to the excitation polarization. The following equation is used to calculate the time-resolved anisotropy:

$$r(t) = \frac{I_{para}(t)-I_{perp}(t)}{I_{para}(t)+2I_{perp}(t)} \tag{2.10}$$

It is also important to consider the relative magnitude of the fluorophores lifetime and the rotational correlation time that one seeks to measure. The lifetime of the fluorophore limits the resolvable correlation time that can be measured. The relationship between the two is given by the Perrin equation:

$$r = \frac{r_0}{1 + (\frac{\tau}{\tau_{rot}})} \tag{2.11}$$

If τ_{rot} is much larger than τ the value measured for anisotropy will be r_0 but if τ is much greater than τ_{rot} the anisotropy will be zero. In time-resolved measurements it is necessary for the lifetime of the fluorophore to be greater than the rotational correlation time in order to get an accurate measurement of the correlation time. This is not always possible and rotational correlation times that are greater than the fluorophore's lifetime result in an infinite value of anisotropy added to the time-dependent decay.

The rotational correlation time of a spherical molecule in a given solvent is

$$\tau_{rot} = \frac{\eta V}{RT} \tag{2.12}$$

where η is the viscosity of the solvent, V is the volume of the spherical fluorophore and T is the temperature of the solution. For a non-spherical molecule the anisotropy decay is more complicated and requires multiple correlation times to explain it. However, a single correlation time can be a good estimate for small molecules in a non-viscous solvent.

The direct dependence of the correlation time on volume of the fluorophore makes it possible to detect the binding of a fluorophore or fluorescently labeled molecule to a larger structure that increases its effective volume significantly. This is one of the main applications of time-resolved anisotropy measurements.

2.4 Fluorescence from Conjugated Polymers

Fluorescence of conjugated polymers is unique because the structure of conjugated polymers is such that they can be accurately thought of as a system of weakly coupled chromophores. Therefore every polymer chain is equivalent to multiple fluorophores covalently attached to one another. These are often referred to as quasi-chromophores or chromophoric units and they have a heterogeneous distribution of band gaps. When one quasi-chromophore on the chain absorbs a photon of light it is likely that the excitation will be transferred non-radiatively to an adjacent quasi-chromophore with a lower band gap. The result is that for a given conjugated polymer chain the majority of emission will take place from only a few quasi-chromophores with the lowest energy excited state.

Chapter 3: Instrument Development and Capabilities

Construction and characterization of a time-correlated single photon counting (TCSPC) spectrophotometer represents a large component of the research presented in this paper. The ability to measure fluorescence lifetimes and time-resolved fluorescence anisotropy enables one to quantify the processes taking place in a molecule's excited state as discussed in the previous chapter. The primary focus of this chapter is a detailed description of the instrumentation that allows these measurements to be made.

3.1 Time-Correlated Single Photon Counting

Fluorescence lifetime decays were measured using a home built time-correlated single photon counting (TCSPC) spectrometer. This instrument combines optical spectroscopy with timing electronics. It acts as a very accurate stopwatch to measure the time that elapses between the near instantaneous electronic excitation of a fluorophore and the emission of a fluorescence photon.

A block diagram of the instrument is presented in Figure 1. Radiation from the excitation source, a mode-locked titanium:sapphire laser, is passed through an electro-optic modulator, reducing its repetition rate from 80 MHz to 8 MHz. It is then frequency-doubled using a β-barium borate crystal. The frequency-doubled radiation is filtered to remove any remaining fundamental frequency, vertically polarized and focused into the sample cuvette. Emission from the sample is

collected at a right angle relative to the excitation radiation's propagation. It is focused through a polarizer set to the magic angle (54.7º) and onto a slit in front of a microchannel plate photomultiplier tube (MCP-PMT). The signal from the MCP-PMT is split. One portion is processed through a pre-amplifier and a constant fraction discriminator (CFD) before arriving at the start input of the time-to-amplitude converter (TAC). The other is used to monitor the count rate for emission with a rate meter. The emission rate should be kept so that less than one photon is being emitted per 20 excitation pulses. For the excitation rate of 8 MHz the emission count rate must be less than 400 kHz. In practice the count rate used is normally 2000 counts per second. Meanwhile the pulse train from the excitation source is detected by a photodiode. This signal is processed by the CFD and passed through a nanosecond delay line before arriving at the stop input of the TAC. The TAC measures the time difference between the emission pulse and the next excitation pulse and creates and output pulse with amplitude proportional to the time difference. A multichannel analyzer (MCA) PCI-card operating in peak height analysis mode sorts these pulses by amplitude into a histogram of times. The excitation pulse train is passed through a nanosecond delay line which allows one to shift the timing of the pulse train by a constant time. Varying the delay time of this line allows one to calibrate the x-axis of the histogram. For example, addition of one nanosecond of delay will move the beginning of the decay by a certain number of bins. This allows one to determine the bin width in units of time.

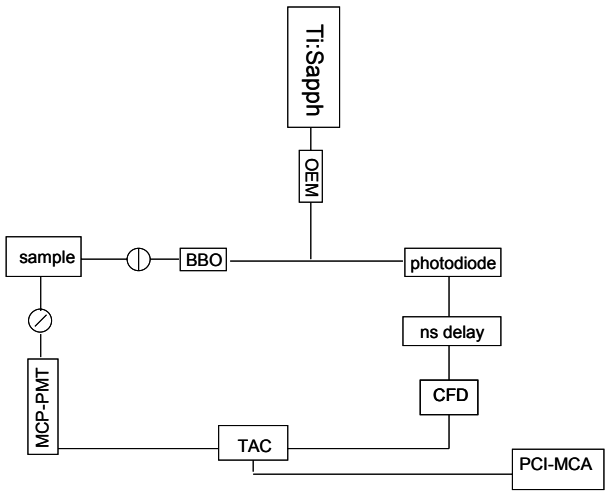

Figure 3.1. Block diagram of TCSPC spectrophotometer.

Due to the limitations of the detectors and timing electronics the instrument response to a sample with a lifetime of zero is non-zero. It known as the instrument response function (IRF). An IRF can be obtained by measuring the response to a very dilute aqueous solution of coffee creamer, which scatters the excitation radiation. A typical instrument response function is presented in Figure 2, it provides information about the temporal resolution of the instrument which is defined by the rise time of the function. Typical rise times obtained from the instrument are ~40 ps. The instrument response function is convoluted with the response of the fluorescent molecule in data collected by the instrument.

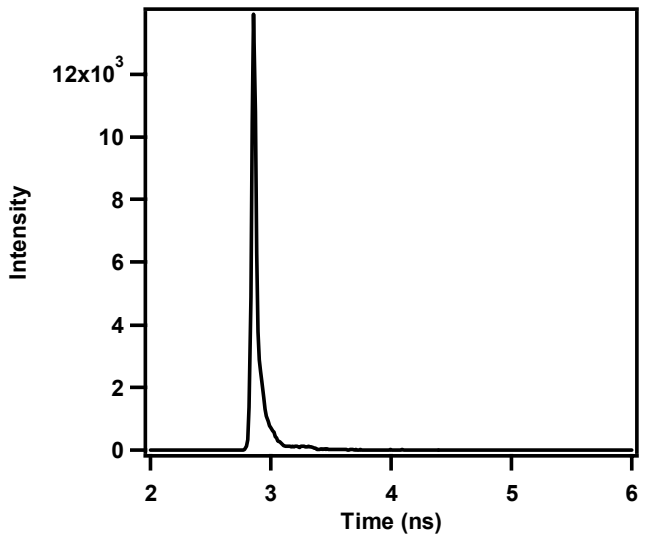

Figure 3.2. Representative IRF from the TCSPC spectrometer.

In general the goal of TCSPC is to measure the average time that an electronically excited molecule remains in the excited state before returning to the ground state. Pulsed light is used to excite the sample at a low intensity and the time is measured between the excitation pulse and the emission of a photon. Emission occurs picoseconds after excitation. The measurement of such a short time period requires that special timing electronics be used.

Each component of the system is described in the following sections.

3.1.1 Ultrafast Laser Excitation

An ultrafast titanium:sapphire laser is the excitation source for the TCSPC spectrophotometer. Specifically the Mai Tai XF-W from Spectra-Physics was purchased for this purpose. It is tunable from 710 nm to 920 nm and has a repetition rate of 80 MHz with the pulse FWHM of 100 fs.

An optoelectronic modulator decreases the repetition rate of the laser by dividing it by an integer value. This works by passing the polarized radiation through a Pockels cell, which is a voltage-controlled waveplate. Applying a certain voltage to the electro-optical material in the cell causes it to act as a half-wave plate, changing the polarization of the incident radiation. A polarizer following the Pockel cell selects for only one polarization orientation. Thus by changing polarization of every nth pulse so that only those pulses have the proper polarization to pass through the exit polarizer the repetition rate can be reduced. In order for the electro-optic modulator to function in this pulse selection mode it is necessary to have a driver to provide the voltage to the EOM and a synchronous countdown to handle the timing of the pulse train and applied voltage.

The excitation radiation is frequency-doubled before reaching the sample by focusing the light onto a β-barium borate crystal. Using this technique of frequency doubling, type I phase matching, results in a train of pulses of radiation with half the wavelength of the input pulses and with its polarization rotated by 90°.

Prior to exciting the sample the radiation is collimated and passes through a half waveplate and vertical polarizer. Any residual fundamental frequency is removed by a filter and the radiation is focused toward the center of the cuvette.

3.1.2 Emission Detection

The emission from the fluorophores is collected at a right angle to the excitation beam propagation. Emission is focused through an emission polarizer and long pass filter onto a slit in front of the detector. The emission polarizer is set to the

magic angle to eliminate any polarization effects. A microchannel plate photomultiplier tube (MCP-PMT) detects the photons emitted from the excited state of the sample. Again the main consideration for choosing an emission detector was temporal resolution. MCP-PMTs provide superior time resolution by reducing the transient time spread, that is, the time between the ejection of an electron from the photocathode and the arrival of an electron at the anode. In a conventional PMT the electron current travels along a trajectory determined by the incident angle of contact with the wall of the tube. An MCP-PMT contains an array of tubules with a thickness on the order of tens of microns after the photocathode. An electron produced at the photocathode will enter one of these tubules and then has a much smaller path to the anode. This reduces the average time that it takes for a photon to be converted into a pulse of electrical current.

The specific MCP-PMT used in the TCSPC spectrophotometer is the R3809U-50 from Hamamatsu. It has a transient time spread of <25 ps and a rise time of 150 ps.

3.1.3 Timing Electronics

A constant fraction discriminator (CFD) is used to provide a temporally accurate pulse from pulses with variable intensities. It is capable of making constant fraction timing pulses from pulses as narrow as 1 ns. It acts by inverting and delaying the input pulse and adding it to the original input pulse. The resulting waveform is bipolar and the zero point crossing is the point when the pulse has risen to 20% of its total intensity. The CFD generates an output pulse that is in time with the zero point

crossing (Figure 3.3). This allows for the accurate timing from pulses with variable intensities from detectors such as MCP-PMTs and fast photodiodes used in the TCSPC spectrophotometer.

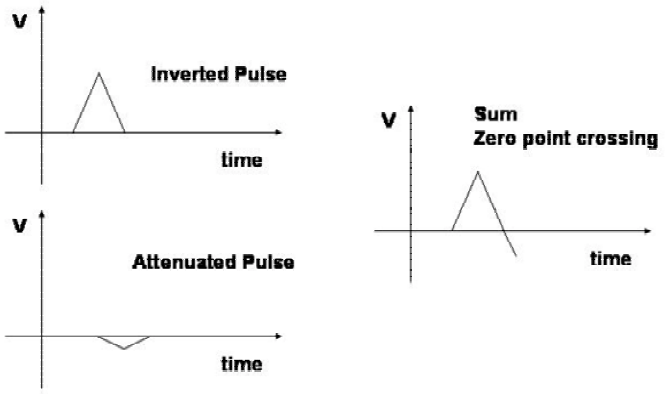

Figure 3.3. The CFD delays a portion of the input pulse and sums it with the same inverted pulse. The zero point crossing of the sum of the two is used to determine the timing of an output which is independent of the intensity of the input pulse.

At the heart of the TCSPC spectrophotometer is the time-to-amplitude converter (TAC). This component measures the time between the start and stop signal that it receives. When a pulse arrives at the start input the TAC begins charging a capacitor. Charging stops when there is a pulse at the stop input or when 50 ns have elapsed. If a stop pulse is detected then the capacitor discharges and creates a pulse with an intensity proportional to the amount of time between the two pulses. Typically the start signal is from the pulse train following the OEM and the stop signal is sent from the MCP-PMT. However this can result in many start signals that do not have a corresponding stop signal. For this reason the start and stop inputs

are reversed from the typical configuration. The result is that each start signal will have a corresponding stop signal within the 50 ns range. Also the data that is collected will be reversed but can easily be modified to the correct shape.

A multichannel analyzer (MCA) sorts the pulses from the TAC by height into a histogram with bins in units of time. The MCA can be set to have two different numbers of bins, 4096 and 8196. The difference between these is in the bin width that results.

3.2 Advantages of TCSPC

Other methods are available for fluorescence lifetime measurements in both the time domain and the frequency domain. Pulse sampling or stroboscopic method is a time domain technique in which a pulsed light source excites the fluorophores and the time-resolved emission is measured at a set point in time following the excitation pulse. The emission sampling takes place by pulsing the photomultiplier gain for a period of time that is short compared with the lifetime of the fluorophore. The time of the emission measurement relative to the excitation is varied and the time-dependent decay is reconstructed. This technique was developed before TCSPC but is not widely used because there are not commercially available instruments.

In the frequency domain fluorescence lifetimes are measured by the phase modulation method. The intensity of the excitation radiation is modulated sinusoidally the result is emission modulated at the same frequency. The emission is delayed by an angle, φ, relative to the excitation radiation and the intensity of the emission is also modulated relative to the excitation. These two factors are used to

calculate the modulation and phase lifetimes, which are the observables in this technique.

3.3 Time-Resolved Anisotropy Measurements

The TCSPC spectrometer was built to allow one to measure the time-resolved anisotropy of fluorophores. The emission polarizer, normally set to the magic angle for collecting lifetime decays, is contained in a mount with a stepper motor that allows one to programmatically control its orientation. The stepper motor was found to have an inconsistent step size and the mount was modified with a lever aligned with the polarizer's fast axis and two digital switches at the 0º (vertical) and 90º positions to detect the polarizer's position. The state of the two switches was monitored using a CB50-LP data acquisition board from National Instruments, which was interfaced with the personal computer via a PCI-6503 board. Labview was used to create a program that allows the input of collection time for each polarizer orientation (vertical or horizontal) and the number of cycles between the two to complete. The user also is able to browse for a folder to write the data files into. When executed the program moves to the vertical position, collects data for the input time, writes the data to a file in the designated folder and moves the polarizer to the horizontal position where data is collected for the same period and written to a file. That completes one cycle for the program.

To begin collecting anisotropy decays the lifetime decay is first collected to 10 000 counts with the emission polarizer at the magic angle. The total time at each

polarizer position (vertical and horizontal) must equal the magic angle collection time.

3.4 Instrument Characterization

The first step in characterizing the instrument was the collection of an instrument response function (IRF), which is presented in Figure 1. The IRF has a FWHM of 40 ps, which is considered a good response from the instrument with our components. In order to determine the bin width of the instrument a ns-delay line was used. By changing the length of the delay by 1 ns the IRF moves within the range of the TAC. Counting the difference in number of bins between the IRF before and after the addition of the 1 ns delay allows one to calculate the width of a single bin of the MCA. A typical bin width for the instrument with the MCA in the 4096 channel setting is 12 ps. With 8192 channels the bins are about 6 ps wide.

3.5 Data Fitting

The fluorescence lifetime decay that is collected by TCSPC is convolved with the IRF. The convolution (R(t)) of the IRF (L(t)) with the fluorophore's radiative decay (F(t)).

$$R(t) = \int_0^t L(t')F(t-t')dt' \tag{3.1}$$

Therefore to fit the data it is necessary to account for the convolution. It becomes especially important for fluorophores with a short lifetime for which the width of the IRF is a significant portion of the decay.

The data analysis programs used were Spectra-Solve and Igor Pro. The method that was used to fit data was a convolute and compare method in both programs. Initial parameters can be entered by the user for the following parameters: background, shift, radiative rate and amplitude and were fit to the equation 3.2.

$$F(t) = A\exp(-(t+s)*k_r) + b \qquad (3.2)$$

where A is amplitude, s is shift between the maximum of the data and IRF, b is the background and k_r is the radiative rate. This is the trial function. It is then convoluted with the IRF chosen by the user and the resulting function is compared to the actual data collected. The parameters are varied to find optimal values to minimize the difference between the convoluted trial function and the data. Multiple lifetimes as well as stretched exponentials can be fit in this manner.

Judging the quality of fit was done by considering the χ^2 parameter and the residual plot. An example of a good fit is shown below.

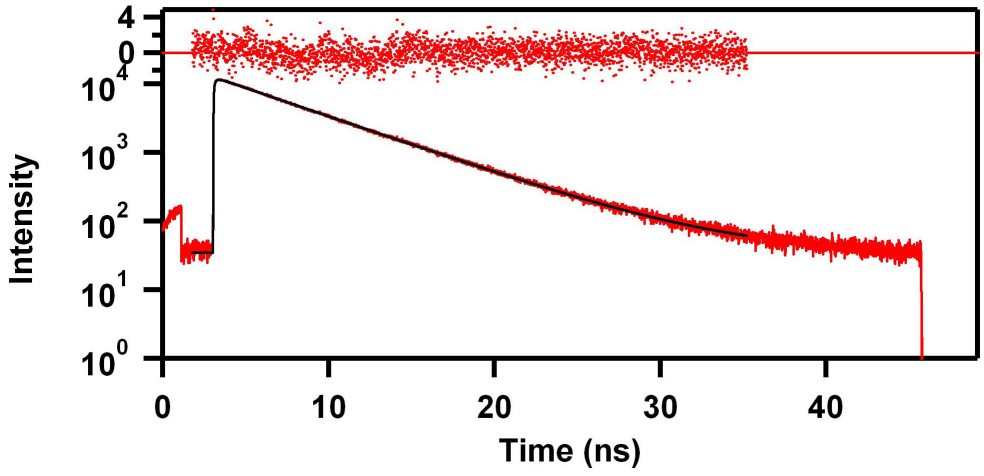

Figure 3.4. An example of the fit and residuals obtained by fitting the data from TCSPC by iterative reconvolution fitting. The data is for Lucifer yellow in water, = 5.1 ns, ^{2} = 1.1.

Testing the time-resolved fluorescence anisotropy measurement was an important step in construction of the instrument. The time-resolved fluorescence anisotropy of coumarin 153 in dimethyl sulfoxide (DMSO) was measured and compared to the results reported by Chowdhury, et. al.[28] The measured r_0 was 0.38 and rotational correlation time was 100 ps which agreed well with the reported values of 0.32 and 110 ps, respectively. The data are shown in Figure 3.5.

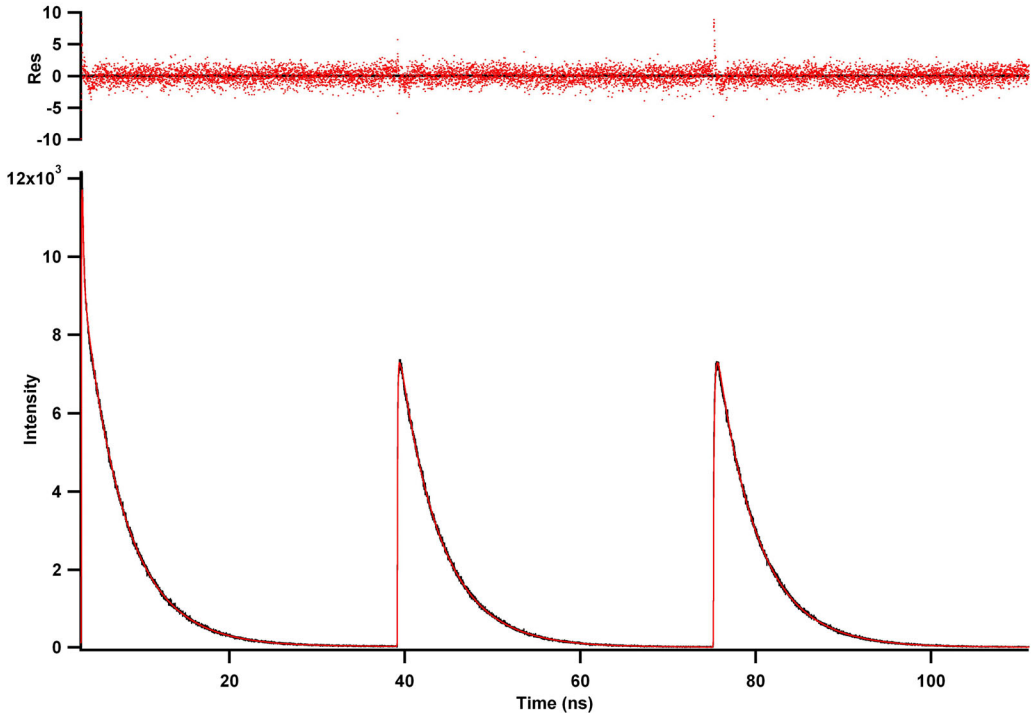

Figure 3.5. Time-resolved fluorescence anisotropy data for coumarin 153 in DMSO. The program concatenates the parallel, magic angle and perpendicular waves and fits the resulting wave.

Construction and optimization of the TCSPC instrument allowed for the research that is presented in the following chapters. Although the technique is well established and has been applied extensively for the past 30 years the construction

and use of a TCSPC spectrometer was an important pedagogical activity and it provides a useful technique for the study of a myriad of systems.

Chapter 4: Time-resolved Fluorescence Anisotropy Measurements

4.1 Introduction

Although not directly related to the focus of this dissertation, the time-resolved fluorescence anisotropy measurements presented in this chapter are an example of the versatile capabilities of TCSPC. Additionally, modification of the instrument for the measurement of time-resolved fluorescence anisotropy is a part of the instrument development that comprises a portion of the work.

In the English laboratory we have been interested in studying the properties of vesicles that form from charged, single tailed surfactant molecules. The two surfactants the have been used are cationic cetyltrimethylammonium tosylate (CTAT) and anionic sodium dodecylbenzenesulfonate (SDBS).

The structures form spontaneously when the cationic and anionic surfactants are combined in the appropriate proportions in solution. An excess of either cationic or anionic surfactant is necessary in order for the vesicles to form. This results in vesicles with net charge. Previous studies conducted by English group members have demonstrated the efficient encapsulation of charged dye molecules in oppositely charge surfactant vesicles and very little encapsulation of dye molecules with the same charge as the vesicle. Dye molecules have also been found to bind to neat vesicles of the opposite net charge. This has led to the hypothesis that electrostatic interactions occur between the small dye molecule and the charge surfactant vesicles that result in efficient encapsulation.

To probe the nature of the interaction between a small, charged molecule and surfactant vesicle time-resolved fluorescence anisotropy measurements were conducted. The specific system studied was positively charged vesicles with the anionic fluorophore, Lucifer yellow. Lucifer yellow (LY) is a lithium salt that has a net charge of -2 in water solution. The encapsulation efficiency of LY by the cation-rich surfactant vesicles is 24% in water.[29] Samples were prepared with 20 uM LY, 3% by weight SDBS and 7% CTAT in water, 50 mM NaCl and 150 mM NaCl. The vesicles were allowed to form over a minimum period of 72 h and were separated from smaller molecules using size exclusion chromatography in the method described previously.[30]

If the large encapsulation efficiency is the result of electrostatic interaction it was expected that the sodium ion would act to shield the net charge of the vesicles and displace LY. This would be observed as a decrease in the encapsulation efficiency. Steady-state fluorescence measurements were conducted in addition to the time-resolved fluorescence and time-resolved fluorescence anisotropy measurements. Comparison of steady-state emission spectra revealed that the vesicles prepared in 150 mM NaCl encapsulated 40% less LY than those prepared in water.

4.2 Time-Resolved Fluorescence Studies

Time-resolved lifetime measurements were useful because the fluorescence lifetime of LY is sensitive to the solvent environment. In water the excited state lifetime of LY is 5.1 ns and the fluorescence decays exponentially. The same value

was measured for the fluorescence lifetime of LY in 150 mM NaCl solution (Figure 4.1, Table 4.1). The measured fluorescence lifetime in water is consistent with that reported by Mishra, et. al.[31]

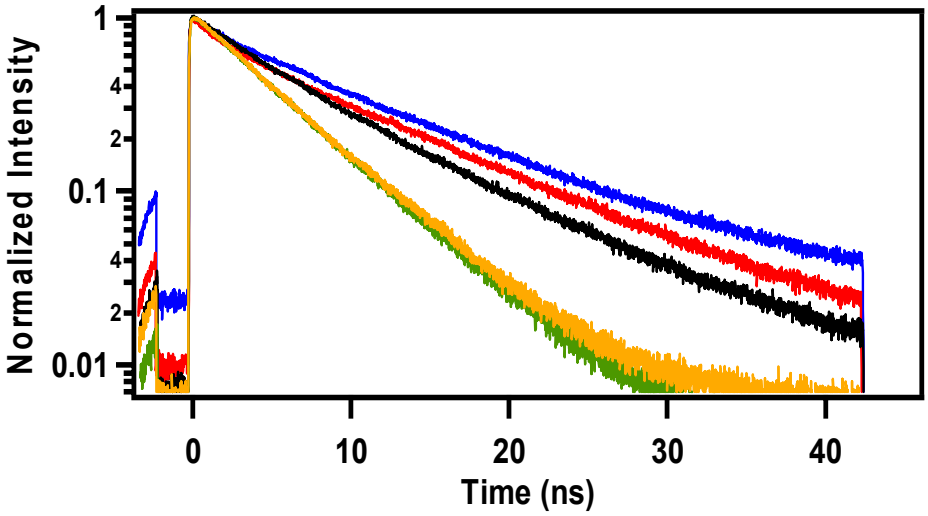

Figure 4.1 Magic angle fluorescence decays of LY in water (green), 150 mM NaCl (gold), CTAT-rich vesicles (black), CTAT-rich vesicles in 50 mM NaCl (red) and CTAT-rich vesicles in 150 mM NaCl.

Table 4.1 Magic-angle fluorescence lifetime measurements for LY in various solutions.

	A_1	τ_1 (ns)	A_2	τ_2 (ns)	$\langle\tau\rangle$
LY in water	1	5.1 ± 0.01	-	-	5.1
LY in 150mM NaCl	1	5.1	-	-	5.1
LY in CTAT-rich vesicles	0.34 ± 0.09	3.5 ± 0.5	0.66 ± 0.09	8.1 ± 0.7	6.5 ± 0.5
LY in CTAT with 50 mM NaCl	0.23 ±0.003	1.2 ±0.1	0.77 ±0.003	10.4 ±0.2	8.3 ±0.2
LY in CTAT with 150 mM Nacl	0.18 ± 0.003	0.99 ± 0.05	0.82 ± 0.003	10.5 ± 0.1	8.9 ±0.1

When prepared in the CTAT-rich vesicle solution the fluorescence lifetime of LY is biexponential. 34% of the LY population has an excited state lifetime of 3.5 ns

and the remaining 66% has a lifetime of 8.1 ns. This indicates that the LY fluorophores are experiencing two different environments in the vesicles.

Preparing the CTAT-rich vesicles in solutions containing NaCl the lifetime of LY has two components, one with a lifetime of about 1 ns and the other with a lifetime of 10.5 ns. The proportion of these two populations changes between the 50mM and 150mM NaCl solutions with the 1 ns component decreasing in proportion (Table 4.1).

4.3 Time-Resolved Fluorescence Anisotropy Results

The results from fitting of the time-resolved fluorescence anisotropy data are presented in Table 4.2. In water, LY rotates quickly, as one would expect for a small molecule in a low viscosity solvent. When prepared in the CTAT-rich vesicles there are two rotational correlation times necessary for a good fit, one is approximately equal to the rotational correlation time of free LY in water and one that is significantly longer. The proportion of the freely rotating population decreased with the addition of NaCl as the proportion and rotational correlation time of the second component increased.

Figure 4.2 shows the calculated fluorescence anisotropy decays for LY in water, in CTAT-rich vesicles in water and 150mM NaCl. From the shape of the curves it is apparent that preparing the vesicle solution in LY results in a longer rotational correlation time than that observed for LY in water.

Table 4.2. Average fit parameters for time-resolved anisotropy data. Data is for free LY in water and LY in CTAT-rich vesicle solutions prepared with 0 to 150 mM NaCl.

	A_1	$\tau_{rot,1}$ (ns)	A_2	$\tau_{rot,2}$ (ns)	r_0
LY in water	1	0.1 ± 0.005	-	-	0.30 ± 0.004
LY in CTAT-rich vesicles	0.72 ± 0.04	.093 ± 0.04	0.28 ± 0.04	2.8 ± 1.3	0.24 ±0.02
LY in CTAT with 50 mM NaCl	0.66 ±0.03	0.11 ±0.01	0.34 ±0.03	4.9 ±0.6	0.29 ±0.02
LY in CTAT with 150 mM Nacl	0.60 ± 0.02	0.094 ± 0.009	0.40 ± 0.02	7.7 ± 0.3	0.27 ±0.02

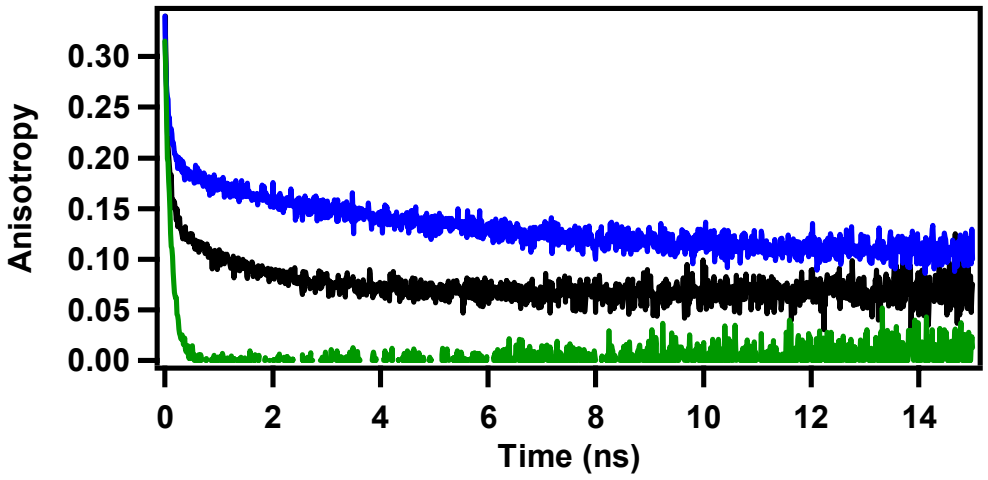

Figure 4.2 Calculated anisotropy decays of LY in water (green), CTAT-rich vesicles in water (black) and CTAT-rich vesicles in 150 mM NaCl solution (blue).

4.4 Discussion and Conclusions

Both magic-angle lifetime and time-resolved anisotropy data indicated that the presence of the vesicles in solution results in two distinct populations of LY fluorophores. It is difficult to definitively determine the location of LY relative to the vesicle bilayer of these two states based on the excited state lifetime. The

dependence of the excited state lifetime of LY on solvent properties is not fully understood.

Considering the fits for LY in CTAT-rich vesicles with no salt in the solution, it is apparent that the larger population (66-72%) of the fluorophore is in an environment where their excited state lifetime is long (8.1 ns) and they are free to rotate. Free rotation implies that there is no strong, static association with the charged vesicle bilayer. We hypothesize that this population exists in the Stern layer of organized water surrounding the vesicles. They may be interacting electrostatically with the charged vesicle surface but are free to rotate. The polarity of the Stern layer is thought to be similar to a short chained alcohol such as methanol or ethanol. LY has been observed to have a longer lifetime in methanol (9 ns) than in water (5.1 ns), meaning that the observed lifetime is consistent with this hypothesis. The remaining population (34-28%) decays with a lifetime of 3.5 ns and has a rotational correlation time of 2.8 ns. This indicates that this population must be strongly interacting with the vesicle bilayer, perhaps incorporated into the bilayer itself.

Addition of salt to the vesicle solution resulted in a large change in the fluorescence lifetimes of the two LY populations. Additionally, it was found to reduce encapsulation of LY by 40% for the 150 NaCl solution. The lifetime of the larger population is 10.5 ns which is similar to that measured for LY in ethanol (10.3 ns). The remaining population decays rapidly (1 ns). The proportion of the longer lifetime population also increases with increasing NaCl concentration.

With increasing NaCl concentration the proportion of freely rotating LY (τ_{rot} ~100 ps) decreases which is consistent with the hypothesis that this population exists

loosely bound through electrostatics in the Stern layer. The slowly rotating population makes up a larger proportion of the total population and τ_{rot} increases with salt concentration. It is tempting to assign the long lifetime population (10.3 ns) detected in the salt-vesicle solutions to the freely rotating LY in a Stern layer environment slight altered by the addition of NaCl. However the proportions of the population in the magic angle lifetime and time-resolved anisotropy fits do not correspond well to one another. Additionally the anomalous fitting parameters for the remaining population make it difficult to corroborate these results. However, from the fluorescence anisotropy decays calculated directly from the data it is clear that addition of salt increases the proportion of slowly rotating, strongly bound fluorophores compared to the case when no NaCl is present. This verifies the hypothesis that electrostatic interactions are important in the efficient, specific encapsulation of charge organic species by surfactant vesicles. However, more experiments are necessary to understand the specific interactions taking place between charge organic molecules and surfactant vesicles.

Chapter 5: Toward Efficient Photomodulation of Conjugated Polymer Emission: Optimizing Differential Energy Transfer in a Azobenzene-Substituted PPV Derivatives

This chapter was published in the Journal of Physical Chemsitry B (2006) vol. 110 .

I collected the fluorescence data presented in this chapter, the polymers studied were synthesized by my collaborators.

5.1 Abstract

We present fluorescence studies of quenching behavior in photoaddressable azobenzene-substituted derivatives of the fluorescent conjugated polymer poly(*p*-phenylenevinylene) (PPV). The azobenzene side chains partially quench the PPV fluorescence, and we have shown previously that the quenching efficiency is greater when the azobenzene side chains are cis than when they are trans. This effect provides a photoaddressable means of modulating the fluorescence intensity of PPV derivatives. To optimize the efficiency of photoinduced intensity modulation, it is important to understand the molecular nature of quenching by both *trans*- and *cis*-azobenzene side chains. Here we investigate the photophysical origins of quenching by the two isomers using steady-state and time-resolved fluorescence spectroscopy. We present results from the azobenzene-modified PPV derivative poly(2-methoxy-5-((10-(4-(phenylazo)phenoxy)decyl)oxy)-1,4-phenylenevinylene) (MPA-10-PPV) and two new related polymers, a copolymer lacking half of the azobenzene side chains and an analogue of MPA-10-PPV with a *tert*-butyl-substituted azobenzene. These

studies reveal that steric interactions strongly influence the extent of PPV emission quenching by *trans*-azobenzene but do not affect the efficient quenching by *cis*-azobenzene. The difference in dynamic quenching efficiencies between *trans*- and *cis*-azobenzene isomers is consistent with fluorescence resonance energy tranfer. These results show that it is possible to control the efficiency of photoswitchable fluorescence modulation through specific structural variations designed to encourage or block quenching by *trans* azobenzene. This is a promising approach to providing useful general guidelines for designing photomodulated PPV derivatives.

5.2 Introduction

Derivatives of the fluorescent conjugated polymer poly(*p*-phenylenevinylene) or PPV have been widely used in applications ranging from organic-based light emitting diodes[32] and solar energy cells[33] to fluorescence-based sensors.[34] The most commonly employed PPV derivative is poly(2-methoxy-5-(2'-ethylhexyloxy)-1,4-phenylenevinylene) (MEH-PPV), in which the alkoxy side chains enhance solubility and processability through side chain-solvent interactions.[35] Polymer-solvent interactions also help determine solution conformations, which in turn affect the fluorescence properties of the polymer by changing the conjugation length and the number of chromophoric units.[36-40] In addition to polymer-solvent interactions, PPV fluorescence properties can also be manipulated through chemical modification of side chains to increase PPV functionality while retaining solubility. We have been engaged in studies of PPV with azobenzene-modified side chains.[41,42] These polymers display interesting photoswitchable intensity modulation, and here we investigate how side chain-backbone interactions influence this photophysical behavior.

To date, conjugated polymers have been functionalized with a variety of pendant side groups for the purpose of tuning fluorescence properties. Pendant dye molecules that can act as energy transfer acceptors have been added to poly(phenylene ethynylene thienylene ethynylene) to create chemosensors for metal ions[43] and to polyfluorene[44,45] and PPV[46] to enable color tuning of polymer emission. In the functionalized polyfluorenes,[44,45] emission is observed primarily from the lower energy pendant dyes due to efficient non-radiative energy transfer from the conjugated polymer backbone. In many cases such color tuning could, in principle, be achieved by blending the conjugated polymer with the dye in a film. However, such non-covalent blends suffer from phase separation and long-term instability due to dye migration, making pendant-functionalized polymers a highly desirable alternative.

We are interested in using pendant photochromic moieties to modulate PPV fluorescence properties. Photochromic molecules have two different forms, reversibly interconvertable by light, that have different absorbance spectra and may also have different shapes, polarities, and other properties. These different properties can be exploited to create various types of photoswitches. When covalently bonded to another molecule, a photochromic moiety's ability to function as an energy transfer donor or acceptor can be turned "on" and "off" by inducing a change in form with light. This approach has been employed to create photoswitches for the purpose of fluorescence modulation, a subject that has been recently reviewed.[47]

Azobenzene shows photochromism through *trans*→*cis* isomerism and exhibits significant changes in geometry, polarity, and absorbance upon isomerization as well as the photomechanical effect of the isomerization itself.[48] It has been

extensively employed as a photochrome in polymeric photoswitch systems, and the photoinduced properties of azobenzene-containing polymers have been reviewed.[49-51] Several small molecule azobenzene photoswitches have taken advantage of azobenzene's ability to act as a nonradiative energy transfer acceptor.[52-54]

Our collaborators have been investigating a family of PPVs functionalized with pendant azobenzenes.[41,42] Poly(2-methoxy-5-((10-(4-(phenylazo)phenoxy)decyl)oxy)-1,4-phenylenevinylene) (MPA-10-PPV, Scheme 5.1) was first synthesized by Yoshino and coworkers[55,56] and has been under study by us for its fluorescence modulation properties.[41] The *cis*-azobenzene acts as an efficient nonradiative energy transfer acceptor for the PPV backbone. Sensitization of the cis → trans azobenzene isomerization is also observed in conjunction with fluorescence quenching, providing clear evidence for energy transfer to the *cis*-azobenzene.[41] The trans azobenzene isomer also quenches the PPV backbone, but photosensitized *trans*→*cis* isomerization is not observed and the quenching mechanism remains unclear. The difference in quenching efficiencies by the *trans*- and *cis*-azobenzene isomers enables modulation of PPV fluorescence by cycling the isomeric state of the side chain with light. Initial work on MPA-10-PPV left open questions regarding the photophysics of the fluorescence modulation, and we present herein results of time-resolved fluorescence studies designed to answer those questions.

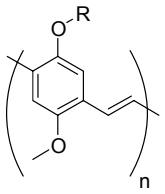

polymer	R
MEH-PPV	R_1 = 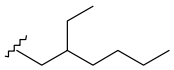
DM-10-PPV	R_2 = 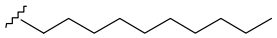
MPA-10-PPV	R_3 = 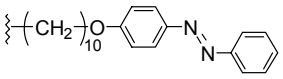
DM-*co*-MPA-10-PPV	50% R_2, 50% R_3
MtBuPA-10-PPV	R_4 = 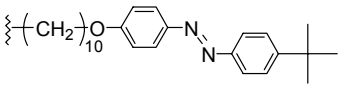

Scheme 5.1. Monomer structures of the polymers discussed and investigated.

One of our primary goals is to optimize the photoswitch abilities of our azobenzene-modified PPV derivatives. We quantify photoswitchable intensity modulation by the fluorescence modulation efficiency (E_{mod}), defined in equation 5.1,

$$E_{\mathrm{mod}} = 1 - \frac{I_{pss}}{I_{trans}} \tag{5.1}$$

where I_{pss} and I_{trans} are the integrated steady-state fluorescence intensities at the photostationary state (*pss*) and in the all-trans form of the polymer, respectively. Preliminary time-resolved data for MPA-10-PPV suggest that a fraction of the PPV chromophoric units undergo highly efficient static quenching by *trans*-azobenzenes but that the strong azobenzene-PPV interaction responsible for the static quenching becomes negligible upon isomerization of the side chain to cis. To maximize E_{mod}, we must limit undesirable static quenching by the *trans*-azobenzene while preserving the

efficient dynamic quenching observed at the photostationary state. Accordingly, we also present herein efforts to demonstrate that we can control static quenching – and, hence, modulation efficiency – through specific structural variations designed to encourage or block static quenching. The largest E_{mod} is observed for a *tert*-butyl-functionalized derivative of MPA-10-PPV in which static quenching is inhibited for steric reasons but dynamic quenching by *trans*- and *cis*-azobenzene is unaffected by the structural perturbation. The addition of the *tert*-butyl group also appears to alter the average distance between PPV donor and azobenzene acceptor. Additionally, fluorescence resonance energy transfer theory appears to account for the isomeric dependence of the dynamic quenching efficiency. Our findings represent an initial step toward defining practical design considerations for photomodulated PPV derivatives.

5.3 Experimental Methods

The syntheses of MPA-10-PPV and poly(5-decyloxy-2-methoxy-1,4-phenylenevinylene) (DM-10-PPV) (Scheme 5.1) were described previously,[41] and the syntheses of other azo polymers presented in this work are given in the Supporting Information. MEH-PPV was purchased from Aldrich and used as received. All samples were prepared the day of use. A small amount of polymer was added to spectral grade toluene and sonicated for 1 h. Samples were transferred to cuvettes equipped with septum caps and degassed with nitrogen for 15 min. Final concentrations gave an optical density of less than 0.1 at 480 nm. Absorption spectra

were recorded on a Varian Cary50. Steady-state fluorescence spectra were measured with a Jobin-Yvon Horiba Fluorolog 3 FL3-11.

For experiments involving measurement of properties of the photostationary state (pss), photoisomerization was induced by exposure to the tip of a Spectroline 11SC-1 longwave UV pen lamp at a distance of 2.5 cm. It was determined that 8 minutes of irradiation in this manner resulted in the photostationary state of the polymer. The sample was continuously monitored during time-correlated single photon counting (TCSPC) experiments by comparing normalized decays to ensure that azobenzene *cis*→*trans* back-isomerization was negligible on the time scale of the experiments, usually 15 min. The composition of the pss was determined by measuring the absorbance of the polymer in the all-trans and pss forms, correcting for the absorbance of the polymer backbone in the UV region, and calculating the ratio of normalized absorbance at the *trans* π-π^* λ_{max} in the pss form to that in the all-trans form. Since the absorbance of the pure cis isomer is very small at the wavelength of the *trans* λ_{max}, this method provides a reasonable estimate of *cis*-and *trans*-azobenzene concentrations.

Fluorescence lifetime decays were collected using a home-built TCSPC spectrometer operated in reverse mode to avoid false start signals and capable of resolving lifetime components as short as 20 ps with deconvolution of the instrument response function. The excitation source for this instrument was a mode-locked titanium sapphire laser with a repetition rate of 80 MHz and a tunable range from 920-710 nm (Wideband Mai Tai, Newport Corp.). A transverse field electrooptic modulator (Model 350-160, Conoptics) was used to reduce the excitation rate to 11.4 MHz. A beam splitter directed a portion of the excitation beam to a high speed

photodiode (Model DET210, Thorlabs) the pulse passed through a nanosecond delay (Model 425A, Ortec) and a constant fraction discriminator (Model 935 Quad CFD, Ortec) to provide the stop pulse to the time-to-amplitude converter (TAC) (Model 567, Ortec). The remaining excitation light was frequency doubled by a barium borate crystal (Photop Technologies), vertically polarized and filtered to remove the remaining fundamental frequency light. Fluorescence emission was collected at a 90º angle relative to the excitation beam, passed through a linear polarizer oriented at 54.7º from vertical and imaged onto an adjustable slit which is used to insure single photon detection by a microchannel plate photomultiplier tube (MCP-PMT) (R3809U-50 Hamamatsu Photonics). The pulses from the MCP-PMT were passed to a pre-amplifier discriminator (model 9327 Ortec) and provided the start pulse to the TAC (model 567 Ortec). A multichannel analyzer card set in peak height analysis mode sorted the pulses from the TAC into a histogram of arrival times (TRUMP-PCI-8K, Ortec). Count rates for the emission detector were kept to less than 2000 counts per second by adjusting the excitation intensity and detection slit width. Typical instrument response functions have full width at half maximum of 45 ps.

All decays were fit to a sum of two or three exponentials by iteratively convoluting trial decay curves, $F(t) = \sum_i a_i e^{-t/\tau_i}$, with the instrument response function and employing a least-squares fitting procedure using Spectra Solve™ software. Best fits were determined by the $\chi 2$ criterion[57] and inspection of the residuals. In certain instances $\chi 2$ values below 1.2 were unachievable using a three-exponential fitting function due to the inability of the model function to adequately describe the heterogeneity of the emitting populations. In these circumstances we are

careful to avoid assigning specific meaning to the amplitudes and populations by limiting our use of this data to the average lifetime as defined in Equation 5.2 below. The normalized pre-exponentials and lifetimes acquired from our best fits were used for deriving an integrated intensity of the time-resolved fluorescence decay, $\bar{\tau}$, using the following equation:

$$\bar{\tau} = \int_{o}^{\infty} F(t)dt = \sum_{i} a_i \tau_i \qquad (5.2)$$

5.4 Results and Discussion

Our collaborators have studied photoinduced changes in PPV emission intensity in an azobenzene-substituted conjugated polymer, MPA-10-PPV (Scheme 5.1).[41,42] MPA-10-PPV is a PPV derivative in which one of the usual alkoxy side chains has been replaced by a decyldioxy-tethered azobenzene. Its absorbance spectrum in dilute toluene solution prepared in the dark (Figure 5.1A) reflects contributions from the *trans*-azobenzene π-π^* transition ($\lambda_{max} \sim 350$ nm) and the PPV backbone ($\lambda_{max} \sim 477$ nm). The fluorescence spectrum of MPA-10-PPV is also shown in Figure 5.1A ($\lambda_{max} = 550$ nm) and is due entirely to emission from the PPV backbone as the azobenzene side chains do not emit. MPA-10-PPV can be compared to a control polymer, DM-10-PPV, which is structurally identical except that it lacks the terminal azobenzene in the side chain (Scheme 5.1). As shown in Figure 5.1B, DM-10-PPV's excitation and emission spectra are essentially identical to those of MPA-10-PPV, demonstrating that the azobenzene side chains of MPA-10-PPV do not

influence the position or shape of the excitation and emission spectra under these conditions.

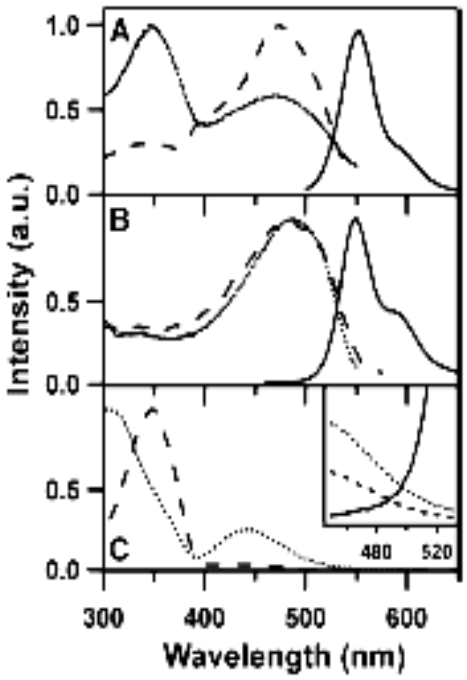

Figure 5.1: Static spectra in dilute toluene solution: (A) MPA-10-PPV absorption (dotted), excitation (dashed), and emission (solid). (B) DM-10-PPV control polymer absorption (dotted), excitation (dashed), and emission (solid). (C) Normalized absorption of model compound decyloxyazobenzene in the trans form (dashed) and at the pss (dotted). Before normalization, the absorption at the peak wavelength in the pss was 3.4 times lower than the absorption at the peak wavelength in the trans form. Inset: Overlap of unnormalized decyloxyazobezene absorption (trans, dashed; pss, dotted) with PPV emission (solid).

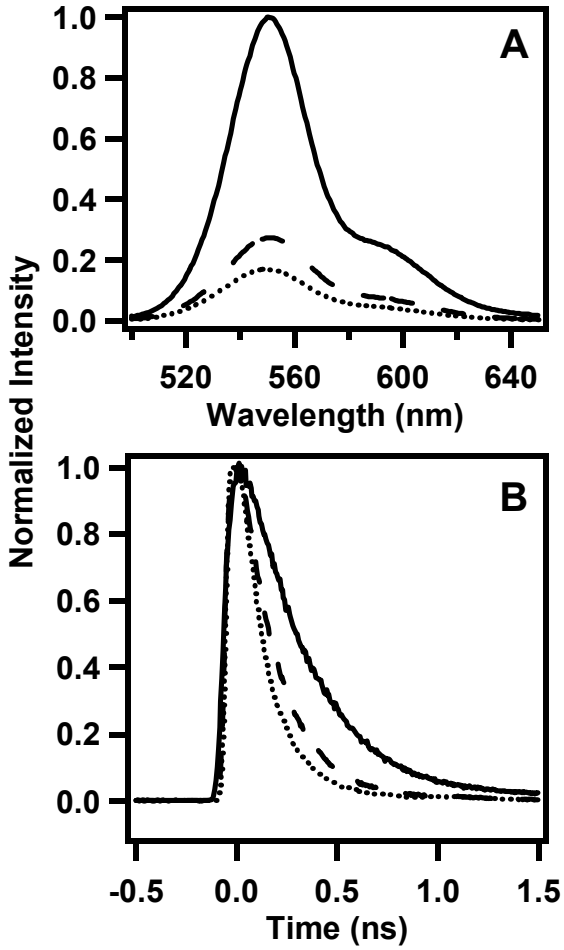

Figure 5.2: Steady-state (A) and time-resolved (B) emission of DM-10-PPV (solid), *trans*-MPA-10-PPV (dashed), and *pss*-MPA-10-PPV (dotted), all in dilute toluene solution.

The azobenzene side chains of MPA-10-PPV do, however, have a major effect on fluorescence intensity. Figure 5.2A and Table 5.1 show the relative intensities of the steady-state fluorescence spectra of DM-10-PPV and the thermally stable form of MPA-10-PPV in which the azobenzenes are trans (*trans*-MPA-10-PPV). The intensity of *trans*-MPA-10-PPV is dramatically quenched relative to the DM-10-PPV control polymer. This quenching is quantified by computing the ratio of steady-state fluorescence intensities for *trans*-MPA-10-PPV (I) to DM-10-PPV (I_0),

yielding an I/I_0 value of 0.35 (Table 5.1). Upon UV irradiation, the azobenzene side chains in MPA-10-PPV photoisomerize to reach a photostationary state in which 55% of the azobenzenes are cis (*pss*-MPA-10-PPV). The fluorescence intensity of *pss*-MPA-10-PPV is quenched further, giving $I/I_0 = 0.21$ and an E_{mod} of 0.41 for MPA-10-PPV (Eq. 5.1). The additional quenching observed upon side chain isomerization is reversed upon irradiation with visible light.

Our collaborators previously determined that the intensity quenching is due to nonradiative energy transfer from the PPV backbone to the azobenzene side chains.[41] The efficiency of the quenching is apparently higher when a portion of the azobenzenes are cis than when they are all trans, a difference we attributed to the improved spectral overlap between the absorption of the cis isomer and the PPV emission. Figure 5.1C shows absorption spectra of an azobenzene model compound, decyloxyazobenzene, in its all-trans and pss forms, and the inset shows the overlap of the azobenzene absorption in both isomeric forms with PPV emission. The overlap is not especially strong, but it is different enough for the two azobenzene isomers to yield different energy transfer efficiencies for *trans*- and *cis*-azobenzene, as will be discussed further below.

The isomeric dependence of quenching efficiencies enables intensity modulation via cycling of the azobenzene isomeric state. Therefore, to achieve maximum modulation efficiency for azobenzene-modified PPV, it is desirable to minimize the quenching by the trans species while maximizing the quenching by the pss. The complexity of this system demands detailed knowledge of the relevant

quenching processes, and time-resolved measurements of the fluorescence decay can provide information to facilitate this understanding.

5.4.1 MPA-10-PPV Time Domain Results

Time-correlated single photon counting (TCSPC) measurements were used to generate a more detailed and complete picture of the photophysics of the MPA-10-PPV system. Time domain experiments can be used to calculate energy transfer efficiency by examining acceptor-induced changes in the donor lifetime. Alternatively, acceptor-induced changes in the integrated lifetime can be compared to changes in the integrated steady-state intensity to check for the presence of a highly-quenched, essentially nonfluorescent population that could occur through strong coupling of the fluorophore and the quencher. The formation of nonfluorescent donor-quencher complexes, often referred to as static quenching, goes undetected in the time-domain.[58]

In order to determine the impact of the side chains on the PPV lifetime, fluorescence decays of the familiar MEH-PPV and the control polymer DM-10-PPV were measured first, and the fitting parameters are shown in Table 5.1. The fluorescence decays of DM-10-PPV and the well-characterized MEH-PPV were both fit to a sum of exponentials in which the major contribution to the decay comes from a component with a 240-270 ps lifetime. These values are in good agreement with previous measurements of MEH-PPV in xylene.[35] The presence of a longer-lived component was needed to describe the data, and this has also been observed previously for MEH-PPV in chloroform.[59] The average lifetimes of MEH-PPV and DM-10-PPV are 272 and 295 ps, respectively, demonstrating that the simple

substitution of a linear alkyl side chain does not perturb the photophysics of the PPV backbone to a significant extent in toluene. Accordingly, DM-10-PPV provides an appropriate control reference with which to compare the steady-state and time-resolved intensities of the azobenzene-substituted PPVs that are the focus of this study.

Table 5.1. Summary of photophysical parameters of PPV derivatives.

[a] I_0 and τ_0 refer to the integrated intensity and average lifetime of the control polymer DM-10-PPV.

PPV Derivative	A_1	τ_1(ps)	A_2	τ_2(ps)	A_3	τ_3(ps)	χ^2	I/I_0 [a]	$\bar{\tau}/\tau_0$
MEH-PPV	0.95	244	0.05	807			1.5		
DM-10-	0.94	269	0.06	980			1.2		
trans-MPA-10-	0.45	21	0.53	177	0.02	1020	1.1	0.35± 0.03	0.41± 0.01
trans-MtBuPA-10-	0.36	71	0.64	211	0.002	950	1.3	0.49± 0.04	0.51± 0.03
trans-DM-*co*-MPA-10-	0.30	94	0.67	238	0.03	588	1.2	0.55± 0.09	0.67± 0.02
pss-MPA-10-	0.50	13	0.49	97	0.003	918	1.5	0.21± 0.02	0.19± 0.01
pss-MtBuPA-10-	0.47	39	0.52	112	0.002	648	1.5	0.24± 0.02	0.25± 0.01
pss-DM-*co*-MPA-10-	0.42	10	0.46	159	0.12	350	1.3	0.45± 0.05	0.43± 0.04

Fluorescence decays for control polymer DM-10-PPV, *trans*-MPA-10-PPV, and *pss*-MPA-10-PPV are shown in Figure 5.2B and follow the same trend observed in Figure 5.2A. A comparison of the DM-10-PPV and *trans*-MPA-10-PPV decays demonstrates that a high degree of quenching is observed upon addition of the azobenzene to the side chain. In the steady state, fluorescence intensity in *trans*-MPA-10-PPV is quenched to 35% relative to the control polymer. Likewise, in the time domain, the decay components are substantially reduced. As shown in Table

5.1, the decay is well-fit by the sum of three exponentials representing three populations: a highly quenched population (a_1 = 0.45, τ_1 = 21 ps), a moderately quenched population (a_2 = 0.53, τ_2 = 177 ps), and a small contribution from a long-lived species. The two principal populations are assigned to PPV chromophores that undergo what we will term *dynamic* quenching,. An average lifetime, $\bar{\tau}$, as defined in Eq. 5.2, was calculated and compared to that of the control polymer, τ_0. For *trans*-MPA-10-PPV, $\bar{\tau}/\tau_0$ is 0.41 whereas I/I_0 is 0.35. Hence, a smaller amount of quenching is measured in the time domain than in the steady state. This discrepancy between steady-state and time-resolved quenching is a classic indicator of the presence of a subpopulation in which the donor and quencher form a ground state complex that is essentially nonfluorescent. We will refer to the quenching of this population as *static* quenching.

Static quenching through the formation of a ground state complex is often observed when a fluorophore and quencher form a stacked structure. For example, static quenching of anionic derivatives of poly(phenylene ethynylene) polymers by cationic electron acceptors in aqueous solution has been studied by Tan, *et al*.[49] They observed extremely efficient quenching due to strong association between the polymer and the quencher ion and rapid migration of the singlet exciton to the quencher site. This conclusion was drawn from the extremely large Stern-Volmer quenching constants. In our case the fact that relative fluorescence intensities are greater in the time domain than in the steady state indicates a substantial degree of static quenching of the PPV backbone by the *trans*-azobenzene side chains. Therefore, a strong electronic coupling between the PPV backbone and the *trans*-

azobenzene side chains must exist and give rise to extremely efficient nonradiative depopulation of the singlet excitons in a subpopulation of PPV chains.

We hypothesize that stacking of the *trans*-azobenzene side chain with the PPV backbone may be responsible for the statically quenched population. *Trans*-azobenzene and the PPV backbone have extremely similar geometries that could enable one azobenzene to interact with two PPV subunits. Evidence for stacking interactions is typically found in steady-state absorption spectra. However, we observe only a slight broadening of the azobenzene absorption of *trans*-MPA-10-PPV relative to an azobenzene model compound. The absence of a substantial change in the azobenzene absorption spectrum suggests that stacking interactions occur in only a small fraction of the azobenzene side chains. It is plausible that even a small fraction of strongly coupled PPV-*trans*-azobenzene complexes could lead to the observed decrease in fluorescence since static quenching could occur by trapping of the singlet exciton during migration or at the PPV chromophoric unit from which emission would occur.[60] It has been shown previously that only a very few traps are necessary for efficient quenching of an entire conjugated polymer chain.[49,61,62] Therefore, the statically quenched population responsible for the intensity loss in MPA-10-PPV is conceivably composed of polymer chains with a single stacked side chain that forms an efficient exciton trap.

5.3.2 MPA-10-PPV Photostationary State

UV-irradiation of MPA-10-PPV produces a photostationary state concentration of *cis*-azobenzenes (55%) and results in additional lifetime quenching in the time domain, as shown in Figure 5.2B. Like *trans*-MPA-10-PPV, *pss*-MPA-

10-PPV is well-fit by the sum of three exponentials with major components that can be interpreted as a highly quenched population (a_1 = 0.50, τ_1 = 13 ps) and a moderately quenched population (a_2 = 0.49, τ_2 = 97 ps). The highly quenched population decays on a timescale that pushes the limits of the instrument's time resolution, even with deconvolution, so we place greater emphasis on the integrated lifetime ($\bar{\tau}$) than on the amplitudes or magnitudes of specific components. The fact that $\bar{\tau}$ for the *pss*-MPA-10-PPV is shorter than $\bar{\tau}$ for *trans*-MPA-10-PPV indicates that the dynamic quenching by *cis*-azobenzene is more efficient than that by the trans isomer.

Quenching of *pss*-MPA-10-PPV relative to the control polymer DM-10-PPV is identical within error in the steady state and the time domain (I/I_0 = 0.21, $\bar{\tau}/\tau_0$ = 0.19), indicating that dynamic quenching dominates in the pss. Therefore, while static quenching plays a major role in the quenching of *trans*-MPA-10-PPV, it is a relatively minor contributor to quenching in the photostationary state. We suggest that trans→cis isomerization disrupts the strongly coupled state responsible for the static quenching in *trans*-MPA-10-PPV. This disruption could have a geometric basis, as stacking of the cis isomer with the PPV backbone would be geometrically disfavored relative to *trans*-azobenzene. Interestingly, these initial results for *trans*- and *pss*-MPA-10-PPV suggest that the *trans*-azobenzene is both a better and worse quencher than the cis: better because it participates in static quenching and worse because its dynamic quenching is less efficient than that of the cis isomer. The picture that emerges from these data is that stacking and static quenching determine the emission intensity (brightness) of the trans state while dynamic quenching is the

dominant factor contributing to the brightness of the pss. The modulation efficiency, as defined in Equation 5.1, is 0.41 for MPA-10-PPV. Ignoring static quenching and recalculating the modulation efficiency based on dynamic quenching from time-resolved integrated intensities yields a value of 0.54, which demonstrates that E_{mod} would be improved if static quenching were reduced. Below we investigate the role of side chain density and steric interactions on static quenching and, hence, modulation efficiency.

The *trans*- and *pss*-MPA-10-PPV time-resolved results indicate that the type of quenching that is observed is largely determined by the differing abilities of *trans*- and *cis*-azobenzene to form a strongly coupled state with the PPV backbone. If stacking is responsible for this effect, then it may be altered by decreasing or increasing steric hindrance. To probe the role of steric factors in quenching behavior, we conducted analogous time-resolved fluorescence experiments with two other polymers in which the structure has been altered to perturb the ability of the azobenzene side chains to participate in azobenzene-azobenzene and/or azobenzene-PPV interactions. First, we synthesized a random copolymer, DM-*co*-MPA-10-PPV, from a 50:50 mixture of the monomers used to synthesize MPA-10-PPV and control polymer DM-10-PPV, yielding a structure that has half as many azobenzenes as MPA-10-PPV. With fewer contiguous azobenzenes, possible azobenzene-azobenzene interactions and general crowding of the side chains should be diminished in this structure relative to MPA-10-PPV, in which every subunit has an azobenzene.

5.4.3 DM-co-MPA-10-PPV

In the time domain, the majority of chromophores in the *trans*-copolymer remain virtually unquenched (a_1 = 0.67, τ_1 = 238 ps) while the remainder are moderately quenched (a_2 = 0.30, τ_2 = 94 ps). Comparison of steady-state and time-resolved relative intensities, however, reveals that static quenching plays a much larger role in the quenching of the trans copolymer than in *trans*-MPA-10-PPV. Relative to control polymer DM-10-PPV, steady-state I/I_0 is 0.55 for the *trans*-copolymer while $\bar{\tau}/\tau_0$ is 0.67. Hence, the trans copolymer shows a significant amount of static quenching even though the number of quenching units has been reduced by half. The increased static quenching observed in trans copolymer may be explained by an increase in the formation of strongly coupled states that is facilitated by the reduction in side chain crowding in the copolymer relative to MPA-10-PPV. With the one-azobenzene-per –subunit structure of MPA-10-PPV, azobenzene side chain organization in the form of self-stacking seems likely and would inhibit azobenzene-PPV interactions by effectively "tying up" the azobenzene side chains. Without this competing interaction, the azobenzene side chains in the copolymer are free to interact with the backbone.

The assumption of reduced crowding in the copolymer is further supported by the pss composition obtained from absorbance measurements: more of the azobenzene side chains are cis in the copolymer (71%) than in MPA-10-PPV (55%). Inhibition of trans→cis isomerization in *trans*-azobenzenes in systems with high azobenzene content has been observed[63,64] and likely limits the cis concentration in *pss*-MPA-10-PPV to a much greater extent than in the copolymer. Various types of *trans*-azobenzene organization in solution have been observed in polypeptides[63,65] and

polymers[66,67] with azobenzene side chains, azobenzene-functionalized dendrimers[68] and oligo(ethylene glycol)s,[69] and in numerous bilayers and vesicles composed of azobenzene-functionalized amphiphiles.[70-72] We attempted to reproduce the static quenching observed in our system by mixing control polymer DM-10-PPV with decyloxyazobenzene, an azobenzene model compound, and monitoring the steady-state and time-resolved intensities. Unfortunately, the high optical densities of decyloxyazobenzene at the concentrations required for this noncovalently tethered system precluded meaningful results.

Upon isomerization to the photostationary state, the fluorescence intensity of the copolymer is further reduced in both the steady state and the time domain. As was the case with MPA-10-PPV, static quenching vanishes once the photostationary state of the copolymer is generated, yielding essentially equal intensity ratios in the steady-state and time-resolved measurements ($I/I_0 = 0.45$, $\bar{\tau}/\tau_0 = 0.43$).

Collectively, the MPA-10-PPV and copolymer results indicate that steric crowding and its influence on azobenzene-azobenzene and azobenzene-PPV interactions are a major factor in *trans*-azobenzene quenching. To investigate this possibility, we synthesized and studied another structural variant of MPA-10-PPV in which we increased the steric bulk of the azobenzene side chain via addition of a *tert*-butyl group in the *para* position of the azobenzene. The resulting polymer, MtBuPA-10-PPV, is shown in Scheme 5.1. The addition of the *tert*-butyl group should increase steric crowding and inhibit azobenzene stacking interactions among neighboring azobenzenes and with the polymer backbone.

5.3.4 MtBuPA-10-PPV

Comparison of the steady-state fluorescence intensities for *trans*-MtBuPA-10-PPV and *trans*-MPA-10-PPV (Figure 5.3, left side) shows that the *tert*-butyl polymer is substantially more intense. Indeed, the steady-state intensity of *trans*-MtBuPA-10-PPV is closer to that of the copolymer, which has half as many quenchers, than it is to its analogue, *trans*-MPA-10-PPV. Clearly, the addition of the bulky *tert*-butyl group significantly diminishes the ability of the trans side chain to quench the PPV backbone. Given that addition of the *tert*-butyl group does not alter the azobenzene enough to affect its resonance with the PPV backbone, these data indicate that a strong physical interaction or close spatial proximity and alignment – rather than spectral overlap – is needed for the efficient quenching observed in *trans*-MPA-10-PPV and the *trans*-copolymer. When taken together with the MPA-10-PPV and copolymer data, these results provide further support for the idea that the extent of quenching by *trans* azobenzene is largely determined by side chain-side chain and side chain-backbone interactions.

Examination of the time-resolved fluorescence of *trans*-MtBuPA-10-PPV reveals the main reason for this significant change in the *trans*-azobenzene's quenching ability: a reduction in static quenching. Steady-state and time-resolved fluorescence intensities of *trans*-MtBuPA-10-PPV relative to the control polymer DM-10-PPV are essentially identical ($I/I_0 = 0.49$, $\bar{\tau}/\tau_0 = 0.51$), indicating that static quenching plays a very minor role in the quenching of PPV fluorescence by the trans *tert*-butyl-functionalized azobenzene.

Addition of the *tert*-butyl group clearly causes a substantial decrease in the quenching ability of *trans* azobenzene in MtBuPA-10-PPV as compared to MPA-10-

PPV, but this difference virtually disappears when the photostationary state concentration of *cis*-azobenzenes (59%) is produced by UV irradiation. Figure 5.3 (right side) shows that the relative steady-state fluorescence intensities of *pss*-MtBu-10-PPV and *pss*-MPA-10-PPV are nearly identical. The time-resolved decays of these two polymers at the *pss* are also extremely similar (Table 5.1), and the quenching behavior of both is dominated by dynamic quenching. As was the case with *pss*-MPA-10-PPV, static quenching plays a negligible role in *pss*-MtBuPA-10-PPV ($I/I_0 = 0.22$, $\bar{\tau}/\tau_0 = 0.24$). Previously, we observed photosensitized cis → trans back-isomerization of the azobenzene side chains in *pss*-MPA-10-PPV and interpreted this as evidence for singlet energy transfer from the PPV backbone to the *cis* azobenzene side chain.[41] Thus, we assign the rapid decay components observed for *pss*-MPA-10-PPV and *pss*-MtBuPA-10-PPV to nonradiative singlet energy transfer.

To determine whether the observed dynamic quenching is consistent with a fluorescence resonance energy transfer (FRET) mechanism, we calculated the Förster radii (R_0) for energy transfer from a PPV donor to *trans*- and *cis*-azobenzene acceptors. We used the trans and cis forms of the decyloxyazobenzene model compound (Figure 5.1C) for the acceptor absorption spectra and a ^{2} value of 2/3, we obtained R_0 values of 15.0 and 18.6 Å for *trans*- and *cis*-azobenzene , respectively. Given these values, the FRET efficiency (E_{FRET}) can be calculated individually for PPV-*trans*-azobenzene and PPV-cis-azobenzene pairs as a function of donor-acceptor separation (r) according to equation 5.3:

$$E_{FRET} = \frac{R_0^6}{R_0^6 + r^6} \qquad (5.3)$$

Figure 5.4 shows E_{FRET} as a function of r for *trans*- and *cis*- azobenzene acceptors. There are clearly donor-acceptor distances at which there are substantial differences in energy transfer efficiency for *trans*- and *cis*-azobenzene.

E_{FRET} can also be calculated from time-resolved fluorescence data according to equation 5.4, and the results of this calculation are listed in Table 5.2.

$$E_{FRET} = 1 - \frac{\bar{\tau}}{\tau_0} \tag{5.4}$$

Figure 5.4 shows that the calculated E_{FRET} value of 0.59 for trans-MPA-10-PPV equates to a donor-acceptor distance of 14.1 Å. Following the curves in Figure 5.4 , this distance yields E_{FRET} = 0.84 for *pss*-MPA-10-PPV, which is extremely close to the measured value of 0.81. For *trans*-MtBuPA-10-PPV, the calculated E_{FRET} of 0.49 yields r = 15.1 Å, which in turn predicts an E_{FRET} of 0.78 for *pss*-MtBuPA-10-PPV. Again, this calculation slightly overestimates the actual value of 0.75. Molecular modeling suggests that there two azobenzene PPVs would have a donor-acceptor distance in the vicinity of 20 Å if the decyldioxy teher were completely extended. Thus, the donor-accpetor distances suggested by the calculated E_{FRET} values are consistent with azobenzene acceptors on a mostly extended chain. It is also possible that the tether conformation changes in response to azobenzene isomerization, which would alter the donor-acceptor distance and, hence, $E_{FRET.}$

Two major points emerge from this FRET analysis. First, it demonstrates that the difference in dynamic quenching efficiencies in all-trans and pss azobenzene can be accounted for by the difference in Förster radii for the two isomeric forms of the azobenzene acceptor. Additionally, it suggests that the differences in dynamic quenching behavior between MPA-10-PPV and its *tert*-butyl-functionalized analogue

may be due to an increase in the average donor-acceptor distance for MtBuPA-10-PPV. The bulky *tert*-butyl group might create sufficient steric hindrance in the side chains to prevent the closer approach to the backbone observed for MPA-10-PPV.

The differing quenching efficiencies by trans- and cis-azobenzenes in all three polymers studied here means that the fluorescence intensity can be modulated in all of them, albeit to differing extents. The fluorescence modulation efficiency, as defined in equation 5.1, is given in the Figure 5.3 inset for the three polymers. E_{mod} values of the copolymer, MPA-10-PPV and MtBuPA-10-PPV are 0.18, 0.41, 0.52, respectively. The highest modulation efficiency was achieved for MtBuPA-10-PPV by adding a structural feature that does not alter the quenching at pss but greatly reduces undesired static quenching by *trans*-azobenzenes. It is interesting to note that the modulation efficiency for MtBuPA-10-PPV calculated from steady-state intensities (0.52) approaches that calculated for MPA-10-PPV from time-resolved intensities, which reflect only dynamic quenching (0.54). Because it eliminates static quenching from the system, functionalization of the azobenzene with the *tert*-butyl group reveals the inherent dynamic quenching abilities of the *trans*- and *cis*-azobenzene isomers. By shedding light on specific molecular-level interactions, these observations provide important insight that could prove useful in designing molecules for PPV-based optoelectronic devices such as pixel-based displays in which control of intensity modulation of initial intensity is desired.

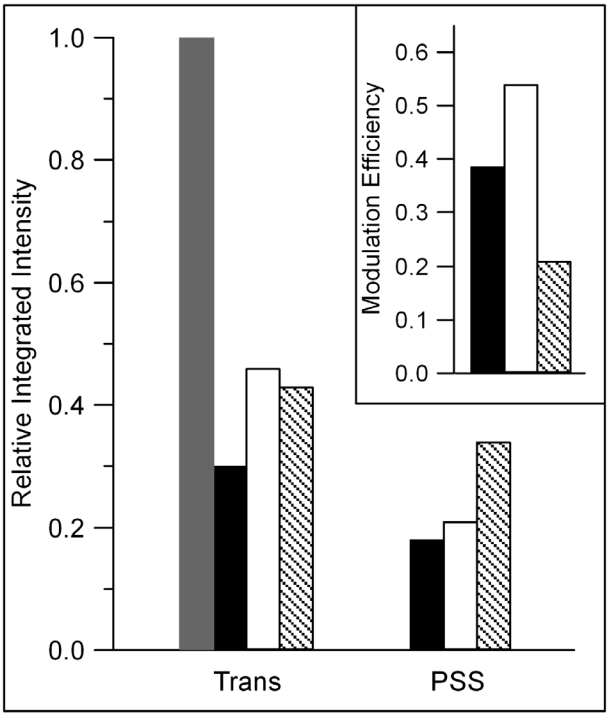

Figure 5.3: Integrated steady-state fluorescence intensities of MPA-10-PPV (black), DM-*co*-MPA-PPV copolymer (diagonal lines), and MtBuPA-10-PPV (white) relative to control polymer DM-10-PPV (gray), all in dilute toluene solution. Inset: Fluorescence modulation efficiencies calculated by Equation 5.1 for each azo polymer.

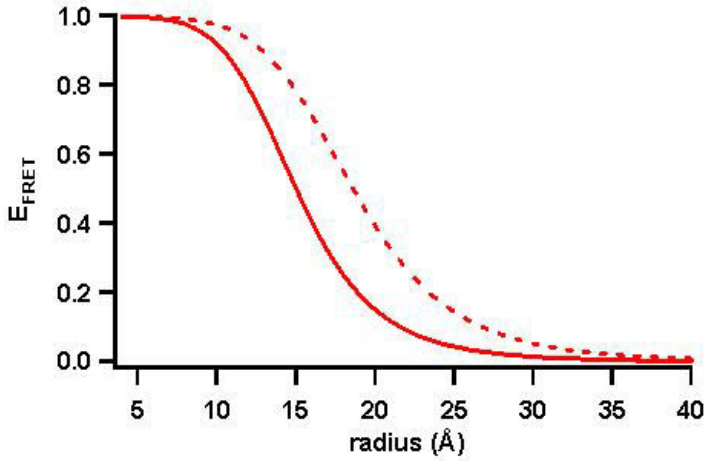

Figure 5.4: FRET efficiencies calculated as a function of donor-acceptor distance, r, by equation 5.3 for trans- (red solid) and cis-azobenzene (red dashed line) acceptors. The lines demonstrate how E_{FRET} calculated from time-resolved data can be used to determine r for MPA-10-PPV, as described in the text.

Table 5.2: E_{FRET} calculated from equation 5.4 with lifetime $_0$ equal to the control polymer DM-10-PPV average lifetime.

PPV Derivative	**E_{FRET}**
trans-MPA-10-	0.59
trans-MtBuPA-10-	0.49
trans-DM-*co*-MPA-10-	0.33
pss-MPA-10-	0.81
pss-MtBuPA-10-	0.75
pss-DM-*co*-MPA-10-	0.57

5.5 Conclusion

We have combined steady-state and time-resolved fluorescence studies to investigate the photomodulation of PPV derivatives functionalized with pendant azobenzenes. We have shown that the mechanisms of quenching by the two isomeric forms of azobenzene differ significantly. Comparison of steady-state and time-resolved data reveals that static quenching of the PPV fluorescence is a major factor in quenching by the *trans* azobenzene side chain. Static quenching by *trans*-azobenzene is facilitated by the formation of an essentially nonfluorescent *trans*-azobenzene-PPV complex that is likely the result of stacking interactions. The occurrence of static quenching varies among the three polymers and is greatest in the polymer with the lowest degree of side chain crowding (*trans*-DM-*co*-MPA) and virtually absent in the sterically hindered *tert*-butyl-substituted polymer (*trans*-MtBuPA-10-PPV). By contrast, quenching by the *cis*-azobenzene side chains in the pss occurs via a dynamic quenching mechansim. Dynamic quenching by both *trans*- and *cis*-azobenzene is consistent with a FRET mechanism, and the difference in trans and cis energy transfer efficiencies is accounted for by the different Förster radii of the two isomeric forms of the azobenzene acceptor with the PPV donor.

Optimization of photomodulation efficiency for these azobenzene-PPV derivatives requires maximization of the difference in steady-state fluorescence intensities between the all-trans and pss forms of the azobenzene-functionalized polymers. We have used the information regarding *trans*- and *cis*-azobenzene quenching mechanisms revealed by the time-resolved measurements to improve modulation efficiency. Addition of a *tert*-butyl group to each azobenzene side chain substantially increases trans state brightness by blocking static quenching while cis

tert-butyl azobenzene side chains retain the powerful quenching efficiency of ordinary *cis*-azobenzene. Therefore, the difference between trans and pss state brightness is increased, enabling an improved modulation efficiency verses MPA-10-PPV. These results suggest that is may be possible to create azobenzene-substituted PPVs with a wide range of initial brightness and modulation efficiencies. Such an array of polymers would prove useful in the development of organic-based optoelectronic devices.

Chapter 6: Wavelength-Resolved Studies of Förster Energy Transfer in Azobenzene-Modified Conjugated Polymers: The Competing Roles of Exciton Migration and Spectral Resonance

This chapter was accepted for publication in the Journal of Physical Chemistry C. I collected the time-resolved fluorescence data presented in this chapter. The polymers were synthesized by my collaborators.

6.1 Abstract

We report results from wavelength-resolved fluorescence lifetime measurements of azobenzene-modified poly(*p*-phenylenevinylene) (PPV). The introduction of an azobenzene side chain enables reversible phototriggered modulation of the PPV emission. Intensity modulation is possible because Förster-type energy transfer from the PPV backbone to the azobenzene side chain acceptors is more efficient for the cis azobenzene isomer than for the trans. Here we explore how side chain quenching competes with intrinsic PPV exciton dynamics. By probing the red and blue edges of the PPV emission, we evaluate the photophysical effects of the side chain on different exciton populations. Prior to UV exposure, when the azobenzene side chains are trans, three exciton subpopulations are detected: (i) rapidly diffusing and unquenched, (ii) non-diffusing and quenched and (iii) low-energy, non-diffusing and unquenched. Exciton diffusion on the far blue edge is extremely efficient and mitigates the effects of side chain quenching, giving rise to the first population. The second population is due to spectral resonance between side chains and non-diffusing excitons. The third population consists of excitons residing

on the longest PPV chain segments. After UV-induced trans→cis photoisomerization, we observe a greater degree of quenching on the red edge as spectral overlap improves and the lowest-energy chromophores become efficiently quenched. Hence, *cis*-azobenzene quenching of (iii) contributes greatly to the efficient photomodulation of these PPV derivatives. In addition, rapid exciton migration on the blue edge may help to improve modulation efficiencies by effectively competing with energy transfer to *trans*-azobenzene. These findings provide improved understanding of the underlying mechanisms of energy transfer to side chains in this important class of polymers.

6.2 Introduction

Luminescent conjugated polymers based on poly(*p*-phenylenevinylene) (PPV) have attracted sustained interest due to their intriguing photophysics and use in applications such as light emitting diodes,[32,73] solar energy cells, [33] and fluorescence-based sensors.[34,61,74] A typical PPV chain contains many individual chromophores, each of which comprises 10-15 repeating units.[75,76] The chromophores are separated by chemical or conformational defects that disrupt conjugation in a non-regular way, such that the chromophores of a given chain will have a range of conjugation lengths. The inherent heterogeneity of chromophoric segments leads to interesting photophysics. After excitation of a given segment, efficient electronic energy transfer funnels the excitation to the lowest-energy chromophores. The exciton migration process has been harnessed to create extraordinarily sensitive fluorescence sensors based on conjugated polymers. A single bound quencher can quench the fluorescence

of many chromophores in a polymer chain due to exciton migration to the quencher site.[77,78] This amplified quenching can occur by electron transfer[79] or energy transfer[80] and has been studied in a variety of conjugated polymer structures.[62] We are interested in the interplay between exciton migration and energy transfer to pendant side chain quenchers and here present wavelength- and time-resolved fluorescence studies of azobenzene-functionalized PPVs.

We have been studying a family of azobenzene-functionalized PPVs, some of which are depicted in Scheme 1. The introduction of an azobenzene-modified side chain increases PPV functionality by enabling photoactivated modulation of PPV emission intensity in both solutions[41,81] and films.[82] Intensity modulation is possible because energy transfer from the PPV backbone to the azobenzene side chain acceptors is more efficient for the cis azobenzene isomer than for the trans. Thus, azobenzene photoisomerization provides a convenient and reversible method by which to control PPV emission intensity through energy transfer to the side chain. We have demonstrated the robustness of emission intensity modulation in both solutions and films through repeated cycling of the side chain isomeric state: ultraviolet (UV) light induces trans→cis azobenzene isomerization, and visible light induces cis→trans back-isomerization. The back-isomerization occurs primarily by sensitized isomerization due to the energy transfer with a very small contribution from direct excitation of *cis*-azobenzene. Thermal back-isomerization also occurs but can generally be neglected due to its slowness (k = 0.003 min^{-1} for MPA-10-PPV in toluene). The effect of side chain isomerization on the PPV emission is easily monitored by either steady-state[41,42,81] or time-resolved fluorescence.[81]

We recently reported that two distinct quenching mechanisms are operative in azobenzene-functionalized PPVs.[81] Using time-correlated single photon counting (TCSPC), we measured fluorescence lifetimes for three different azobenzene-substituted PPV derivatives and for an unmodified model PPV. We computed fluorescence lifetimes and steady-state emission intensities of azobenzene PPVs relative to the unquenched control polymer to evaluate the degree of dynamic and static quenching, respectively. This comparison revealed that quenching of the PPV backbone by *trans*-azobenzene occurs by a combination of static (stacking) and dynamic (Förster) mechanisms. Addition of a bulky *tert*-butyl group to the *para* position of the azobenzene has two major effects on quenching by *trans*-azobenzene: 1) static quenching is greatly diminished and 2) dynamic quenching becomes somewhat less efficient. Since the *tert*-butyl substituent is unlikely to substantially alter the electronics of *trans*-azobenzene, the origin of these effects must be steric in nature. The *tert*-butyl group prevents the *trans*-azobenzene stacking interactions with PPV that are responsible for the static quenching. Additionally, a Förster analysis indicates that the average donor-acceptor distance is slightly longer in the case of *tert*-butyl-functionalized azobenzene acceptors. This result is not unexpected given the steric bulk of the *tert*-butyl group and explains the decreased dynamic quenching efficiency.

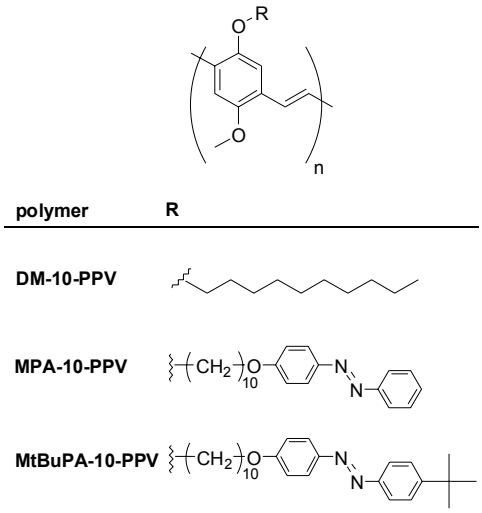

Scheme 6.1. Structures of the conjugated polymers studied.

Photoisomerization of either unmodified or *tert*-butyl-substituted azobenzene to the cis isomer yields increased quenching that is dominated by dynamic quenching with virtually no contribution from static quenching. These results and those above collectively indicate that static quenching is due to a *trans*-azobenzene-PPV complex that likely forms through stacking interactions that are disfavored for *cis*-azobenzene and *tert*-butyl-substituted azobenzene in both forms. *Cis*-azobenzene quenching in all azobenzene-PPV derivatives is dominated by dynamic quenching that is more efficient than that measured for *trans*-azobenzene. The dynamic quenching for both isomers appears to be consistent with Förster energy transfer. Trans→cis azobenzene photoisomerization increases the Förster radius due to greater spectral overlap between PPV and the cis side chain, resulting in more efficient energy transfer to the cis isomer. The emission of a typical PPV and the absorption of an azobenzene model compound in trans and cis forms are shown in Figure 6.1, with the increase in overlap upon photoisomerization depicted in the inset to Figure 6.1B.

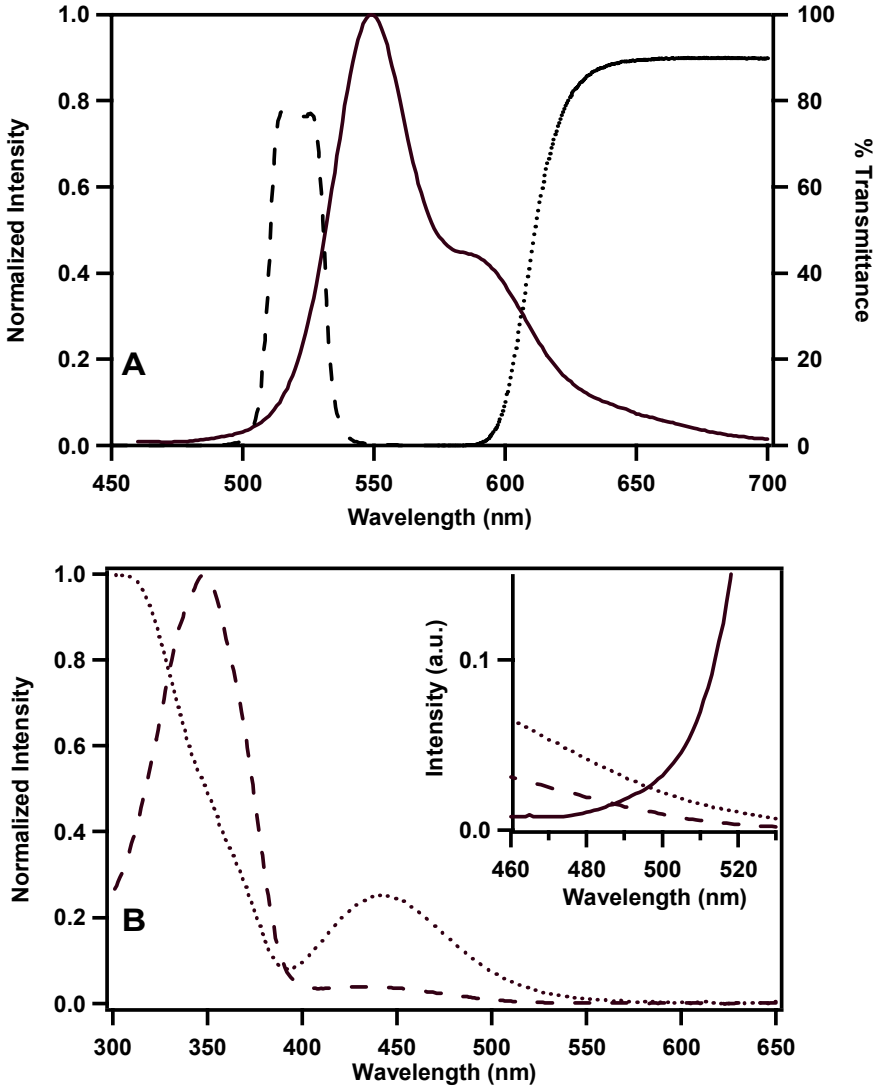

Figure 6.1. (A) Emission spectrum of DM-10-PPV overlaid with the transmission spectra of the filters used to select the red and blue wavelength regions. (B) Normalized absorption spectra of trans-decycloxyazobenzene (dashed) and pss-decycloxyazobenzne (dotted). The inset shows the overlap of the unnormalized decycloxyazobenzene absorption spectra with the emission spectrum of DM-10-PPV (solid)

Energetic resonance between donor and acceptor is required for Förster energy transfer and is typically depicted in textbook examples by showing overlap of the acceptor absorption spectrum on the red edge of the donor emission spectrum.[58]

An unusual aspect of the PPV-donor/azobenzene-acceptor system is that spectral overlap occurs on the blue edge of the PPV emission band. This raises the interesting question of how intrinsic nonradiative processes of high-energy excitons may compete with energy transfer. Brunner, et al. studied energy transfer in acceptor-doped PPV films and concluded that not only energetic resonance but also inherent exciton kinetics must be considered when predicting energy transfer efficiencies in PPV derivatives.[83] These findings represent a departure from the conventional view that considers spectral overlap (resonance) as the principal governing factor in predicting Förster resonance energy transfer and will be important in interpreting our data.

Here we present a wavelength-resolved TCSPC study of two azobenzene-modified PPVs. We make comparisons between dynamic quenching occurring on the PPV blue edge and red edge. Data are presented from both *trans*- and *cis*-azobenzene samples. The wavelength-resolved data expose populations that are obscured in the total emission and enable us to make several new observations. Blue-edge emission measurements for *trans*-state polymers reveal that exciton migration is the dominant pathway for high-energy excitons despite the fact that azobenzene spectral overlap is greatest on the PPV blue edge. However, these data also reveal a minor population of blue-emitting chromophores that do not experience rapid migration and instead are strongly quenched by azobenzenes. For polymers with *cis*-azobenzene side chains, the greatest observable change in dynamic quenching occurs on the red edge of the polymer emission even though the increase in spectral overlap upon trans→cis isomerization is more apparent on the blue edge. These new

observations enable us to conclude that PPV-to-azobenzene energy transfer is too slow to compete with efficient exciton migration but is an effective quenching mechanism for longer-lived excitons on both the blue and red edges of PPV emission. These new observations are important for the design of photomodulated PPV derivatives and for energy transfer in conjugated polymers in general.

6.3 Experimental

The syntheses of PPV derivatives poly(5-decyloxy-2-methoxy-1,4-phenylenevinylene) (DM-10-PPV),[41] poly(2-methoxy-5-((10-(4-(phenylazo)phenoxy)decyl)oxy-1,4-phenylenevinylene) (MPA-10-PPV),[41] and poly(2-methoxy-5-((10-(4-(4-*tert*-butylphenylazo)phenoxy)decyl)oxy)-1,4-phenylenevinylene (MtBuPA-10-PPV)[81] have been described previously.[41,81] All samples were prepared by dissolving a small quantity of polymer in spectral grade toluene and sonicating the solution for 1 h. The sample was then purged of oxygen by passing nitrogen gas through the sample contained in a septum-capped cuvette for 15 minutes. All samples were first prepared in the dark in order to maintain the azobenzene side chains in the thermally equilibrated trans isomeric form. To prepare polymers with side chain azobenzene groups in the cis isomeric form, isomerization was induced by exposure to a long wave UV pencil lamp (Spectroline 360-380 Long Wave UV Pencil Lamp, Spectronics Corporation) at a distance of 2.5 cm for 8 minutes. UV illumination under these conditions induces a photostationary state (pss) with approximately 55% of the azobenzene side chains in their cis conformation.[81]

Time-resolved fluorescence measurements were performed using a time-correlated single photon counting spectrometer operated in reverse mode which was

described in detail previously.[81] All experiments were conducted using a 420 nm excitation wavelength obtained by frequency doubling the 840 nm fundamental wavelength of a mode-locked titanium-sapphire laser (Wideband Mai Tai, Newport Corporation). At 420 nm, there is sufficient photon energy to excite PPV segments with a wide range of conjugation lengths.[59] The excitation intensity for our TCSPC experiments is ~ 3μJ/cm^2, an intensity at which only a single exciton is created on the individual PPV chains.[84] Emission was detected on a microchannel plate photomultiplier tube (R3809U-50, Hammamatsu) and the system had an instrument response function with 45 ps FWHM. All emission decays were collected until the peak channel counts reached 10,000. Steps were taken to ensure that back-isomerization (cis → trans) was negligible for TCSPC experiments performed on UV-exposed samples. UV-vis spectra were acquired before and after the TCSPC data acquisition, and it was found that fewer than 15% of the *cis* side chains underwent back-isomerization during the typical TCSPC experiment. Intermediate decays with peak counts < 10,000 were captured throughout an individual run and were normalized and overlaid with each other. During all experiments these decay profiles overlaid well, showing that the small amount of back-isomerization did not change the decay kinetics. Wavelength-resolved data was obtained using either a 519 ± 10 nm band pass filter (519/20/25D, Andover Corporation) for the blue edge or a 610 nm long pass filter (03FCG501, Melles Griot) for the red edge. The transmittance spectra of these two filters are shown in Figure 6.1. Total emission fluorescence decays were collected using a 435 nm long pass filter (03FCG461, Melles Griot).

All decays were fit to a sum of two or three exponentials by iteratively convoluting trial decay curves, $F(t) = \sum_i a_i e^{-t/\tau_i}$, with the instrument response function and employing a least-squares fitting procedure using Spectra Solve™ software. Several representative fits with their residuals are provided in the Supporting Information. The integrated average lifetime, $\bar{\tau}$, was calculated according to Equation 6.1:

$$\bar{\tau} = \int_0^\infty F(t)dt = \sum_i a_i \tau_i \quad (1)$$

The $\bar{\tau}$ values provide a useful quantitative measure in circumstances where decays are complex and it is difficult to find a single unique fit. In these instances, $\bar{\tau}$ changes much less than the individual fit parameters from experiment to experiment and is particularly useful for calculating overall dynamic quenching

6.4 Results

We conducted TCSPC measurements on two different azobenzene-substituted PPV polymers, MPA-10-PPV and MtBuPA-10-PPV, and a reference polymer, DM-10-PPV. Structures for the three polymers are shown in Scheme 6.1. For each of the polymers, we measured emission decays from the blue and red edges of the emission spectra as well as the total emission. Wavelength-resolved measurements are aimed at detecting fluorescence decay components originating from different exciton subpopulations,[35,59] i.e. blue-emitting *vs*. red-emitting. Figure 6.2 shows decays collected at each wavelength range for DM-10-PPV (Panel A) and MPA-10-PPV

with trans azobenzene side chains (Panel B). Emission decays for both polymers show the same general trend, with the fastest decay observed on the blue edge. There are also substantial differences between the two polymers. The three decays for MPA-10-PPV are not only faster than those of DM-10-PPV but also more conspicuously different from each other. Differences between the time-resolved emission of the two polymers are directly attributable to the presence of the *trans*-azobenzene side chain in MPA-10-PPV.

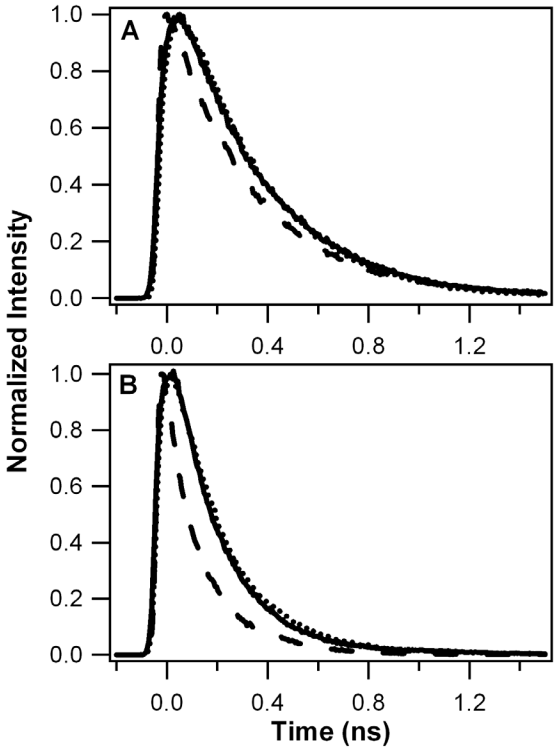

Figure 6.2. Fluorescence decays for DM-10-PPV (A) and *trans*-MPA-10-PPV (B) at the three different wavelength ranges. The total emission decay (solid line), blue edge decay (dashed line) and red edge decay (dotted line) are shown for both polymers.

We acquired fluorescence decays for dark-prepared samples and UV-exposed samples to evaluate the effect of the azobenzene side chain photoisomerization on PPV decay kinetics and emission modulation. Prior to UV exposure, the side chains of the azobenzene-substituted polymers are all in their thermodynamically favored trans state. These dark-prepared samples are denoted by the prefix *trans*-. Under UV illumination a photostationary state is reached in which approximately 55% of the azobenzene side chains are in their *cis* conformations.[81] Samples in which the photostationary state has been induced are denoted by the prefix *pss*-. The control polymer, DM-10-PPV, showed no changes in its decay profiles after UV exposure (Appendix 3). Decays for each polymer and wavelength range were fit as described in the experimental section. Table 6.1 shows the best-fit data for the *trans*-states of each sample along with corresponding χ^2 values. Table 6.2 shows the best-fit data for the *pss*-state of each sample. These data and fits were consistent from day to day and from sample to sample as demonstrated by the small standard deviations for the average decay times, $\bar{\tau}$, in Tables 1 and 2 ($N \geq 3$).

Table 6.1. Best fitting parameters acquired from the thermally-equilibrated polymer samples prepared in the dark. All emission decays were collected until the peak channel counts reached 10,000.

PPV Derivative	A_1	τ_1 (ps)	A_2	τ_2 (ps)	A_3	τ_3 (ps)	χ^2	$\bar{\tau}$ (ps)	$\bar{\tau}/\tau_0$	$k_{ET}/10^9$ s^{-1}
Total Emission										
DM-10-	0.94	269	0.06	980	--	--	1.2	312±10	--	
trans-MPA-10-	0.45	21	0.53	177	0.02	1020	1.1	124±4	0.35	4.8
trans-MtBuPA-10-	0.36	71	0.64	211	0.002	950	1.3	163±10	0.49	2.9
Blue Emission										
DM-10-	0.67	19	0.32	291	0.02	977	1.2	126±5	--	
trans-MPA-10-	0.67	25	0.32	154	0.0144	533	1.5	66±8	0.52	7.2
trans-MtBuPA-10-	0.73	28	0.27	193	0.001	360	1.6	75±1.5	0.59	5.4
Red Emission										
DM-10-	1	299	-0.08	68	--	--	1.2	298±1	--	
trans-MPA-10-	0.72	142	0.28	268	0.0001	5200	1.2	177±10	0.59	2.3
trans-MtBuPA-10-	0.15	48	0.84	220	0.008	725	1.2	184±12	0.62	2.1

Table 6.2. Best fitting parameters for UV-exposed polymers. All emission decays were collected until the peak channel counts were 10,000.

PPV Derivative	A_1	τ_1 (ps)	A_2	τ_2 (ps)	A_3	τ_3 (ps)	χ^2	$\bar{\tau}$ (ps)	$\bar{\tau}/\tau_0$	$k_{ET}/10^9$ s^{-1}
Total Emission										
DM-10-	0.94	269	0.06	747	--	--	1.2	302±11	--	
pss-MPA-10-	0.50	13	0.49	97	0.003	918	1.5	57±3	0.18	14
pss-MtBuPA-10-	0.47	39	0.52	112	0.002	648	1.5	78±4	0.25	9.5
Blue Emission										
DM-10-	0.59	25	0.37	278	0.04	936	1.0	148±8	--	
pss-MPA-10-	0.61	13	0.36	80	0.03	311	1.2	49±7	0.33	14
pss-MtBuPA-10-	0.86	22	0.13	153	0.01	1012	1.5	54±2	0.36	12
Red Emission										
DM-10-	0.96	281	0.04	808	--	--	1.1	299±1	--	
pss-MPA-10-	0.63	65	0.37	155	0.004	1003	1.4	97±14	0.33	7.0
pss-MtBuPA-10-	0.68	50	0.32	137	0.001	563	1.4	76±2	0.26	9.8

6.4.1 Total-Emission Time-Resolved

Dark-Prepared Samples. : Figure 6.3A is an overlay of the total emission decays for all three polymers. For control polymer DM-10-PPV the total emission decay is nearly exponential with a lifetime of 270 ps, which corresponds to previously reported values of the familiar MEH-PPV in a good solvent.[35,59,85] For *trans*-MPA-10-PPV the total emission decays 2.5 times faster than DM-10-PPV, and there is no observable unquenched decay component. Likewise, *trans*-MtBuPA-10-PPV decays faster than the control, and its decay components, while longer than those of MPA-10-PPV, are also all quenched relative to the control polymer. These comparisons show that *trans*-azobenzene-substituted PPV is dynamically quenched by the side chain. We showed in our previous paper that this quenching was consistent with resonant energy transfer to the side chains.[81] Quenching of *trans*-MtBuPA-10-PPV is slightly less than *trans*-MPA-10-PPV and this is attributed to a greater donor-acceptor separation distance due to steric effects introduced by the *tert*-butyl group.[81]

UV-exposed samples: Exposure to UV establishes a cis-rich photostationary state in the azobenzene side chains as described above. Relaxation to the trans state through back isomerization is extremely slow and occurs both thermally and indirectly through energy transfer from the PPV backbone (i.e. photosensitization). During a typical TCSPC experiment, return to the trans state is less than 15% complete. Hence, we are able to conduct accurate TCSPC measurements on the *pss* for comparison with the *trans*-state.

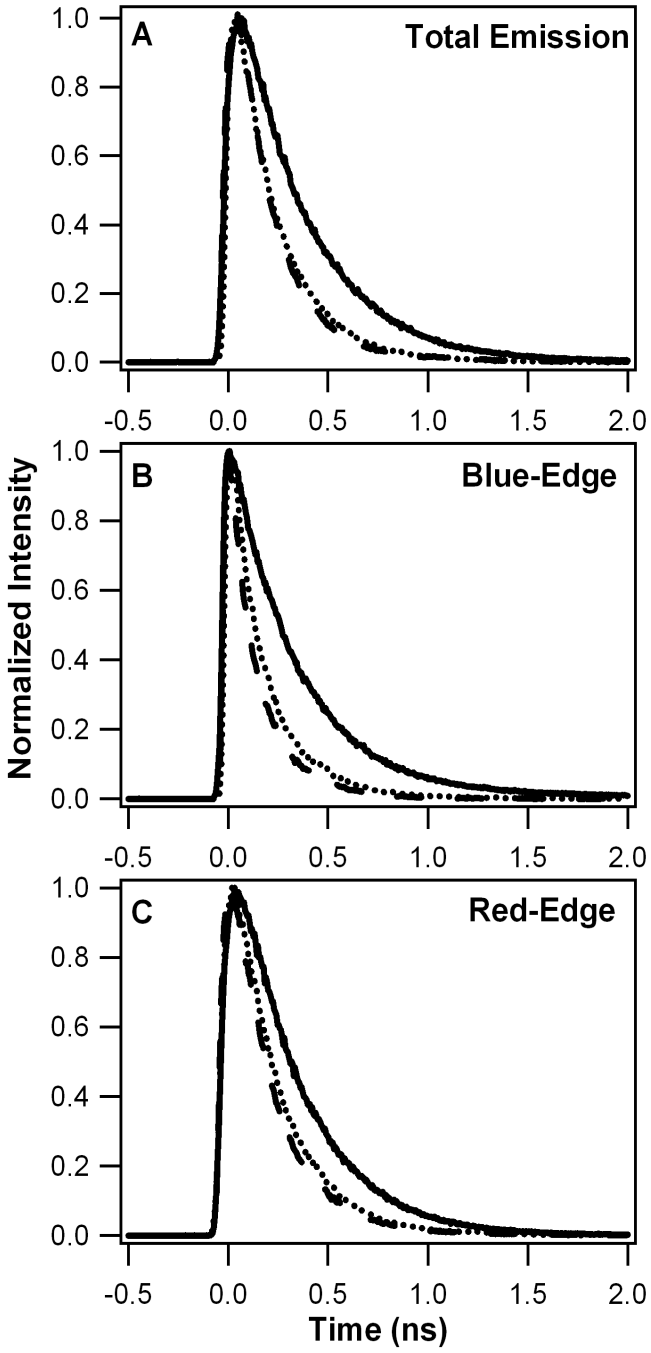

Figure 6.3. Comparison of fluorescence decays of DM-10-PPV (solid), *trans*-MPA-10-PPV (dashed) and *trans*-MtBuPA-10-PPV (dotted) collected from the entire emission band (A), the blue edge (B) and red edge (C).

Table 6.2 documents the fits used to describe the decays of UV-exposed samples. As expected, the total emission decay of DM-10-PPV does not change after

UV exposure. However, the total emission decays for both *pss*-MPA-10-PPV and *pss*-MtBuPA-10-PPV reveal increased dynamic quenching. Unlike DM-10-PPV, both azobenzene-modified polymers have decays dominated by highly quenched components. The excited state of *pss*-MtBuPA-10-PPV decays slightly slower than *pss*-MPA-10-PPV due to increased backbone/side chain separation. This increased separation reduces the amount of dynamic quenching in accordance with Förster energy transfer.[81] The excitation wavelength used in these experiments (420 nm) overlaps with the azobenzene $n \rightarrow \pi^*$ excitation band; thus, there is some direct excitation of the azobenzene side chain. To eliminate the possibility that the increased quenching is due to an azobenzene excited state, we conducted experiments over a range of excitation wavelengths (350 nm to 490 nm) and found that photomodulation is independent of the PPV excitation wavelength.

6.4.2 Blue-Edge Time-Resolved Fluorescence

Dark-prepared samples: The blue-edge emission decays of all three polymers are compared in Figure 6.3B, and the corresponding fits are given in Table 6.1. The blue-edge decay of each polymer contains a significant fast component (ca. 20-30 ps, 67-70%). The integrated intensity of the blue-edge region (509-529 nm) is only 6.7% of the total emission; thus, this fast component is masked in the total emission decay profile but is easily detectable by measuring only blue-edge emission. When fitting the blue-edge data for the azobenzene-substituted polymers with a sum of three decaying exponentials, we were unable to obtain χ^2 values as low as those reported for other samples in Table 6.1. The high χ^2 values for the azobenzene-substituted

polymers are due to the inability of the fitting function to adequately describe the additional complexity introduced by the azobenzene moieties.

In addition to the fast decay component, the blue-edge emission from the control polymer contains a 32% contribution from an unquenched species (291 ps). The azobenzene polymers differ in that they both show substantial quenching in the remaining emission (ca. 30%, τ<200 ps). The absence of an unquenched or native component in the azobenzene-substituted polymers indicates that all blue-emitting states decay rapidly by either exciton migration (~67 %) or are quenched by the *trans*-azobenzene side chain. Between *trans*-MPA-10-PPV and *trans*-MtBuPA-10-PPV there is a slight but distinguishable difference in the average lifetimes with the *trans*-MPA-10-PPV decaying about 5% faster than *trans*-MtBuPA-10-PPV.

UV-exposed samples: Fits for the blue-edge decays of all three UV-exposed samples are given in Table 6.2. For the control polymer no significant change was observed. For the two azobenzene-substituted polymers, photoisomerization of the side chains decreases the blue-edge integrated average lifetime by 25-30%. In the case of *pss*-MPA-10-PPV, the relative weights of the two major components change only slightly after UV irradiation but their decay times decrease by nearly 50%. The results for *pss*-MtBuPA-10-PPV are somewhat different in that the component lifetimes decrease to a lesser extent but the relative weights change substantially. However, these differences may be due to inaccuracies in the fitting and more emphasis should be placed on the integrated average lifetime to avoid incorrect interpretations based on individual components.

6.4.3 Red-Edge Time-Resolved Fluorescence

Dark-prepared samples: The red-edge emission for DM-10-PPV is nearly exponential with a 300 ps lifetime representative of unquenched PPV emission. A small but reproducible rise time is also observed. The red-edge decay for DM-10-PPV is about 10% slower than that of the total emission since the red-edge decay lacks contributions from the fast blue-edge components. Similar to DM-10-PPV, the emission decay of *trans*-MPA-10-PPV has a decay component approaching that of unquenched PPV, though here it is a minor component (τ= 268 ps, 28%). This component is completely absent in both the blue-edge and total-emission decays of *trans*-MPA-10-PPV (Table 6.1). The major red-edge component (142 ps, 72%) for *trans*-MPA-10-PPV is a quenched subpopulation and, unlike with DM-10-PPV, no detectable rise time is observed. The red-edge fluorescence decay of *trans*-MtBuPA-10-PPV is markedly different from both DM-10-PPV and *trans*-MPA-10-PPV and is described by two components with decay times of 48 ps and 220 ps.

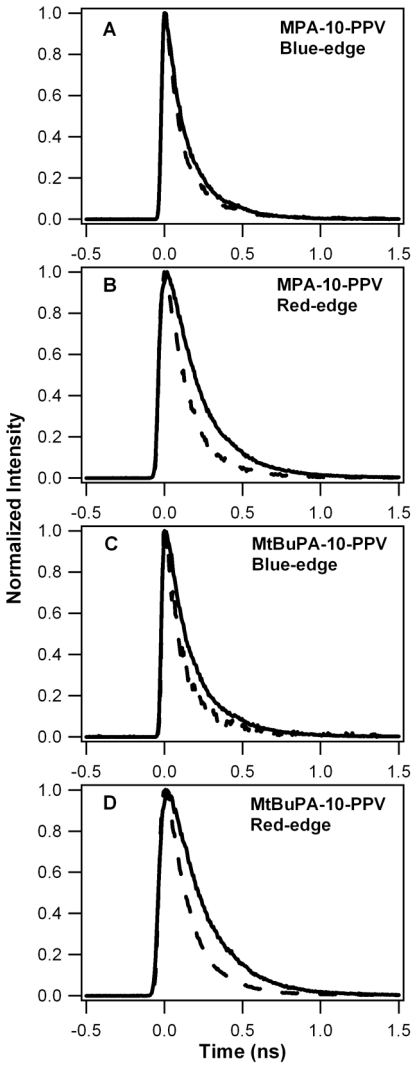

Figure 6.4. Effect of UV-exposure on the red- and blue-edge decays of both azobenzene-substituted polymers. Lifetimes for both dark-prepared (solid line) and UV-exposed (dashed line) samples were measured and compared. Less quenching is observed on the blue edge (A and C) than on the red edge (B and D) when the *pss* is established.

UV-exposed samples: The red-edge emission decays of DM-10-PPV before and after UV irradiation overlay well with the exception that it was no longer necessary to include a rising component to achieve a good fit for DM-10-PPV after UV exposure. For the azobenzene-modified polymers the post-UV decays are very

similar to one another, each consisting of two major components in which 60-70% of the observed population has a lifetime less than 100 ps and the remaining 30-40% has a lifetime of approximately 150 ps.

6.5 Discussion

Major goals of this paper are to elucidate how side-chain quenching competes with innate PPV photophysical processes and to evaluate how azobenzene isomerization affects the interactions between the azobenzene side chains and different PPV exciton subpopulations. Site selective fluorescence spectroscopy[86] and single molecule measurements[78] confirm that the bulk PPV emission spectrum reflects an inhomogeneously broadened ensemble of states. By measuring emission from the extreme blue and red edges, we obtain a good degree of photoselection. Fluorescence from the blue-edge emission wavelength range contains a substantial contribution from radiative recombination of higher-energy excitons that have not yet reached the lowest-energy segments. Data collected at wavelengths longer than 610 nm favor detection of emission originating from the lowest-energy chromophoric segments, arising either through direct excitation of lower-energy chromophores or through migration from higher-lying chromophores. By comparing data collected from the different emission wavelength ranges, we can examine differences in exciton population dynamics and by doing so evaluate the nature of the interactions between the azobenzene side chain and PPV singlet excitons of differing energies. We will first discuss interactions involving *trans*-azobenzene in dark prepared samples then turn to the effects of *cis*-azobenzene side chains in UV-exposed samples.

6.5.1 Dark-Prepared Samples

Data from dark-prepared samples are used to evaluate the effects of the *trans*-azobenzene side chain on PPV emission kinetics. In order to quantify the effects of the side chain quencher we will compare our results with those from the control polymer, DM-10-PPV. The decay kinetics for the total and red-edge emission ranges of DM-10-PPV are extremely similar and are both dominated by a component that is characteristic of emission from PPV in a good solvent ($\tau \cong 300$ ps). Their nearly single-exponential decay profiles also suggest a characteristic lifetime for emitting chromophores in accordance with conventional models of PPV emission.[87] The red-edge trace requires the addition of a rising component in order to achieve a good fit, and we assign this rise time to the growing-in of a subpopulation of low-energy chromophores due to exciton migration. The blue-edge decay for DM-10-PPV is non-exponential and is dominated by a fast decay component that stems from rapid intramolecular relaxation of high-energy excitons moving from shorter to longer chain segments. The DM-10-PPV blue-edge decay also has a substantial component that decays with a time constant of 291 ps. This component stems from radiative recombination occurring on lower-energy segments. The appearance of unquenched emission in both the blue- and red-edge decays of DM-10-PPV shows that there is a significant degree of heterogeneous broadening for the lowest-energy chromophores, in accordance with room temperature single molecule experiments.[78]

Figure 6.2 shows that the average decay times for *trans*-MPA-10-PPV are shorter than those of DM-10-PPV at all three wavelength ranges, illustrating the dynamic quenching effect of the *trans*-azobenzene side chain on PPV emission. The

overall trend in wavelength dependence is the same in both panels of Figure 6.2, but with larger differences among the three decays of the azobenzene-modified polymer. Figure 6.3B shows the blue-edge decays of all three polymers. Both azobenzene polymers and the control polymer have a fast blue-edge component (ca. 20-30 ps) that accounts for approximately two-thirds of the decay. Hayes *et al.* measured a sub-picosecond blue-edge decay component in PPV films that they assigned to exciton "hopping" from the highest-energy sites.[88] They also observed a slower component that decayed on a time scale similar to ours that they assigned to diffusion-like exciton migration that occurs as fewer energetically available sites became available. Similarly, Kersting *et al.* measured ps red shifts in the PPV transient emission spectra that were not present in PPV oligomers.[89] Therefore, we attribute the fast blue-edge component in our polymers to diffusional intrachain migration. The fast blue-edge decay component is essentially the same for all three polymers. From this we can conclude that quenching by side chains is negligible for diffusing excitons. The balance of the blue-edge decays consists of quenched populations for MPA-10-PPV (154 ps) and MtBuPA-10-PPV (193 ps) and unquenched emission for DM-10-PPV (291 ps). Thus, energy transfer to side chains effectively quenches non-diffusing excitons on low-energy segments and is responsible for the shortening of the blue-edge decay in the azobenzene-substituted polymers.

The red-edge data for both *trans*-azobenzene polymers contain contributions from a quenched population and a population with a lifetime approaching that of the unquenched emission. For *trans*-MPA-10-PPV, the major component (72%, 142 ps) closely matches the minor component observed on the blue edge (154 ps) and shows

that PPV segments resonant with the *trans*-azobenzene side chain are detected at both wavelength ranges. The minor component (28%, 268 ps) is essentially unquenched, showing that there is also a small population comprising the lowest-energy PPV chromophores for which there is insufficient spectral overlap to produce energy transfer. Note also that, unlike DM-10-PPV, no rise time was required to fit the *trans*-azobenzene red-edge decays. This result suggests that energy transfer to the side chain may compete with exciton migration when diffusion rates are significantly slow, i.e. when the end of the energy funnel has nearly been reached. These intermediate energy excitons that produce the rise time in DM-10-PPV migrate more slowly because there are fewer neighboring segments of lower energy. In the *trans*-azobenzene-substituted polymers this population is quenched by the side chain during migration.

From our wavelength-resolved measurements of dark-prepared samples, we conclude that intrinsic exciton migration mitigates the effects of spectral overlap for blue-edge excitonic populations. The blue-edge measurements show there is an exciton population that diffuses so fast it is essentially unaffected by the *trans*-azobenzene side chains, despite good spectral overlap. On the red edge, where spectral overlap is poor, we observe some emission quenching due to energy transfer from low-energy segments where there is no competition with intrinsic exciton diffusion. There is also a significant red-edge population that is essentially unquenched, showing that excitons residing on the longest segments can escape quenching by the *trans*-side chain. Some interesting questions arise from these observations. Will improved spectral overlap allow competition with diffusion? Can

we increase overlap enough to quench even the lowest-energy chromophores? We can explore these questions by investigating the *pss* state since spectral overlap improves when the *cis*-azobenzene isomers are created. In the following sections we answer these questions and discuss their relevance to understanding photomodulation.

6.5.2 UV-Exposed Samples

Trans→cis photoisomerization causes an increase in the intensity of $n \rightarrow \pi^*$ band near 440 nm.[81,90] This change in absorbance and its effect on azobenzene-PPV spectral overlap is depicted in the inset of Figure 6.1B. Concomitant with side chain isomerization, a large increase in quenching of the PPV emission is observed, as evidenced by comparing the total emission integrated average lifetimes in Table 6.2 with those in Table 6.1. Figure 6.4 documents the increase in dynamic quenching after UV exposure in both the blue- and red-edge emission of the two azobenzene-substituted polymers. Evaluation of the differential quenching observed between red and blue emission should provide answers to the questions posed above. Visually, the increase in quenching for the *pss* polymers is greater in the red-edge data (Panels 6.4B and 6.4D) than in the blue-edge data (Panels 6.4A and 6.4C). Fits to the Figure 6.4 *pss* decays are shown in Table 6.2 and support this visual observation. Hence, side chain photoisomerization appears to improve energy transfer efficiency from the lowest-energy PPV chromophores more than from the higher-energy segments. The blue-edge fits of the *pss* data show that there is an increase in quenching, particularly of the minor longer-lived component, which is consistent with a picture in which the increase in spectral overlap primarily influences slow diffusing populations.

6.5.3 The Competing Effects of Spectral Overlap and Exciton Diffusion

Our wavelength-resolved TCSPC experiments provide a way to compare quenching dynamics of different exciton populations. To facilitate comparisons between the different data, we have calculated the ratios of integrated average lifetimes ($\bar{\tau}$) of the azobenzene-containing polymers and those of DM-10-PPV (τ_0) and included them in Tables 6.1 and 6.2. Data in Table 6.1 show that the $\bar{\tau}/\tau_0$ values are only slightly larger on the red edge than on the blue edge for both of the *trans*-azobenzene-substituted polymers. This is somewhat unexpected since spectral overlap is much greater on the blue edge, which should lead to more quenching and a smaller $\bar{\tau}/\tau_0$. However, quenching by side chains must compete with exciton relaxation in the inhomogeneous density of states of the polymer; and therefore, a significantly greater rate will be necessary on the blue edge to induce the same apparent quenching. We can estimate the energy transfer rate constant, k_{ET}, for the blue- and red-edge data using the equation:

$$k_{ET} = 1/\bar{\tau} - 1/\tau_o \qquad (6.2)$$

The calculated k_{ET} values are given in Tables 6.1 and 6.2. These values are *apparent* rate constants and are useful for comparison but do not accurately account for the inhomogeneous density of states. In Table 6.1, the apparent energy transfer rates calculated from the blue-edge data are roughly three times higher than those from the red-edge data for both *trans*-MPA-10-PPV and *trans*-MtBuPA-10-PPV. This comparison illustrates that quenching rates are at least three times greater on the

blue edge due to better spectral overlap, but have a diminished effect due to competition with inherent exciton diffusion.

For Förster-type energy transfer the rate of energy transfer is proportional to the spectral overlap integral, *J*, and is given by:[58]

$$k_{ET} = \frac{9000 \ln 10 \kappa^2 Q_D}{128 \pi^5 N_A n^4 \tau_D r^6} J(\lambda) \tag{6.3}$$

where N_A is Avogadro's number, n is the solvent index of refraction, κ is an orientation factor, r is the separation between donor and acceptor and Q_D and τ_D are the emission quantum yield and lifetime of the donor. $J(\lambda)$ is the overlap integral calculated from the normalized donor emission spectra ($f_D(\lambda)$) and the acceptor absorption cross section ($\sigma_A(\lambda)$):[58]

$$J = \int f_D(\lambda) \sigma_A(\lambda) \lambda^4 d\lambda \tag{6.4}$$

We have calculated the overlap integrals for the two polymers and side chain isomeric states. The values of the overlap integrals are given in Table 6.3. In Figure 6.5A we have plotted k_{ET} values calculated from equation 6.2 and using the average integrated lifetime of the total emission decay against *J* values for the two isomeric states of both polymers. Fits through these points and the origin suggest that a linear relationship exists in accordance with Förster-energy transfer. The difference in the two slopes is attributable to different side chain-backbone separation distances. The ratio of the two slopes is 1.49 and its sixth root is 1.07, which should be proportional to the ratio of the two separation distances according to Equation 6.3. Indeed, we previously calculated separations of 15.1 Å and 14.1 Å for which the ratio is 1.06.[81]

This remarkably good agreement provides further support for Förster energy transfer. From the energy transfer rates calculated from the red and blue-edge decays using Equation 6.2, we can infer that spectral overlap with blue-emitting excitons is three times greater than red-emitting populations prior to side chain isomerization.

The effect of side chain photoisomerization and its resulting change in spectral overlap on energy transfer rates can be quantified by comparing k_{ET} values in Table 6.2 with those in Table 6.1. The blue-edge k_{ET} roughly doubles for both polymers upon creation of the pss. On the red edge, the changes are even greater. For MPA-10-PPV there is a three-fold increase in k_{ET} upon photoisomerization, and for MtBuPA-10-PPV the increase is nearly five-fold. Since the value of k_{ET} is proportional to spectral overlap, this comparison shows that the increase in spectral overlap is proportionally much larger on the red edge. The major impact of improved spectral overlap is that the previously unquenched red-edge populations are now strongly quenched, as seen from the fits in Table 6.2. Hence, the improved spectral overlap of PPV with *cis*-azobenzene leads to quenching of red-emitting PPV segments that were previously unquenched by *trans* side chains, and this effect is responsible for the greater photomodulated quenching observed in the red-edge emission in Figure 6.4. That there is a significantly greater increase in spectral overlap for *pss*-MtBuPA-10-PPV than for *pss*-MPA-10-PPV could be due to differences in the PPV emission spectra of the two polymers. Indeed, Figure 6.5B shows that MtBuPA-10-PPV does have a slightly blue-shifted spectrum relative to MPA-10-PPV and, hence, improved overlap with azobenzene acceptors. The blue-

shifted emission spectrum could reflect a polymer backbone that adopts a more kinked conformation to accommodate the bulky *tert*-butyl-terminated side chains.

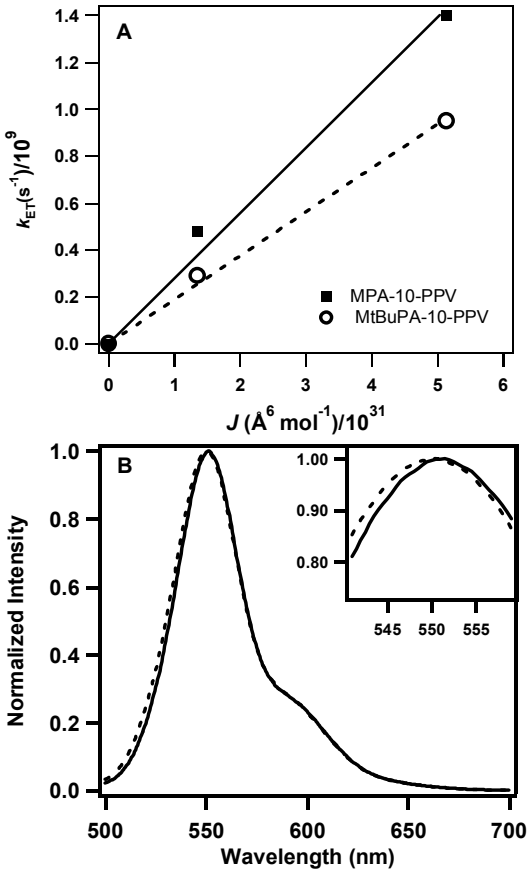

Figure 6.5. (A) Plot of energy transfer rate *vs*. overlap integral. The energy transfer rate was calculated using Equation 2 and the $\bar{\tau}$ of the total emission. The overlap integrals were calculated using the emission spectra of the PPV derivative and the absorbance spectrum of a model azobenzene compound. (B) Normalized steady-state emission spectra of MPA-10-PPV (solid) and MtBuPA-10-PPV (dashed) in toluene. Inset is the enlargement of the emission peaks to highlight the blue shift of the MtBuPA-10-PPV emission spectrum relative to MPA-10-PPV.

A major motivation of our studies has been the desire to establish better design principles of functional polymers for advanced applications. For

photomodulated polymers, an important figure of merit is the modulation efficiency, E_{mod}, which is defined as:[81]

$$E_{\text{mod}} = 1 - \frac{I_{pss}}{I_{trans}} \tag{6.5}$$

where I_{pss} and I_{trans} correspond to the steady state emission intensities of the photostationary-state and dark-prepared samples, respectively. Addition of the *tert*-butyl group causes a 24% improvement in E_{mod}, from 0.41 for MPA-10-PPV to 0.52 for MtBuPA-10-PPV.[81] To quantitatively compare the relative blue- and red-edge contributions to E_{mod}, we calculated effective E_{mod} values using the integrated average lifetimes on the red edge and blue edge of both polymers. This quantity, which we will refer to as the dynamic modulation efficiency or ε_{mod}, was calculated using the average integrated lifetimes for the trans and pss states:

$$\varepsilon_{\text{mod}} = 1 - \frac{\bar{\tau}_{pss}}{\bar{\tau}_{trans}} \tag{6.6}$$

and the values are reported in Table 4. The ε_{mod} values are greatest for the red edge in both polymers and the difference between $\varepsilon_{mod,blue}$ and $\varepsilon_{mod,red}$ is larger for MtBuPA-10-PPV. MtBuPA-10-PPV gives superior modulation efficiency overall, in part due to improved red-edge dynamic modulation efficiency. As mentioned earlier this system is somewhat unusual in that the donor emission is red-shifted relative to the main acceptor absorbance band. Similar scenarios have been observed in dye-doped PPV films.[83] It is interesting to note that this arrangement favors efficient photomodulation since some initial spectral overlap will always be difficult to avoid. Thus, when the initial energy transfer competes with exciton migration, its quenching

effect is reduced, leading to a greater overall modulation. If the initial overlap were on the red edge, the modulation efficiency would be reduced due to greater undesired quenching in the initial bright state, leading to a smaller E_{mod}.

Table 6.3. Spectral overlap integrals calculated from Equation 6.4.

J (Å^6/mol)		
	trans	*pss*
MPA-10-PPV	1.35 x 10^{31}	5.14 x 10^{31}
MtBuPA-10-PPV	1.35 x 10^{31}	5.14 x 10^{31}

Table 6.4. Dynamic modulation efficiencies from the red and blue edges of the two azobenzene-modified polymers.

	$\varepsilon_{mod,\ blue}$	$\varepsilon_{mod,\ red}$
MPA-10-PPV	0.26	0.45
MtBuPA-10-PPV	0.28	0.59

6.6 Conclusion

We have used wavelength-resolved TCSPC to study photomodulation mechanisms in two azobenzene-modified PPV polymers. Wavelength-resolved studies reveal exciton sub-populations that are otherwise obscured in the total emission decay. These measurements have revealed the dynamic interplay between side chain-induced quenching and exciton diffusion. This interplay depends on spectral resonance and exciton diffusion rates, which vary greatly between the red- and blue-edge data. Prior to UV exposure three exciton subpopulations are detected

in azobenzene-substituted PPVs: i) rapidly diffusing and unquenched, ii) non-diffusing and quenched and iii) low-energy, non-diffusing and unquenched. Exciton diffusion on the far blue edge is extremely efficient and minimizes the effects of side chain quenching, giving rise to the first population. The second population is due to spectral resonance between side chains and non-diffusing excitons. The third population consists of excitons residing on the longest PPV chain segments. After UV exposure and photoisomerization, additional quenching is observed and even the lowest-energy segments are quenched due to increases in spectral overlap. This effect is particularly pronounced for MtBuPA-10-PPV. For our purposes *tert*-butyl modified azobenzene is a much better side chain quencher because of its lack of static quenching and improved spectral overlap from blue shifting of the PPV emission. These effects are attributed to increased chain kinking and conformational changes brought about by the bulky side chain. In addition, using an "uphill" energy transfer scheme may facilitate better modulation due to the ability of efficient exciton migration to mitigate the effects of weak spectral overlap in the initial bright state configuration.

Chapter 7: Conclusion

Important advances have been made in recent years in the understanding and application of conjugated polymers. Exciting innovations in photovoltaics and sensing are being realized with conjugated polymers serving as the key material enabling this progress. One interesting conjugated polymer that was synthesized[56] and left uncharacterized is the starting point of this research. Conjugated polymers derived from the PPV family and modified with a photochromic azobenzene side chain were investigated. These polymers exhibit intriguing responses to UV and visible light, which alters the side chain azobenzene isomeric conformation. Exposure to UV results in photoisomerization of the azobenzene side chain from its thermally equilibrated trans form to a photostationary state with 55% of the side chains in the cis form. Concomitantly UV exposure diminishes the emission intensity of the PPV. Reverse isomerization can be induced by exposure to visible light and the emission intensity of the PPV backbone is subsequently recovered.

In order to conduct a detailed investigation into the photophysical processes resulting in the differential quenching observed in the azobenzene-modified PPV derivation time-resolved fluorescence measurements were conducted using a TCSPC spectrometer. Construction and characterization of this instrument are described as it was first used for these experiments. Also its application to resolving fluorescence anisotropy decays was presented, fully demonstrating the capabilities and potential uses of the instrument.

When considering the qualities of the polymers studied, they were judged by the efficiency of modulation that could be induced via exposure to light. The closer the polymer came to being switched from "on" to "off" the better the quenching properties from our perspective. An understanding of the causes of the modulation efficiency can be applied to delineate some guidelines for the design of side chain modified conjugated polymers with specific properties.

The studies that have been conducted on azobenzene-modified PPV derivatives have proven the strong effect that static quenching can have on emission of conjugated polymers and that side chain substituents can also be the source of static quenching. This is important when adding a side chain group because those that are conjugated have the potential to closely approach the polymer backbone and form a π-stacking interaction, which results in a low energy segment on the polymer backbone that is non-emissive.

Another important consideration for the addition of a side chain group to be used as an energy transfer acceptor is the competition between exciton migration along the polymer backbone and energy transfer. The rate of energy transfer to the side chain group must be comparable to the exciton migration rate (typically 4×10^5 cm^2/s) otherwise no energy transfer will take place until the exciton reaches a lowest energy state on the conjugated polymer chain.[87] In order for energy transfer to a side chain acceptor to occur efficiently the acceptor must be spectrally resonant with equilibrated excitons. The unique spectral overlap that exists between higher energy azobenzene absorption spectrum and the lower energy PPV backbone emission was

found to be advantageous to provide the differential energy transfer efficiencies between the two isomeric forms of azobenzene.

7.1 Proposed experiments

In order to extend the understanding of how side chain modification by energy transfer acceptors can be used to create and photoswitchable conjugated polymer with maximum efficiency I propose the following experiments.

1. Varying the length of the alkoxy side chain tethering the azobenzene group to study the effect of the tether length on the efficiency of quenching by static and dynamic mechanisms. I expect that decreasing the length of the tether will result in an increase in dynamic quenching as the azobenzene becomes closer to the PPV backbone. The effect of tether shortening on static quenching could be to decrease the effect as there is less flexibility of the tether and, at the same concentration, less chance of an azobenzene from one chain coming in close contact with the backbone on another chain. Increasing the length of the tether should decrease the dynamic quenching and may not have a large effect on static quenching. Exploring this effect will allow for the optimization of the tether length for which modulation efficiency is greatest. It may also elucidate the extent of interaction taking place between side chains and backbones from different polymer chains.

2. Use of other photochromic side chain groups may also prove to be a method of optimizing modulation efficiency or will at least be instructive. One good candidate is spriopyran which has an absorption band centered at 600 nm which increases 1.5-fold upon exposure to UV light. It is different from

azobenzene in that the shape of the absorption spectrum does not change upon UV exposure, only the intensity of the 600 nm band increases. The overlap of this absorption band with the emission spectrum of PPV would be quite large but increasing the tether length may allow for appropriate difference in energy transfer efficicncy.

In conclusion, the research presented here represents an important contribution to the knowledge base of conjugated polymer photophysics. The design guidelines that have been defined will be useful to future researchers seeking to synthesize conjugated polymers with specific emission properties. The development of the TCSPC spectrophotometer has been an instructive exercise and will provide an important resource to the department for years to come.

Appendix 1: Programming information for anisotropy measurements.

Time-resolved anisotropy measurements require that data be collected over a relatively long period of time, usually for about 1 h. It is also important that the excitation intensity be stable over this period of time because the relative emission intensities for the three polarizer orientations are compared. One method used to minimize the effects of excitation intensity fluctuation that is normally employed for time-resolved fluorescence anisotropy measurements is two alternate between vertical and horizontal orientations during data collections. That is, data is collected with the excitation and emission polarizers parallel to one another for a given period of time and then perpendicular for the same period and this cycle is repeated over an appropriate period of time (equal to the amount of time magic angle decay collected). The data from each orientation is written into a separate file. In order to conduct this experiment it is very useful for the experiment to be automated in order to eliminate human error in the data collection. A LabView program was written to coordinate the stepper motor for the polarizer, the data acquisition board to detect the switch states and the data collection program.

An image of the user interface panel of the LabView program is shown below in Figure A1.1. The user can enter the data collection time, number of cycles to complete, MCA bin width and choose the folder to write the data files to.

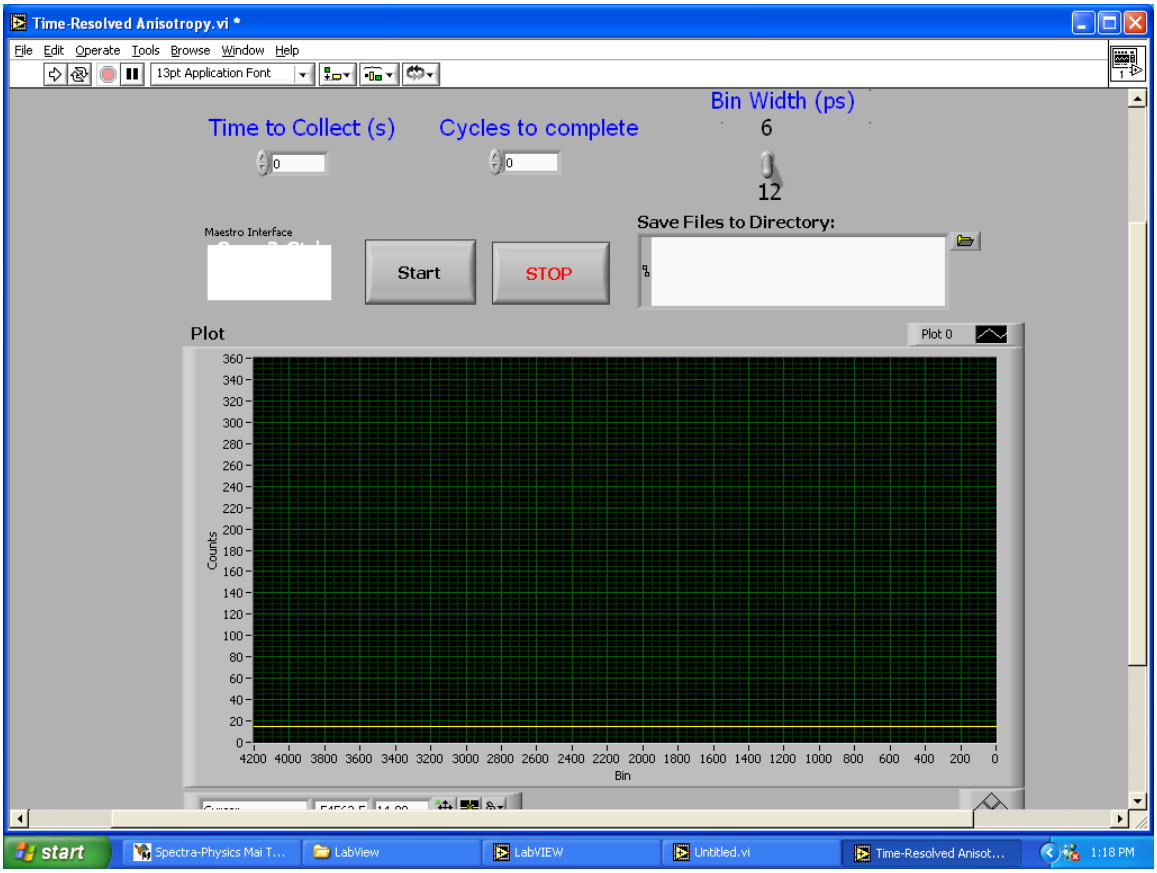

Figure A1.1 Screen shot of user interface of the time-resolved anisotropy LabView program.

The structure of the program is most clearly expressed by a flow chart shown in Figure A1.2.

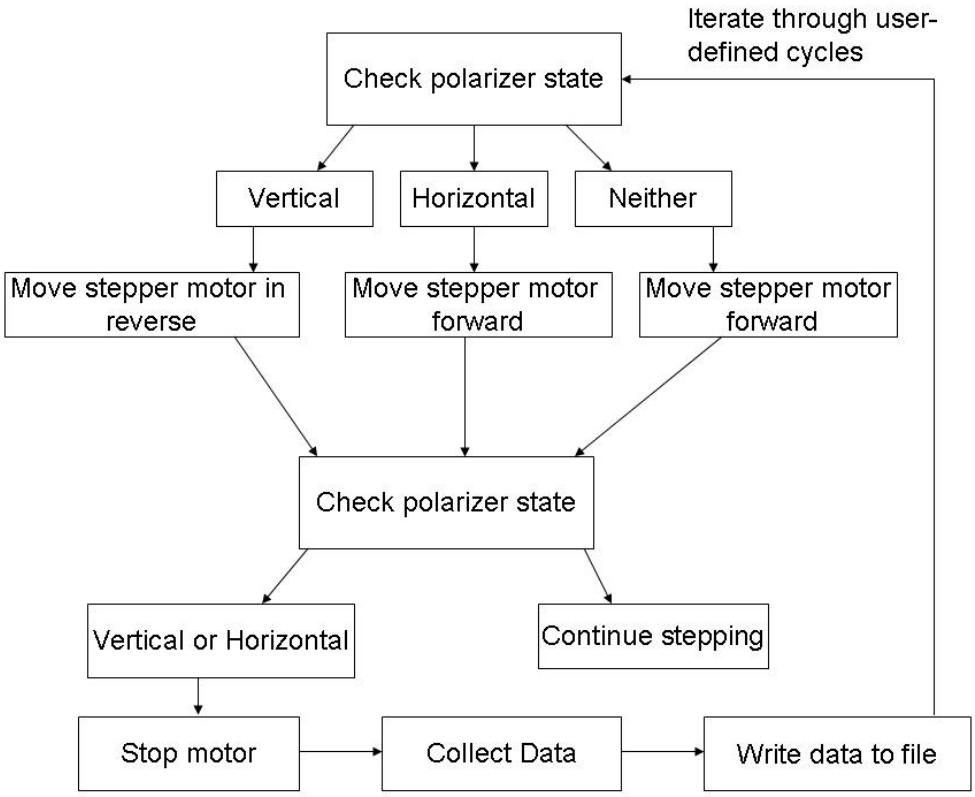

Figure A1.2 Flow chart showing the program designed to automate collection of time-resolved anisotropy data.

Appendix 2: Supporting Information for Chapter 5

Synthesis. All chemicals were purchased from Acros Organics and used as received unless otherwise noted. Acetone was distilled from anhydrous potassium carbonate prior to use. 1,10-dibromodecane was recrystallized from methanol. Polymer structures are shown in Scheme 1. The syntheses of MPA-10-PPV (**1**) and DM-10-PPV (**2**) were described previously.[41] ^{1}H and ^{13}C NMR spectra were measured on a 400 MHz Varian Mercury spectrometer, and chemical shifts are reported in ppm downfield from TMS.

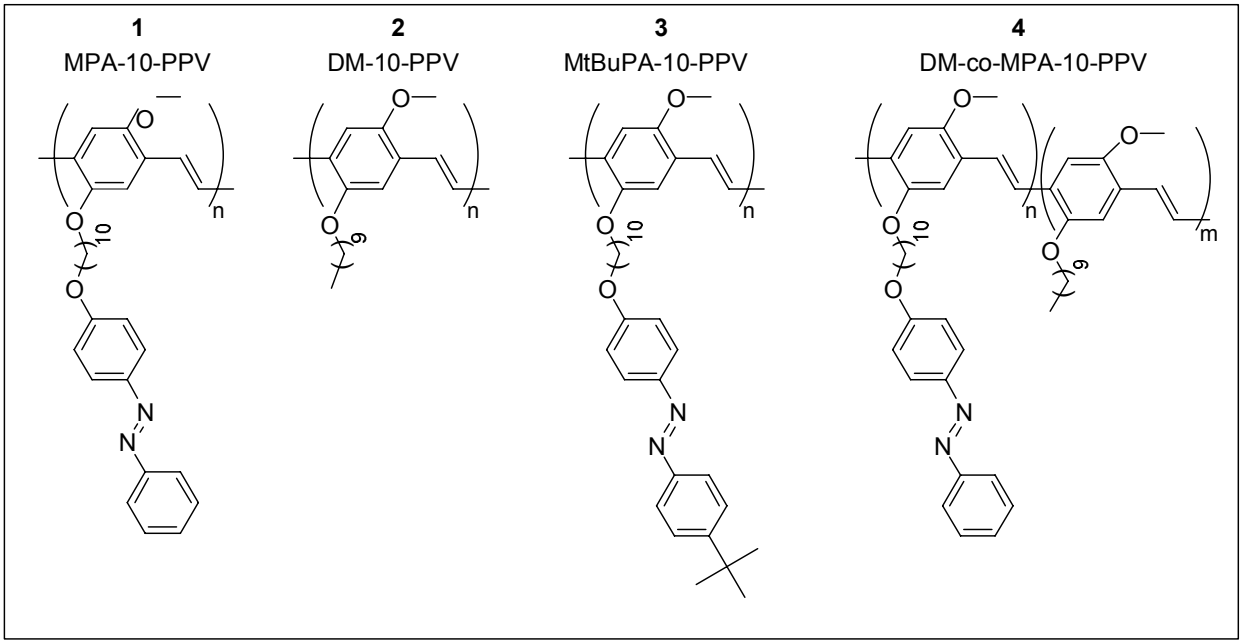

Scheme A2.1. Polymer structures.

Poly(2-methoxy-5-((10-(4-(4-*tert*-butylphenylazo)phenoxy)decyl)oxy)-1,4-phenylenevinylene (MtBuPA-10-PPV). The synthesis of MtBuPA-10-PPV (**3**) is outlined in Scheme A2.2.

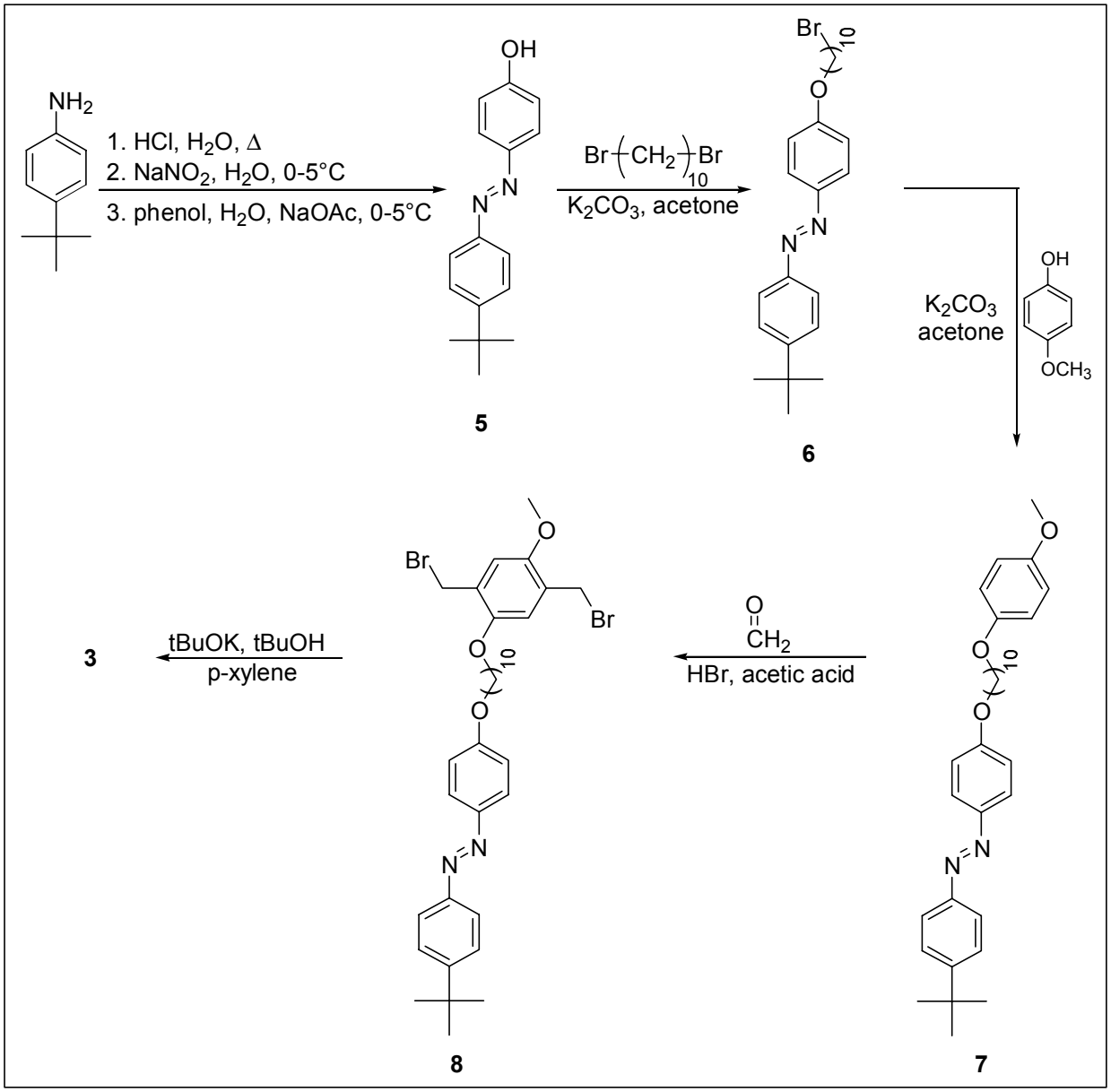

Scheme A2.2. Synthesis of polymer 3.

4-*tert*-butyl-4'-hydroxyazobenzene (5). Compound 5 was synthesized and purified according to the procedure of Kocakutgen.[91] ^{1}H NMR ($CDCl_3$): 7.87-7.85 (d, 2H), 7.82-7.80 (d, 2H), 7.52-7.50 (d, 2 H), 6.94-6.92 (d, 2H), 5.39 (br. s, 1 H),

1.37 (s, 9 H). ^{13}C NMR ($CDCl_3$): 158.09, 154.03, 150.73, 147.42, 126.10, 124.94, 122.42, 115.92, 35.31, 31.66.

1-(4-(10-bromodecyloxy)phenyl)-2-(4-*tert*-butylphenyl)diazene (**6**). Azobenzene **5** (8.3 g, 33 mmol), anhydrous potassium carbonate (33.9 g, 245 mmol), 1,10-dibromodecane (81.6 g, 271 mmol), and dry acetone (150 mL) were added to a round bottom flask equipped with a condenser. An argon atmosphere was established, and the solution was refluxed for 23 hours. After partial cooling, the reaction mixture was filtered to remove salts, and the acetone was removed by rotary evaporation. The product was precipitated by addition of hexanes, collected by suction filtration, and purified by recrystallization from methanol. Purified yield 7.2 g (46%). ^{1}H NMR ($CDCl_3$): 7.90-7.88 (d, 2 H), 7.82-7.80 (d, 2 H), 7.52-7.50 (d, 2 H), 7.00-6.98 (d, 2 H), 4.05-4.02 (t, 2 H), 3.43-3.39 (t, 2 H), 1.87-1.79 (m, 4 H), 1.48-1.41 (m, 4 H), 1.36 (s, 9 H), 1.32 (br. m, 8 H). ^{13}C NMR ($CDCl_3$): 161.51, 153.86, 150.83, 147.11, 126.06, 124.70, 122.37, 114.84, 68.60, 35.30, 34.36, 33.19, 31.67, 29.80, 29.73, 29.69, 29.57, 29.12, 28.54, 26.38.

1-(4-(10-(4-methoxyphenoxy)decyloxy)phenyl)-2-(4-*tert*-butylphenyl)diazene (**7**). Compound **6** (7.2 g, 15 mmol), *p*-methoxyphenol (2.0 g, 16 mmol), anhydrous potassium carbonate(15.1 g, 109 mmol)), and dry acetone (90 mL) were added to a round bottom flask equipped with a condenser. An argon atmosphere was established, and the solution was refluxed for 23 hours. After cooling to room temperature, the product was precipitated by pouring into ice cold water and collected by suction filtration. The product was recrystallized from hexanes. Purified yield 7.1 g (91%). ^{1}H NMR ($CDCl_3$): 7.90-7.88 (d, 2 H), 7.82-7.80

(d, 2 H), 7.52-7.50 (d, 2 H), 7.00-6.98 (d, 2 H), 6.83 (s, 4 H), 4.05-4.02 (t, 2 H), 3.92-3.89 (t, 2 H), 3.76 (s, 3 H), 1.86-1.80 (m, 4 H), 1.48-1.46 (m, 4 H), 1.37 (s, 9 H), 1.33-1.32 (m, 8 H). . ^{13}C NMR ($CDCl_3$): 161.63, 153.94, 153.81, 153.46, 150.88, 147.15, 126.15, 124.78, 122.43, 115.63, 114.88, 114.82, 68.92, 68.61, 56.06, 35.27, 31.63, 29.83, 29.73, 29.70, 29.53, 29.09, 28.50, 26.40, 26.35.

1-(4-(10-(2,5-bis(bromomethyl)-4-methoxyphenoxy)decyloxy)phenyl)-2-(4-*tert*-butylphenyl)diazene (**8**). Compound **8** was synthesized by an adaptation of the method of Neef and Farraris.[92] Compound **7** (7.1 g, 14 mmol), paraformaldehyde (2.0 g, 67 mmol), acetic acid (100 mL), and a 33% solution of HBr in acetic acid (8.8 mL, 53 mmol of HBr) were added to a round bottom flask equipped with a condenser. An argon atmosphere was established, and the solution was heated in an 80 °C oil bath for 4 hours. After cooling, the reaction mixture was diluted with chloroform and then extracted with water, saturated $NaHCO_3$, and brine. The solution was dried over $MgSO_4$, and the solvent was removed by rotary evaporation. The crude product was purified by washing with hot methanol and was dried under vacuum. Purified yield 3.7 g (38%). ^{1}H NMR ($CDCl_3$): 7.90-7.88 (d, 2 H), 7.82-7.80 (d, 2 H), 7.52-7.50 (d, 2 H), 7.00-6.98 (d, 2 H), 6.86 (s, 2 H), 4.53 (s, 2 H), 4.52 (s, 2 H), 4.05-4.02 (t, 2 H), 4.00-3.97 (t, 2 H), 3.86 (s, 3 H), 1.83-1.82 (m, 4 H), 1.50 (m, 4 H), 1.36 (br. m, 21 H). ^{13}C NMR ($CDCl_3$): 161.55, 153.85, 151.22, 150.92, 150.82, 147.08, 127.75, 127.52, 126.07, 124.71, 122.38, 114.95, 114.86, 113.94, 69.31, 68.64, 56.56, 35.30, 31.67, 29.85, 29.73, 29.70, 29.58, 29.04, 29.00, 26.46, 26.40.

Poly(2-methoxy-5-((10-(4-(4-*tert*-butylphenylazo)phenoxy)decyl)oxy)-1,4-phenylenevinylene (MtBuPA-10-PPV) (**3**). A round bottom flask equipped with a

condenser and powder dispensing funnel was placed under argon and flame dried. *P*-xylene (40 mL) and a solution of potassium *tert*-butoxide (1.8 g, 16 mmol) in *tert*-butanol (13 mL) were added to the flask, which was immersed in a 105 °C oil bath. Monomer **8** (2.5 g, 3.6 mmol) was added quickly to the powder dispensing funnel and then added gradually to the reaction solution over a period of 1 hour. The reaction solution was stirred for 18 hours, cooled, filtered, and precipitated into methanol. Polymer was isolated as a red solid (2.0 g). The polymer was dried under vacuum prior to use. ^{1}H NMR ($CDCl_3$): 7.87-7.78 (4 H), 7.52-7.47 (3 H), 7.25 (1 H), 6.95 (3 H), 6.70 (1 H), 4.04-3.59 (7 H), 1.82-1.74 (4 H), 1.52-1.27 (21 H).

DM-co-MPA-10-PPV. Copolymer **4** is a random copolymer synthesized from monomers 1-(4-(10-(2,5-bis(bromomethyl)-4-methoxyphenoxy)decyloxy)phenyl)-2-phenyldiazene and 1,4-bis(bromomethyl)-2-(decyloxy)-5-methoxy-benzene, both of which have been described previously.[41] A round bottom flask equipped with a condenser and powder dispensing funnel was placed under argon and flame dried. *P*-xylene (50 mL) and a solution of potassium *tert*-butoxide (1.0 g, 9.3 mmol) in *tert*-butanol (12 mL) were added to the flask, which was immersed in a 105 °C oil bath. Monomers 1-(4-(10-(2,5-bis(bromomethyl)-4-methoxyphenoxy)decyloxy)phenyl)-2-phenyldiazene (1.4 g, 2.2 mmol) and 1,4-bis(bromomethyl)-2-(decyloxy)-5-methoxy-benzene (1.0 g, 2.2 mmol) were mixed thoroughly together and then added quickly to the powder dispensing funnel. The monomers were added gradually to the reaction solution over a period of 50 minutes. The reaction solution was stirred for 18 hours, cooled, filtered, and precipitated into methanol. ^{1}H NMR ($CDCl_3$): 7.91-7.86, 7.51-7.43, 7.00, 6.69, 4.04-3.40, 1.79-1.75,

1.32-1.26, 0.87. The ratio of azobenzene-containing units (MPA) to non-azobenzene-containing units (DM) was determined by comparing the integrals of the peaks at 7.91-7.87, which contains 4 azobenzene protons from MPA units, and the peak at 0.87, which corresponds to the methyl group in the DM units according to: $n_{MPA}/n_{DM} = 3A_{azo}/4A_{methyl}$, where A represents the integral area of the specified peak.[93] This analysis yielded a ratio of 1.04, indicating that the copolymer contains 50% MPA units and 50% DM units.

Appendix 3: Supporting Information for Chapter 6.

Example Fits. Fluorescence decays of conjugated polymer emission collected at three wavelength ranges were fit by a "convolute and compare" technique and simplex method that minimized the chi-squared parameter. Goodness of fit was judged by considering the residual plot and chi-squared value. The data range to be fit was defined by the channels with intensity equal to 0.01% to 0.05% of the intensity of the peak channel. In some cases it was not possible to obtain a fit with a chi-squared value <1.2. Examples of data, fit and residuals with chi-squared values at the low and high ends of the range presented in our data tables are presented in Figures A3.1-3. Figure A3.1 shows the total fluorescence decay of *trans*-MPA-10-PPV, fit with the parameters in Table A3.1 of the main text.

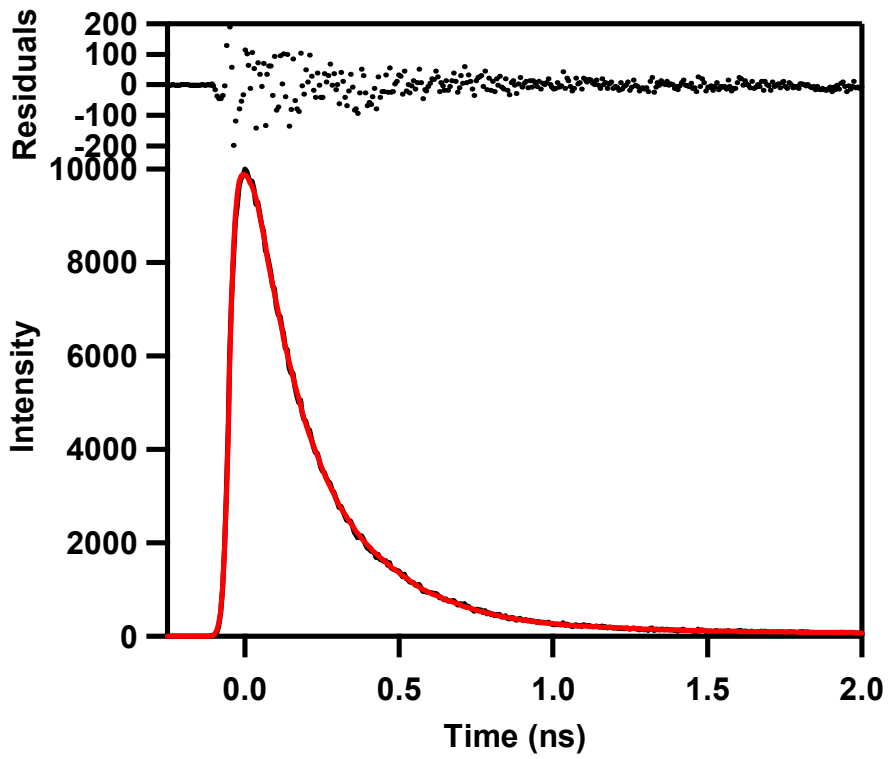

Figure A3.1. Total emission decay of *trans*-MPA-10-PPV (black) with best fit (red) and residuals (dots), $\chi^2 = 1.1$.

Another example of a fit that returned a chi-squared value below 1.2 is the blue edge emission of DM-10-PPV after UV irradiation, shown in Figure 2.

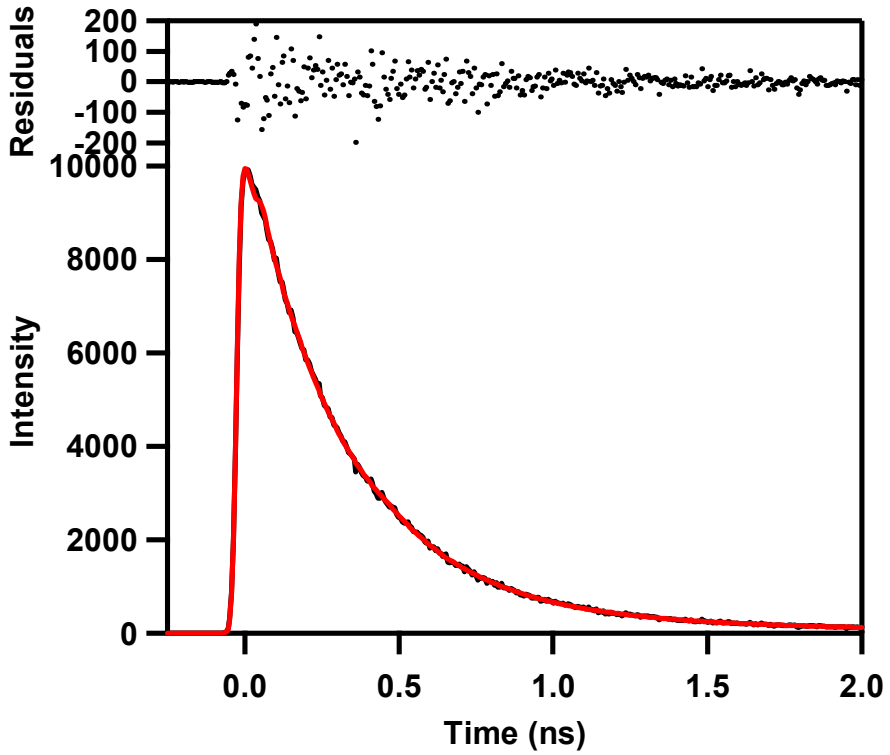

Figure A3. 2. Blue edge emission of UV-irradiated DM-10-PPV (black) with best fit (red) and residuals (dots), $^2 = 1.0$.

Figure A3.3 shows the best fit for blue emission of *trans*-MtBuPA-10-PPV, which returned a chi-squared value of 1.6, greater than the typically desired limit of 1.2 or less. We attribute the increased chi-squared value to the heterogeneous nature of the emitting species, which is especially significant for the blue edge of the emission spectrum. However, as seen by the residuals, the fit describes the data trace well. For this reason we place most emphasis on the comparison of integrated lifetimes between species and place less confidence in assignments based on individual fitting parameters.

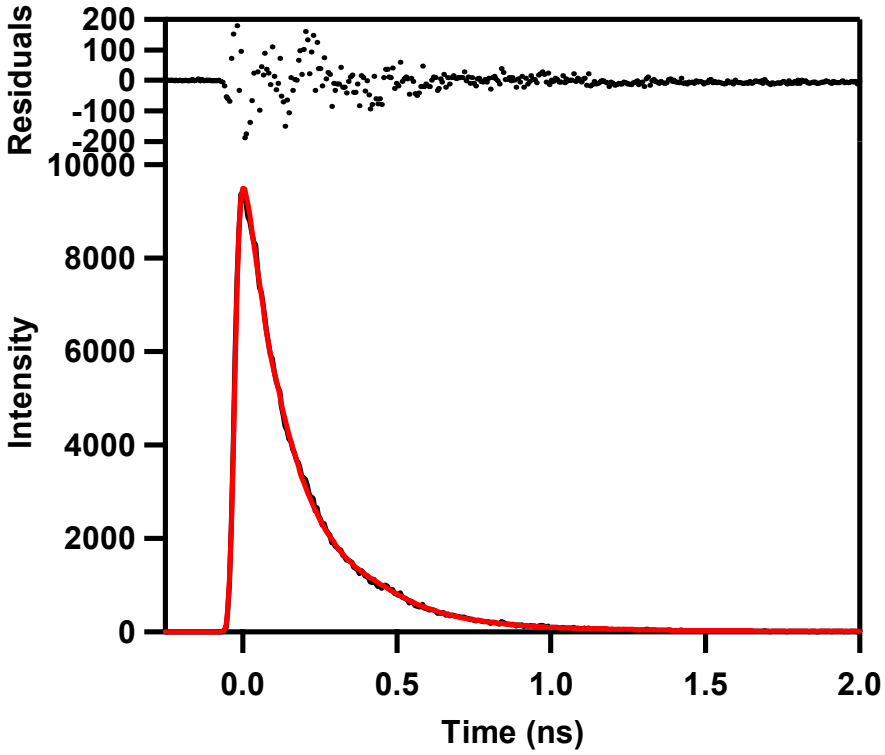

Figure A3.3. Blue emission of *trans*-MtBuPA-10-PPV (black), fit (red) and residuals (dots), $^2 = 1.6$.

Fitting of the control polymer total emission data required two exponential components but that number increased to three for the control polymer's blue edge as well as all of the azo-modified polymer decays. Examining the fitting parameters in Tables A3.2 and A3.3, it is easy to be convinced that the components each represent an independent decay process as they are sufficiently different from one another. Figure A3.4 shows the fluorescence decay data, best fit and residuals for blue emission from DM-10-PPV.

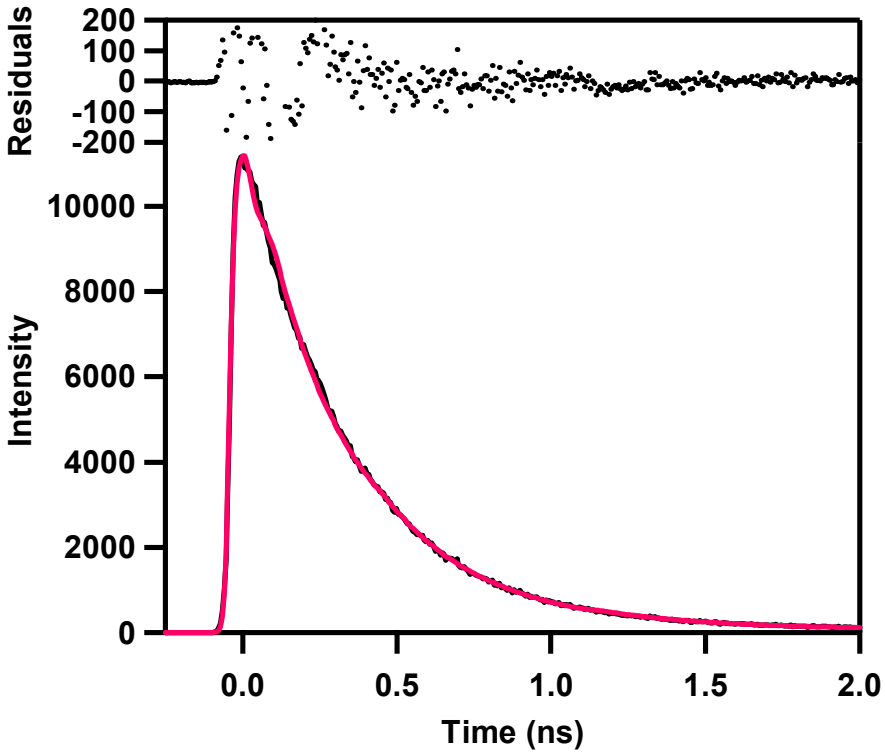

Figure A3.4. Blue edge emission from DM-10-PPV (black), best fit (red) and residuals (dotted), $^2 = 1.2$.

We also present a sample fit for the red edge emission of DM-10-PPV in Figure A3.5. A rising component was added to the fitting parameters for this fit. We attribute it to the migration of excitons into lower energy state following the excitation pulse.

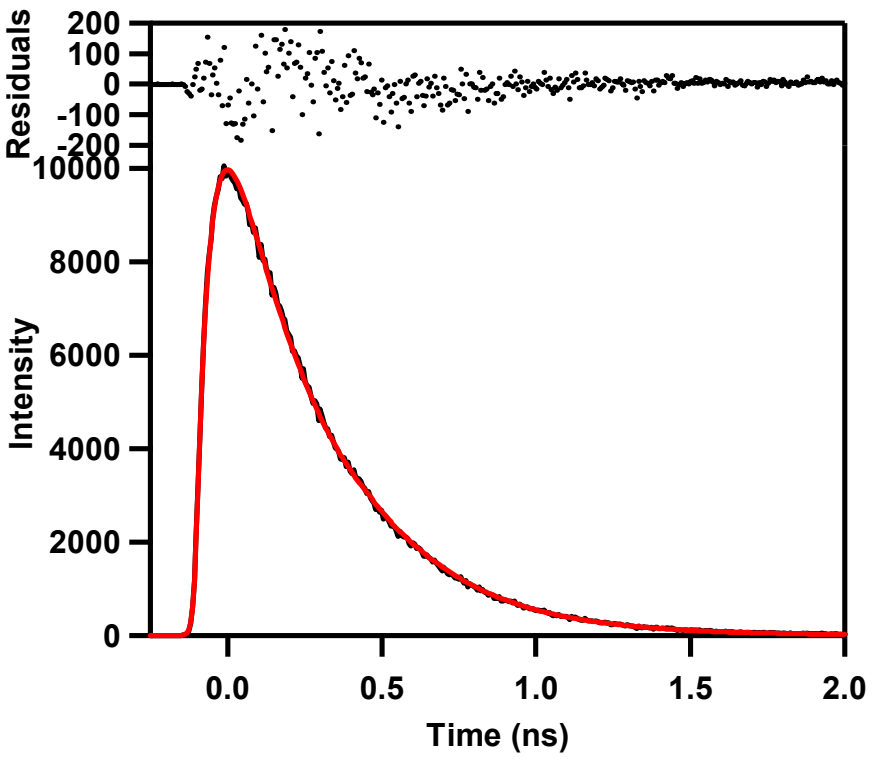

Figure A3.5. Red emission from DM-10-PPV (black), fit (red) and residuals (dotted), ^{2} = 1.2.

Control UV Exposure. Exposure of the control polymer, DM-10-PPV, to UV irradiation was performed to identify any changes in emission independent of azobenzene photoisomerization. The results in Table A3.2 of the main text show that there are no significant changes induced by UV irradiation for the total and blue emission of DM-10-PPV. Disappearance of the negative amplitude component of the red emission fit following UV irradiation is the only change. Figure A3.6 shows the traces of dark prepared DM-10-PPV overlaid with those of UV irradiated DM-10-PPV for the three wavelength ranges.

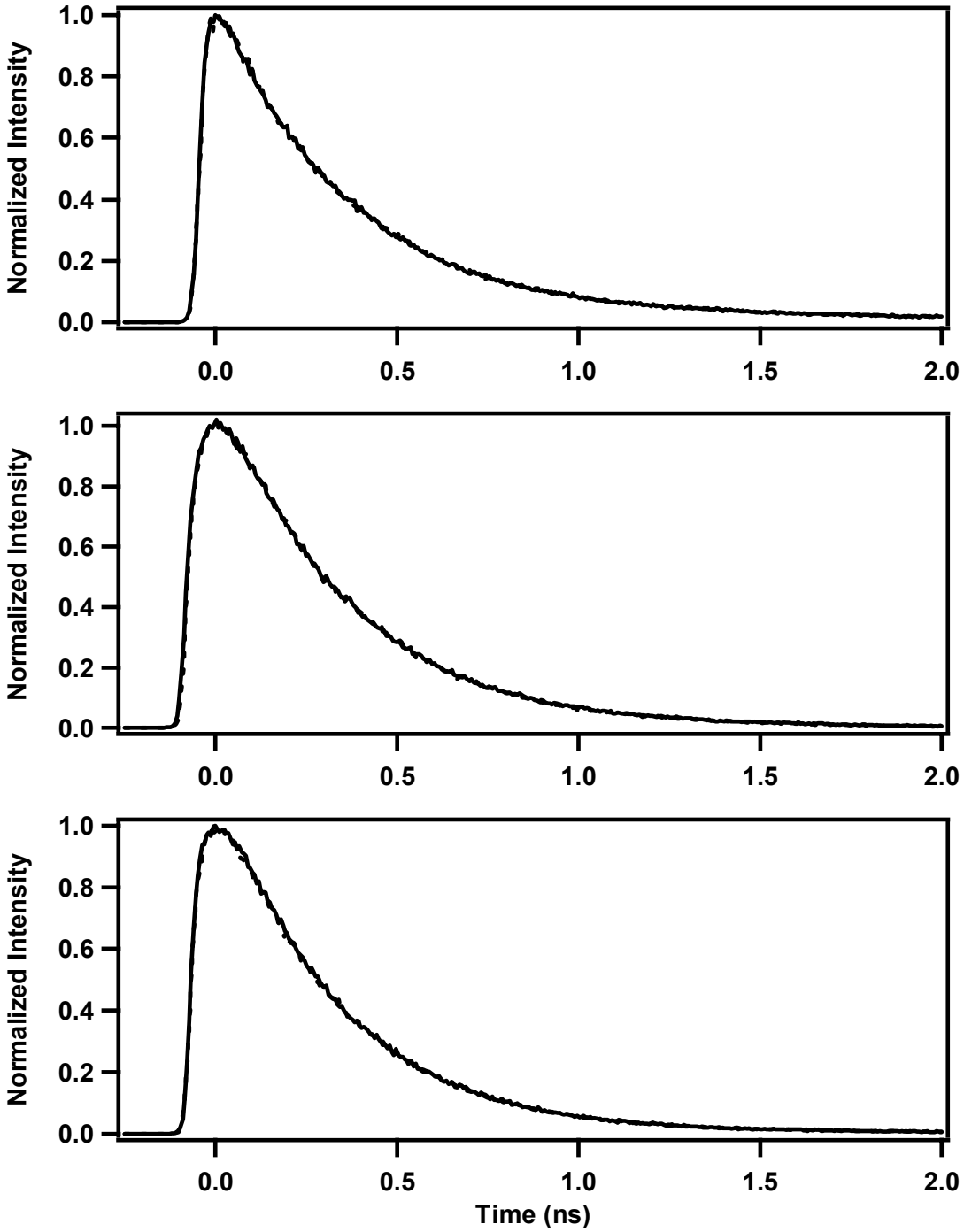

Figure A3.6. DM-10-PPV (solid) and UV irradiated DM-10-PPV (dashed) decays from the blue (top), red (center) and total (bottom) emission.

Abbreviations

TCSPC – time-correlated single photon counting

PPV – poly(p-phenylenevinylene)

IRF – instrument response function

CTAT – cetyl trimethylammonion tosylate

SDBS – sodium dodecyl benzenesulfonate

TAC – time-to-amplitude converter

MCA – multichannel analyzer card

CFD – constant fraction discriminator

EOM – optoelectronic modulator

LY – Lucifer yellow

Bibliography

(1) Bolto, B. A.; Weiss, D. E. *Aust. J. Chem.* **1963**, *16*, 1076.

(2) Bolto, B. A.; McNeill, R.; Weiss, D. E. *Aust. J. Chem.* **1963**, *16*, 1090.

(3) McNeill, R.; Siudack, R.; Wardlaw, G. H.; Weiss, D. E. *Aust. J. Chem.* **1963**, *16*, 1056.

(4) Bolto, B. A.; Weiss, D. E.; Willis, D. *Aust. J. Chem.* **1965**, *18*, 487.

(5) McNeill, R.; Weiss, D. E.; Willis, D. *Aust. J. Chem.* **1965**, *18*, 477.

(6) McGinness, J., *et al.*. *Science* **1974**, *183*, 853855.

(7) Nobel Prize Homepage. http://nobelprize.org/nobel_prizes/chemistry/laureates/2000/index.html (accessed September 17, 2007.)

(8) Chiang, C. K.; Fincher, C. R.; Park, Y. W.; Heeger, A. J.; Shirakawa, H.; Louis, E. J.; Gau, S. C.; MacDiarmid, A. G. *Phys. Rev. Lett.* **1977**, *39*, 1098.

(9) Burroughes, J. H.; Bradley, D. D. C.; Brown, A. R.; Marks, R. N.; Mackay, K.; Friend, R. H.; Burn, P. L.; Holmes, A. B. *Nature* **1990**, *347*.

(10) Baignet, D. R.; Hamer, P. J.; Friend, R. H.; Morratti, S. C.; Holmes, A. B. *Synth. Met.* **1995**, *71*.

(11) Burn, P. L.; Holmes, A. B.; Kraft, A.; Bradley, D. D. C.; Brown, A. R.; Friend, R. H. *J. Chem. Soc. Chem. Commun.* **1992**, 32.

(12) Greenham, N. C.; Moratti, S. C.; Bradley, D. D. C.; Friend, R. H.; Holmes, A. B. *Nature* **1993**, *365*.

(13) Staring, E. G. J.; *et al.*. *Synth. Met.* **1995**, *71*.

(14) Sirringhaus, H.; Kawase, T.; Friend, R. H.; Shimoda, T.; Inbasekaran, M.; Wu, W.; Woo, E. P. *Science* **2000**, *290*, 2123.

(15) Beenken, W. J. D.; Pullerits, T. *J. Phys. Chem. B* **2004**, *108*, 6164.

(16) Chang, R.; Hsu, J. H.; Fann, W. S.; Liang, K. K.; Chiang, C. H.; Hayashi, M.; Yu, J.; Lin, S. H.; Chang, E. C.; Chuang, K. R.; Chen, S. A. *Chem. Phys. Lett.* **2000**, *317*, 142.

(17) Wohlgenannt, M.; Jiang, X. M.; Vardeny, Z. V. *Phys. Rev. B: Condens. Matter* **2004**, *69*.

(18) Gustafsson, G.; Cao, Y.; Treacy, G. M.; Klacetter, F.; Colaneri, N.; Heeger, A. J. *Nature* **1992**, *357*.

(19) Trad, H.; Ltaief, A.; Majdoub, M.; Bouazizi, A.; Davenas, J. *Mater. Sci. Eng., C* **2006**, *26*, 340.

(20) Jin, J. I.; Park, C. K.; Shim, H. K.; Park, Y. W. *J. Chem. Soc. Chem. Commun.* **1989**, 1205.

(21) Yu, G.; Gao, J.; Hummelen, J. C.; Wudl, F.; Heeger, A. J. *Science* **1995**, *270*.

(22) Saricifti, N. S.; Braun, D.; Zhang, C.; Srdanov, V. I.; Heeger, A. J.; Stucky, G.; Wudl, F. *Appl. Phys. Lett.* **1993**, *62*, 585.

(23) Smith, R. C.; Tennyson, A. G.; Lim, M. H.; Lippard, S. J. *Org. Lett.* **2005**, *7*, 3573.

(24) Wang, D.; Gong, X.; Heeger, P. S.; Rininsland, F.; Bazan, G.; Heeger, A. J. *PNAS* **2001**, *99*, 49.

(25) Tian, N.; Tang, Y.; Xu, Q.; Wang, S. *Macromol. Rapid Commun.* **2007**, *28*, 729.

(26) Kalinowski, J. *J. Phys. D: Appl. Phys.* **1999**, *32*, R179.

(27) Rajeswaran, G.; al., e. *Proc. 20th Int. Display Research Conf.* **2000**, 974.

(28) Chowdhury, P. K.; Halder, M.; Sanders, L.; Arnold, R. A.; Liu, Y.; Armstrong, D. W.; Kundu, S.; Hargrove, M. S.; Song, X.; Petrich, J. W. *Photochem. Photobiol.* **2004**, *79*, 440.

(29) Danoff, E. J.; Wang, X.; Tung, S. H.; Sinkov, N. A.; Kemme, A. M.; Raghavan, S. R.; English, D. S. *Langmuir* **2007**, *23*, 8965.

(30) Wang, X.; Danoff, E. J.; Sinkov, N. A.; Lee, J. H.; Raghavan, S. R.; English, D. S. *Langmuir* **2006**, *22*, 6461.

(31) Mishra, P. P.; Apurba, L. K.; Datta, A. *Chem. Phys. Lett.* **2004**, *400*, 128.

(32) Yu, G.; Zhang, C.; Pakbaz, K.; Heeger, A. J. *Synth. Met.* **1995**, *71*, 2241.

(33) Kietzke, T.; Horhold, H. H.; Neher, D. *Chem. Mat.* **2005**, *17*, 6532.

(34) Lee, T. S.; Na, J.; Lee, J. K.; Park, W. H. *Opt. Mat.* **2003**, *21*, 429.

(35) Smilowitz, L.; Hays, A.; Heeger, A. J.; Wang, G.; Bowers, J. E. *J. Chem. Phys.* **1993**, *98*, 6504.

(36) Gill, R. E.; Malliaras, G. G.; Widleman, G.; Hadziioannou, G. *Adv. Mater.* **1994**, *6*, 132.

(37) Peng, Z.; Zhang, J.; Xu, B. *Macromolecules* **1999**, *32*, 5162.

(38) Schwartz, B. J. *Annu. Rev. Phys. Chem.* **2003**, *141*, 54.

(39) Collison, C. J.; Rothberg, L. J.; Treemaneekarn, V.; Li, Y. *Macromolecules* **2001**, *34*, 2346.

(40) Szymanski, C.; Wu, C.; Hooper, J.; Salazar, M. A.; Perdomo, A.; Dukes, A.; McNeill, J. *J. Phys. Chem. B* **2005**, *109*, 8543.

(41) Harbron, E. J.; Vicente, D. A.; Hoyt, M. T. *J. Phys. Chem. B* **2004**, *108*, 18789.

(42) Harbron, E. J.; Vicente, D. A.; Hadley, D. H.; Imm, M. R. *J. Phys. Chem. A* **2005**, *109*, 10846.

(43) Murphy, C. B.; Zhang, Y.; Troxler, T.; Ferry, V.; Martin, J. J.; Jones, W. E. *J. Phys. Chem. B* **2004**, *108*, 1537.

(44) Ego, C.; Marsitzky, D.; Becker, S.; Zhang, J.; Grimsdale, A. C.; Müllen, K.; MacKenzie, J. D.; Silva, C.; Friend, R. H. *J. Am. Chem. Soc.* **2003**, *125*, 437.

(45) Su, H.-J.; Wu, F.-I.; Shu, C.-F. *Macromolecules* **2004**, *37*, 7197.

(46) Morgado, J.; Cacialli, F.; Friend, R. H.; Iqbal, R.; Yahioglu, G.; Milgrom, L. R.; Moratti, S. C.; Holmes, A. B. *Chem. Phys. Lett.* **2000**, *325*, 552.

(47) Raymo, F. M.; Tomasulo, M. *J. Phys. Chem. A* **2005**, *109*, 7343.

(48) Rau, H. Photoisomerization of Azobenzenes. In *Photochemistry and Photophysics*; Rabek, J. F., Ed.; CRC Press: Boca Raton, 1990; Vol. II; pp 119.

(49) Natansohn, A. R.. *Chem. Rev.* **2002**, *102*, 4139.

(50) Kumar, G. S.; Neckers, D. C. *Chem. Rev.* **1989**, *89*, 1915.

(51) Irie, M. Photoresponsive Polymers: Reversible Control of Polymer Conformation in Solution and Gel Phases. In *Applied Photochromic Polymer Systems*; McArdle, C. B., Ed.; Blackie: Glasgow, 1992; pp 174.

(52) Jin, M.; Lu, R.; Bao, C. Y.; Xu, T. H.; Zhao, Y. Y. *Opt. Mat.* **2004**, *26*, 85.

(53) Ceroni, P.; Laghi, I.; Maestri, M.; Balzani, V.; Gestermann, S.; Gorka, M.; Vögtle, F. *New J. Chem.* **2002**, *26*, 66.

(54) Asakawa, M.; Ashton, P. R.; Balzani, V.; Brown, C. L.; Credi, A.; Matthews, O. A.; Newton, S. P.; Raymo, F. M.; Shipway, A. N.; Spencer, N.; Quick, A.; Stoddart, J. F.; White, A. J. P.; Williams, D. J. *Chem. Eur. J.* **1999**, *5*, 860.

(55) Matsui, T.; Nagata, T.; Ozaki, M.; Fujii, A.; Onoda, M.; Teraguchi, M.; Masuda, T.; Yoshino, K. *Synth. Met.* **2001**, *119*, 599.

(56) Yoshino, K.; Nagata, T.; Nakayama, K.; Fujii, A.; Ozaki, M.; Onoda, M. *Mol. Cryst. Liq. Cryst. Sci. Technol., Sect. C:* **2000**, *12*, 143.

(57) Cross, A. J.; Fleming, G. R. *Biophys. J.* **1984**, *46*, 45.

(58) Lakowicz, J. R. *Principles of Fluorescence Spectroscopy*; Kluwer Academic/Plenum: New York, 1999.

(59) Samuel, I. D. W.; Crystall, B.; Rumbles, G.; Burn, P. L.; Holmes, A. B.; Friend, R. H. *Chem. Phys. Lett.* **1993**, *213*, 472.

(60) Hu, D.; Yu, J.; Barbara, P. F. *J. Am. Chem. Soc.* **1999**, *121*, 6936.

(61) Hsu, J.-H.; Fann, W.; Tsao, P.-H.; Chuang, K.-R.; Chen, S.-A. *J. Phys. Chem. A* **1999**, *103*, 2375.

(62) Zheng, M.; Bai, F.; Zhu, D. *J. Photochem. Photobiol., A: Chemistry* **1998**, *116*, 143.

(63) Fissi, A.; Pieroni, O. *Macromolecules* **1989**, *22*, 1115.

(64) Jung, B.-D.; Stumpe, J.; Hong, J.-D. *Thin Solid Films* **2003**, *441*, 261.

(65) Pieroni, O.; Fissi, A.; Houben, J. L.; Ciardelli, F. *J. Am. Chem. Soc.* **1985**, *107*, 2990.

(66) Menzel, H.; Weichart, B.; Schmidt, A.; Paul, S.; Knoll, W.; Stumpe, J.; Fischer, T. *Langmuir* **1994**, *10*, 1926.

(67) Sugiyama, K.; Sono, K. *J. Appl. Polym. Sci.* **2001**, *81*, 3056.

(68) Tsuda, K.; Dol, G. C.; Gensch, T.; Hofkens, J.; Latterini, L.; Weener, J. W.; Meijer, E. W.; De Schryver, F. C. *J. Am. Chem. Soc.* **2000**, *122*, 3445.

(69) Rivera, E.; Belletête, M.; Natansohn, A.; Durocher, G. *Can. J. Chem.* **2003**, *81*, 1076.

(70) Shimomura, M.; Kunitake, T. *J. Am. Chem. Soc.* **1987**, *109*, 5175.

(71) Kuiper, J. M.; Engberts, J. B. F. N. *Langmuir* **2004**, *20*, 1152.

(72) Song, X.; Perlstein, J.; Whitten, D. G. *J. Am. Chem. Soc.* **1997**, *119*, 9144.

(73) Halls, J. J. M.; Pichler, K.; Friend, R. H.; Moratti, S. C.; Holmes, A. B. *Synth. Met.* **1996**, *77*, 277.

(74) Fan, C.; Hirasa, T.; Plaxco, K. W.; Heeger, A. J. *Langmuir* **2003**, *19*, 3554.

(75) Gettinger, C. L.; Heeger, A. J.; Drake, J. M.; Pine, D. J. *J. Chem. Phys.* **1994**, *101*, 1673.

(76) Woo, H. S.; Lhost, O.; Graham, S. C.; Bradley, D. D. C.; Friend, R. H.; Quattrocchi, C.; Bredas, J. L.; Schenk, R.; Mullen, K. *Synth. Met.* **1993**, *59*, 13.

(77) Itoh, T.; Kamioka, K.; Webber, S. E. *Macromolecules* **1989**, *22*, 2851.

(78) Kim, S. H.; Zyung, T.; Chu, H. Y.; Do, L.-M.; Hwang, D.-H. *Phys. Rev.B: Condens. Matter* **2000**, *61*, 15854.

(79) Wang, J.; Wang, D. L.; Moses, D.; Heeger, A. J. *J. Appl. Polym. Sci.* **2001**, *82*, 2553.

(80) Bassler, H.; Brandl, V.; Deussen, M.; Gobel, E. O.; Kersting, R.; Kurz, H.; Lemmer, U.; Mahrt, R. F.; Ochse, A. *Pure Appl. Chem.* **1995**, *67*, 377.

(81) Grimes, A. F.; Call, S. E.; Vicente, D. A.; English, D. S.; Harbron, E. J. *J. Phys. Chem. B* **2006**, *110*, 19183.

(82) Lewis, S. M.; Harbron, E. J. *J. Phys. Chem. C* **2007**, *111*, 4425.

(83) Brunner, K.; van Haare, J. A. E. H.; Langeveld-Voss, B. M. W.; Schoo, H. F. M.; Hofstraat, J. W.; van Dijken, A. *J. Phys. Chem. B* **2002**, *106*, 6834.

(84) Martini, I. B.; Smith, A. D.; Schwartz, B. J. *Phys. Rev. B* **2004**, *69*.

(85) Nguyen, T.-Q.; Doan, V.; Schwartz, B. J. *J. Chem. Phys.* **1999**, *110*, 4068.

(86) Bassler, H.; Schweitzer, B. *Acc. Chem. Res.* **1999**, *32*, 173.

(87) Barbara, P. F.; Gesquiere, A. J.; Park, S.-J.; Lee, Y. J. *Acc. Chem. Res.* **2005**, *38*, 602.

(88) Hayes, G. R.; Samuel, I. D. W.; Phillips, R. T. *Phys. Rev. B* **1995**, *52*, 11569.

(89) Kersting, R.; Lemmer, U.; Mahrt, R. F.; Leo, K.; Kurz, H.; Bassler, H.; Gobel, E. O. *Phys. Rev. Lett.* **1993**, *70*, 3820.

(90) Satzger, H.; Root, C.; Braun, M. *J. Phys. Chem. A* **2004**, *108*, 6265.

(91) Kocaokutgen, H.; Gumrukcuoglu, I. *Turk. J. Chem.* **1995**, *19*, 219.

(92) Neef, C. J.; Ferraris, J. P. *Macromolecules* **2000**, *33*, 2311.

(93) Wang, G.; Min, L.; Guo, C.; Wu, F.; Tian, W.; Chen, X.; Shen, J. *Polymer J.* **2000**, *41*, 2309.